

AD-A252 881



2

Low Dielectric Constant insulators and Gold Metallization for GHz Multi-Chip Modules

DARPA BAA#90-09, Part II
Contract: N00014-91-J-4008

Annual Performance Report
Due 920630

Principal Investigators:

Paul Kohl and Sue Ann Bidstrup
School of Chemical Engineering
Georgia Institute of Technology
Atlanta, GA 30332-0100
JUNE 1992

DTIC
ELECTE
JUL 16 1992
S A D

This document has been approved
for public release and sale; its
distribution is unlimited.

GEORGIA INSTITUTE OF TECHNOLOGY



92-17391



Low Dielectric Constant insulators and Gold Metallization for GHz Multi-Chip Modules

DARPA BAA#90-09, Part II
Contract: N00014-91-J-4008

Annual Performance Report
Due 920630

Principal Investigators:

Paul Kohl and Sue Ann Bidstrup
School of Chemical Engineering
Georgia Institute of Technology
Atlanta, GA 30332-0100

Accession For	
NTIS CRA&I	<input checked="checked" type="checkbox"/>
DTIC TAB	<input type="checkbox"/>
Unannounced	<input type="checkbox"/>
Justification	
By	
Distribution /	
Availability Codes	
Dist	Availability and/or Special
A-1	

Statement A per telecon Larry Kabocoff
ONR/Code 1131
Arlington, VA 22217-5000

NWW 7/15/92

Table of Contents

<u>Topic</u>	<u>Page</u>
1. Overview.....	3
1.1 Milestones.....	6
1.2 Collaborators.....	7
2. Metallization.....	10
2.1 Process for Gold MCMs.....	10
2.2 Adhesion to Gold.....	11
2.21 Adhesion and Electrical Isolation tests.....	20
2.22 XPS Analysis of Adhesion Layer.....	22
2.3 Electroless Deposition of Gold.....	34
3. Low Dielectric Constant Polymers.....	61
3.1 Polyimides and bis-benzocyclobutene.....	62
3.2 Polyquinoline.....	90
3.3 Photodefinable Polyimides.....	93
3.4 Low Temperature Measurements.....	103
3.5 Moisture Measurements.....	108
4. Inorganic Insulators.....	113
4.1 Silicon dioxide.....	113
4.2 Porous Silica.....	131
5. Electrical Characterization.....	148
6. Students	151
References.....	153
Appendix 1.....	156
Appendix 2.....	161
Appendix 3.....	165

1. Overview

The goal of this program is to investigate new dielectrics, metals and processes for the fabrication of multi-chip modules which hold the promise of exceptional electrical performance in the GHz region in addition to high yield and high reliability. The low dielectric constant insulators are being evaluated through the fabrication of in-situ test structures using gold as the metallization. In the course of doing this evaluation, a simple process for gold MCMs has been investigated.

A processing scheme using gold as the interconnection metallization in the module has been developed and is being characterized. The gold process has fewer process steps than the equivalent copper process and is potentially lower cost, particularly when high reliability is important. A unique adhesion material is under investigation and is currently being evaluated by n-Chip. This adhesion material would result in a significant cost reduction in the manufacture of copper or gold MCMs. Future plans are included in section 2.

A series of organic and inorganic materials have been selected for evaluation as interlevel dielectrics with the gold metallization. In-situ test structures are being fabricated to determine the electrical, mechanical and chemical properties of the dielectrics. Novel approaches to low dielectric constant insulators are being investigated in addition to the evaluation of existing materials.

Selection of thin film dielectrics is a key element in the performance and long-term reliability of GHz multichip modules. The overall performance depends on the ease of processing, chemical structure, electrical behavior and mechanical properties. Crucial characteristics which must be considered in the selection of materials to be used as interlevel dielectrics include: dielectric properties; moisture absorption; coefficient of thermal expansion; modulus; residual stress; adhesion; processing temperature; thermal stability; and thermal conductivity. The series of polyimides currently being investigated for use in GHz frequency MCMs include:

DuPont PI2545 (PMDA-ODA)
DuPont PI2566 (Fluorinated)
DuPont PI2611 (Low Stress)
Amoco Ultadel 7501 (Photosensitive)
Ciba-Geigy 200 Series (Pre-imidized)
Ciba-Geigy 400 Series (Pre-imidized and Photosensitive)

Other exploratory polymer systems being investigated include:

Allied-Maxdem polyquinolines
Dow Chemical benzocyclobutenes

These exploratory systems have not yet achieved a significant commercial market as interlevel dielectrics. However, preliminary results indicate that these polymers possess a lower dielectric constant and superior moisture barrier properties than some of the traditional polyimides used as dielectrics.

A number of inorganic materials are also being explored for interlevel dielectric applications, including:

Plasma Enhanced CVD Silicon Dioxide
Spin-on Glasses
Porous Silica

Studies are underway to investigate the improvement in silicon dioxide performance through variations in deposition conditions. The effect of the measurement frequency on the dielectric properties of silicon dioxide is also being explored. Currently, spin-on glasses and porous silica are not used in interlevel dielectric applications; however, they possess a number of properties that would be advantageous for this application. Spin on glasses have a low dielectric constant and the ability to planarize the underlying topography. Porous silica possesses an extremely low dielectric constant (i.e. 1.6- 2.5). In both these materials, one of the serious limitations is the ability to achieve thin films ranging from five to ten micrometers. Currently, we are attempting to overcome this processing limitations and compare their performance properties to those of the polymer interlevel dielectrics.

In order to compare the performance properties of the various dielectric materials, in-situ characterization techniques are required. Thermal cure history, fabrication environment and type

of substrate upon which the pre-polymer is cast all can have a significant effect on the final film properties. Therefore, a polymer film cured on a particular surface may have significantly different properties than a film of the same material cured free of the substrate. In order that the characterization test results actually reflect the behavior of the polymer in a performance environment, it is necessary to measure the critical film properties directly on the substrate.

A number of methods are being used or developed for characterizing film properties directly on a silicon or metallized substrate. The in-plane modulus is characterized using micro-machined low deflection sites or microfabricated vibrating polymer strings. The residual stress and in-plane coefficient of thermal expansion are measured using a Flexus Wafer Curvature Apparatus. The film thickness, refractive indices and degree of orientation are obtained using a Metricon Prism Coupler.

In applications requiring multilayer coatings, polymer properties normal to the plane are as crucial to the performance of the coating as polymer properties in the plane. Each of the characterization techniques mentioned above are restricted to the characterization of in-plane properties. The spin coat processing of polymer films may lead to molecules which are oriented in the plane of the film; this orientation will cause the mechanical and thermal properties in the plane of the film to be different from those properties through the plane of the film. Currently, there is no test method for measuring mechanical and thermal properties normal to the plane of the film. In this study the microfabricated electrodes will be used to determine small changes in film thickness that result when the temperature or pressure in the film is varied. From these measurements, we can directly determine the modulus and the coefficient of thermal expansion normal to the plane of the film.

In summary, gold-insulator test structures have been fabricated. A series of promising organic and inorganic dielectrics have been selected for evaluation for use in GHz multi-chip modules. A series of in-situ characterization techniques have been developed for measuring electrical, mechanical and thermal properties of the interlevel dielectrics. The effect of the chemical system and processing variations on the performance properties of thin film dielectrics is currently being explored. Processing

variations include spin speed, film thickness, reaction temperature and degree of molecular orientation.

1.1 Milestones

<u>Date</u>		<u>Technical Objective</u>
<u>Proposed</u>	<u>Completed</u>	
8/1991	9/1991	Initiate Program.
9/1991	9/1991	Training of graduate and undergraduate students on specific processing and testing equipment.
10/1991	10/1991	Selection of "Long List" of low dielectric constant materials and structures.
12/1991	11/1991	Fixtures for HP8510 completed.
12/1991	12/1991	Completion of process log for test structure processing to evaluate low dielectric constant materials and processes.
1/1992	12/1991	Design of in-situ stress and mechanical property testing.
1/1992	12/1991	Fabrication of first generation test structures for characterization.
3/1992	2/1992	Identification of layer to layer adhesion test.
4/1992	1/1991	First Georgia Tech electrical characterization of microstrips at >1 GHz.
7/1992		Preliminary design of second test structure in collaboration with outside institution of DARPA's choosing.
8/1992	partial	Preliminary evaluation of stress and high frequency electrical properties of low dielectric constant material.

10/1992		Selected short list of low dielectric constant materials and processes.
11/1992	3/1992	Design of experiments for moisture uptake.
1/1993		Evaluation of adhesive properties and development of processing techniques to improve adhesion.
2/1993	partial	Preliminary evaluation of gold vs. copper completed.
3/1993		Lithography masks of second test structure completed.
9/1993		Models of second test structure completed.
11/1993		Evaluation of stress, adhesion and high frequency electrical properties at ambient conditions.
3/1994		In-depth high frequency characterization of chemical structure vs. equivalent circuit.
7/1994		Effect of moisture and temperature cycling on adhesion and high frequency electrical properties.
8/1994		Documentation completed.

1.2 Collaborators

There are several groups of collaborators in which we are working with. The first group (listed below) are those participating in the High Performance MCM program. We have pursued these interactions and have had some success in maintaining a meaningful level of interaction. In spite of multiple attempts to interact with other organizations, collaborations have not materialized. We most heartily welcome additional collaborations and we recognize that official channels are sometimes needed in order to initiate such interactions. We also recognize that meaningful collaborations require a significant commitment resources.

We have initiated interactions with numerous organizations outside of the program in order to achieve our program objectives. These include materials suppliers and equipment vendors. The interaction with Maxdem was suggested by DARPA and we are evaluating their products (section 3.2). The interaction with MTI is to help develop the processing tools necessary for dielectric processing in parallel with material development. The Army Missile command has had an interest in high reliability MCMs using gold as the metallizations and has used our experiences as a source of information in interacting with their suppliers.

Program Participants:

n-Chip

Materials: properties of SiO₂
Processing: Spin-On-Glass
Metallization: Copper vs. Gold

Mayo and University of Wisconsin

High frequency measurements
Test structures for evaluation

Additional Industrial Collaborators:

Dupont

Low dielectric constant polyimides- processing, properties and uses.

Dow Chemical

Bis-benzocyclobutene- processing, properties and uses.

Allied Signal

Exploratory spin-on-glass for planarizing SiO₂ applications.

Maxden Corporation

Polyquinolines- processing, properties and uses.

Goodrich

Exploratory materials for interlayer dielectrics which have a low dielectric constant and have been developed for other uses.

Army Missile Command (MICOM):

The use and reliability of gold in DoD MCMs.

Machine Technology Inc.

Processing tools.

2. METALLIZATION.

The low dielectric constant insulators are being evaluated through the fabrication of in-situ test structures using gold as the metallization. In the course of doing this evaluation, a simple process for gold MCMs has been investigated. The unique adhesion layer (record of invention March 1991) is documented in Section 2.2. The process travelers for the Au-SiO₂ and Au-polymer are in Appendix 1 and 2 respectively. The process instructions are given in Appendix 3.

2.1 Process for Gold MCMs.

A cross sectional diagram of the structure is shown below in Figure 2.1.

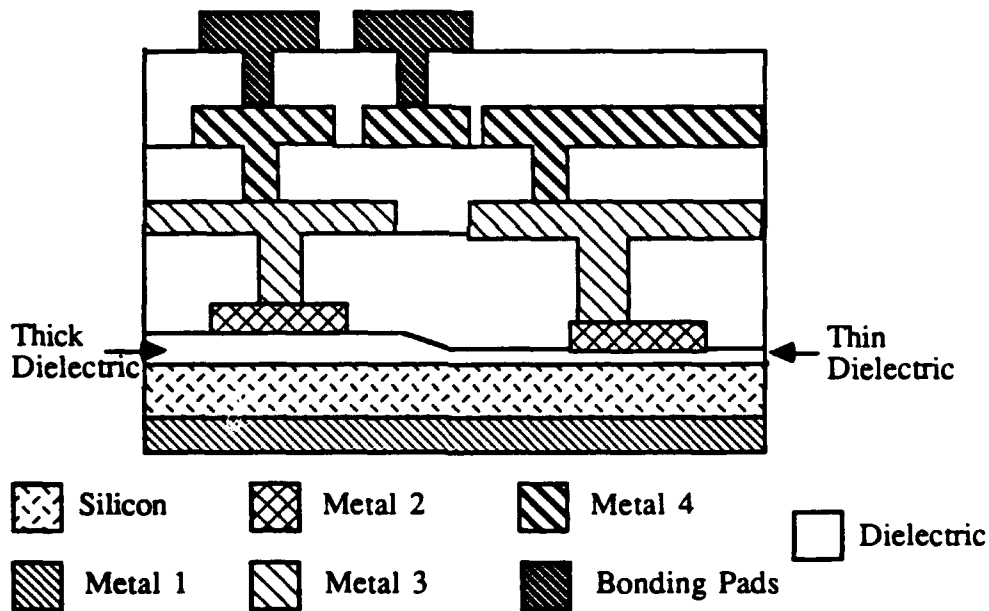


Figure 2.1. Cross-section of Typical MCM Structure (not drawn to scale)

Each metal layer was formed by sputtering a 1000Å seed layer of gold and appropriate adhesion layer, followed by photolithography defining the final gold pattern. The pattern was then electroplated to its final thickness using an additive free soft gold plating bath. The photoresist and seed layer of gold were then chemically stripped.

Most of the processes followed conventional semiconductor processing (i.e. photolithography, reactive ion etching, plasma enhanced chemical vapor deposition). However, a gold electroplating apparatus was needed for electroplating the gold patterns. A device for simultaneously electroplating three silicon wafer was designed and constructed. The metal thickness was measured in five places (#5 is the center of the wafer) and the thickness is shown in Figures 2.2 through 2.7.

The anodes were platinized titanium and an additive free, pH 7, gold bath was selected because of its purity (absence of additives which effect gold conductivity) and neutral pH. The neutral pH allows us to use any insulator without chemical attack. The plating cell was constructed from PVC. The wafer to wafer plating uniformity is shown in Figure 2.3-2.7. The inter-wafer uniformity is shown in Figure 2.2.

A critical issue in the processing of MCMs is the residual stress in the metallization when high temperature processes ($>200^{\circ}\text{C}$) are required for processing the dielectric material. The residual stress of the gold after successive temperature cycles was 142 MPa as shown in Figure 2.8. On the first heating cycle compressive stress is developed in the metal due to the CTE mismatch with the silicon substrate. At about 200°C , the metal recrystallizes, the grains grow, and the stress is relieved. Upon cooling, a high degree of residual stress (tensile) is developed again due to the CTE mismatch, which cannot be annealed out. Control of residual stress is the motivating force for us to investigate dielectric materials which can be processed at low temperatures ($<200^{\circ}\text{C}$).

2.2 Adhesion

The chemical bonding of insulators to noble metals, such as gold, is generally very difficult without the use of a bonding layer. The adhesive force is directly correlated to the free energy of formation of the metal oxide. Table 2.1 shows the free energy of formation of a variety of metal oxides.^(2.1)

Figure 2.2
Average Thickness vs Position

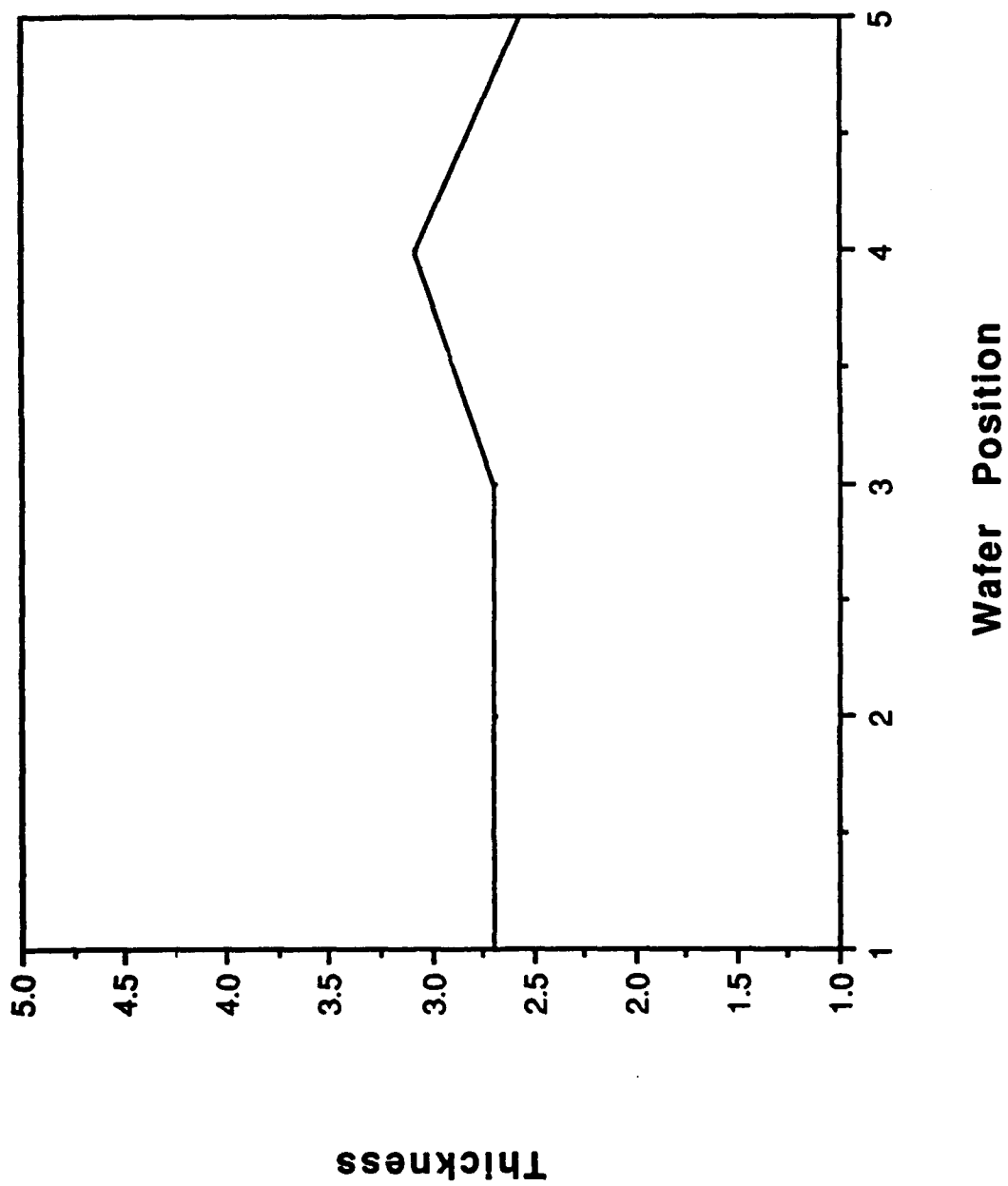


Figure 2.3
Position 1 vs Wafer #

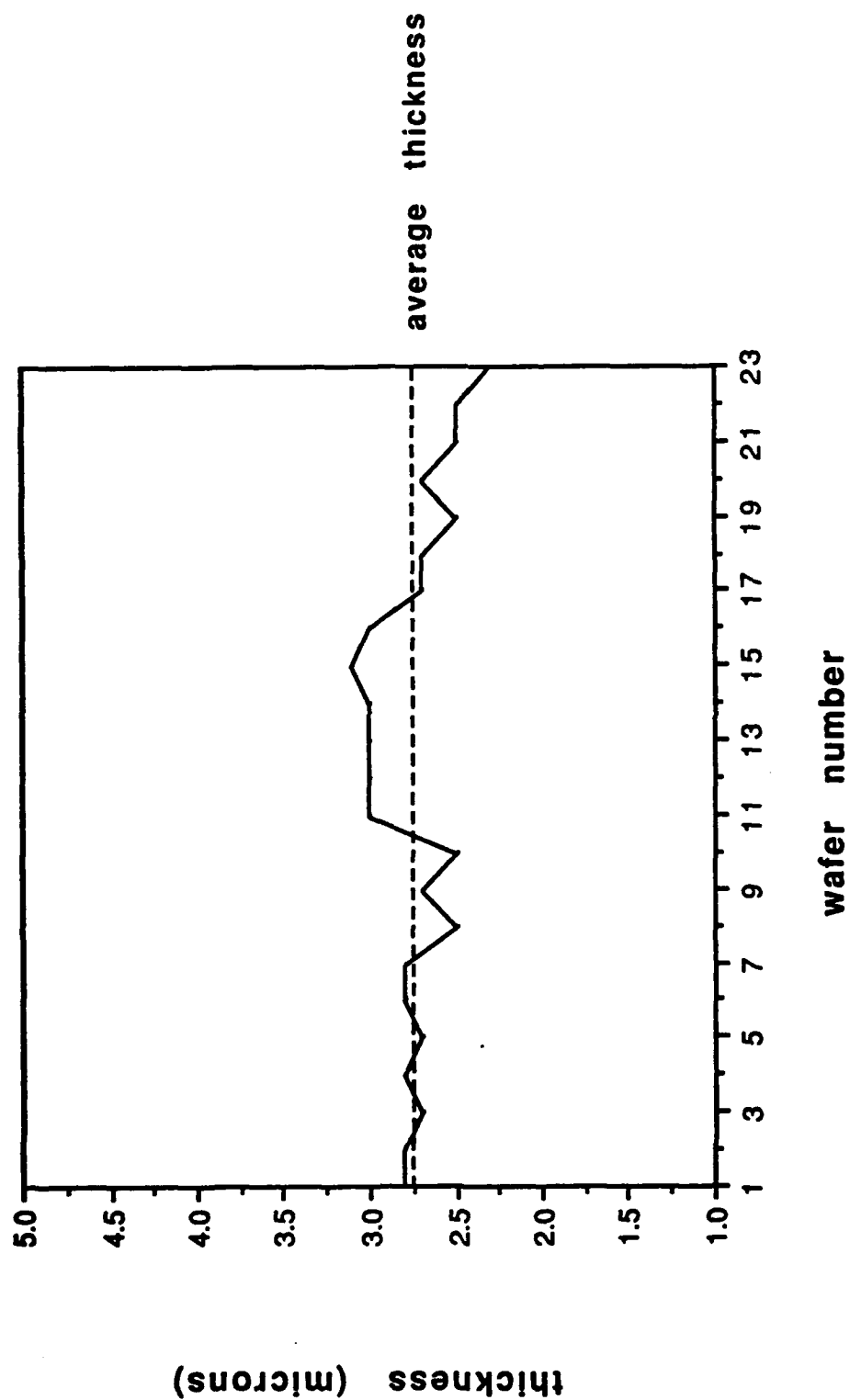


Figure 2.4
Position 2 vs Wafer #

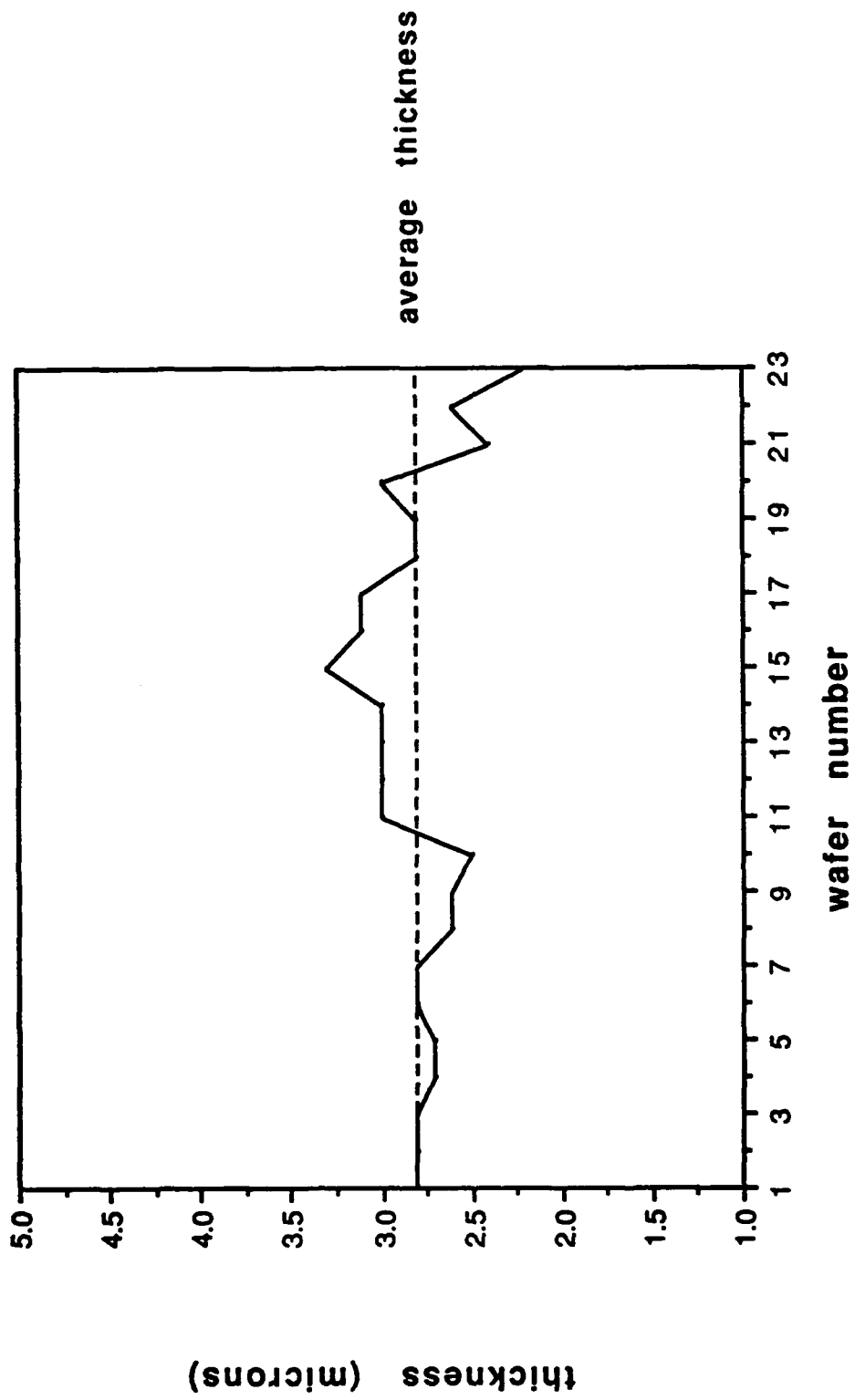


Figure 2.5
Position 3 vs Wafer #

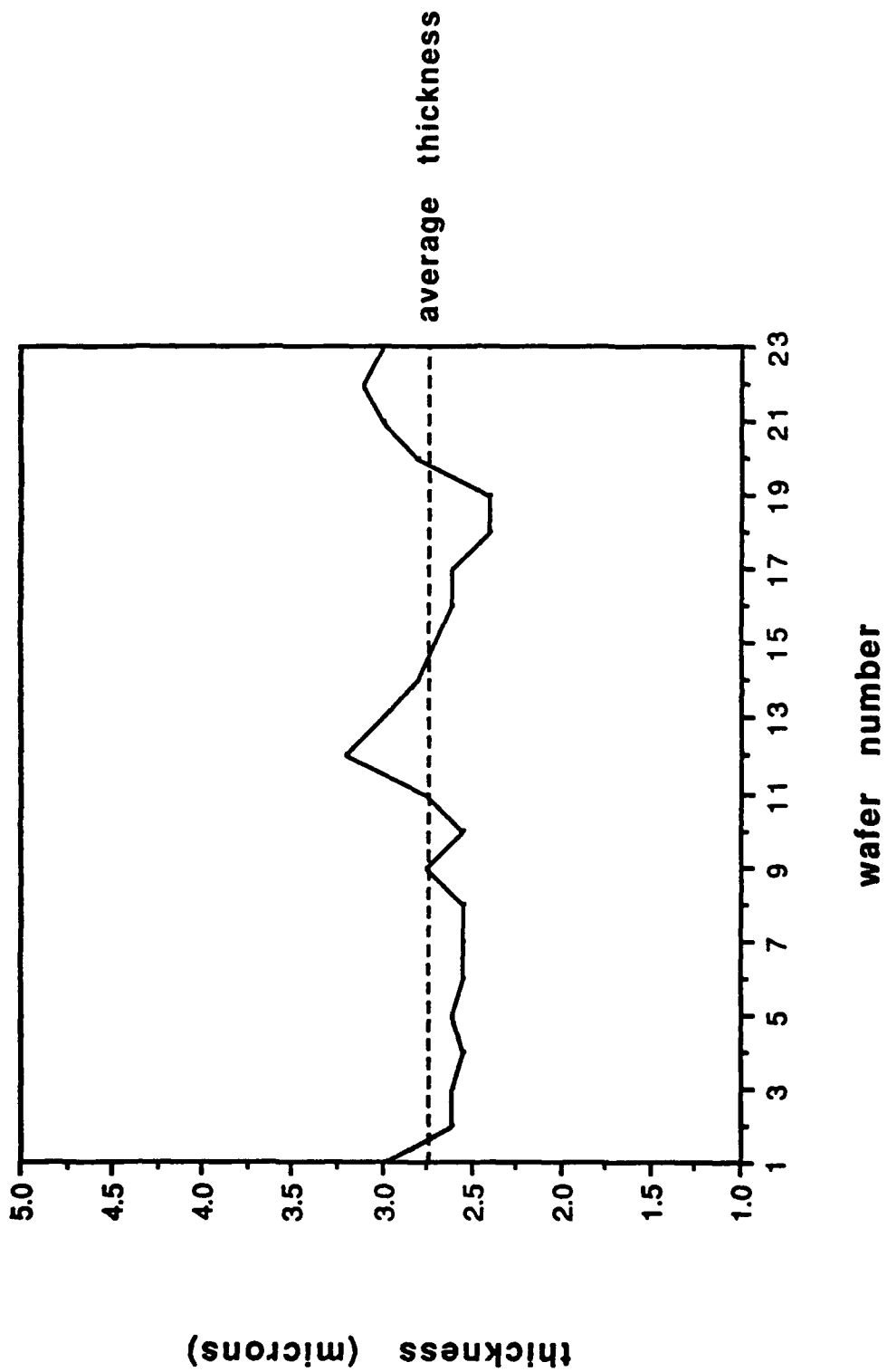


Figure 2.6
Position 4 vs wafer #

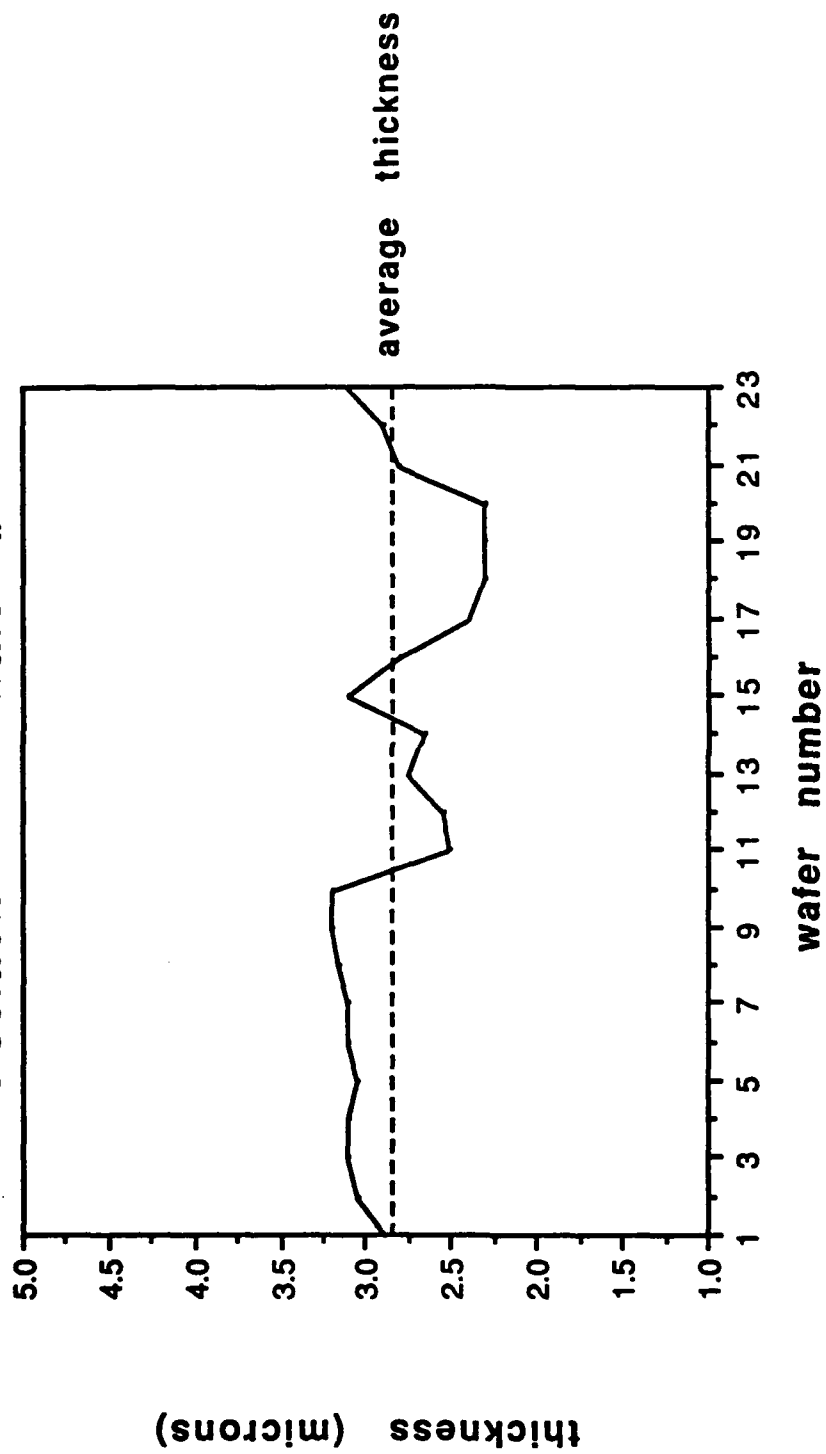


Figure 2.7
Position 5 vs Wafer #

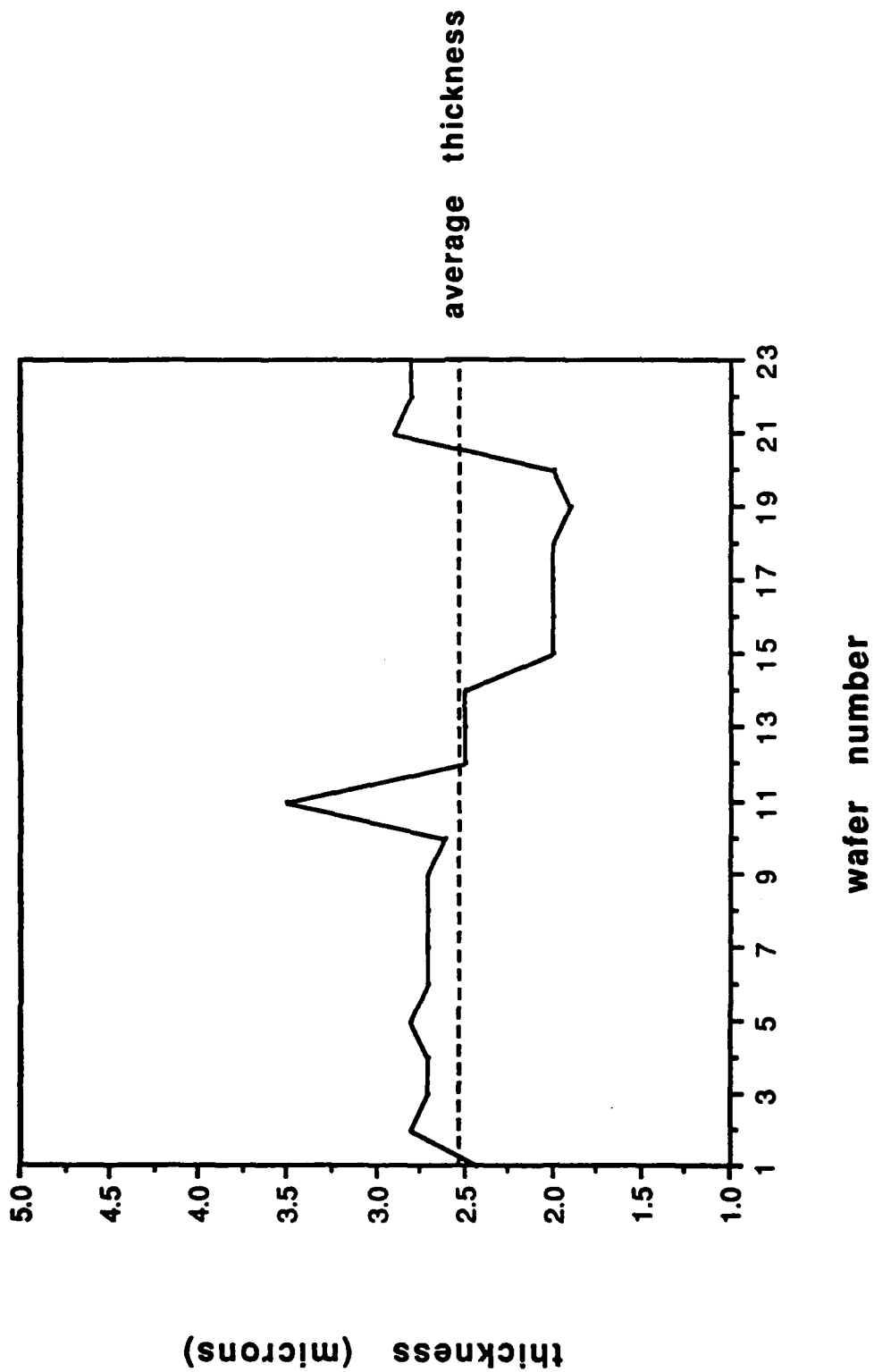


Figure 2.8

Gold Residual Stress vs. Temperature Reheat Temperature Cycle

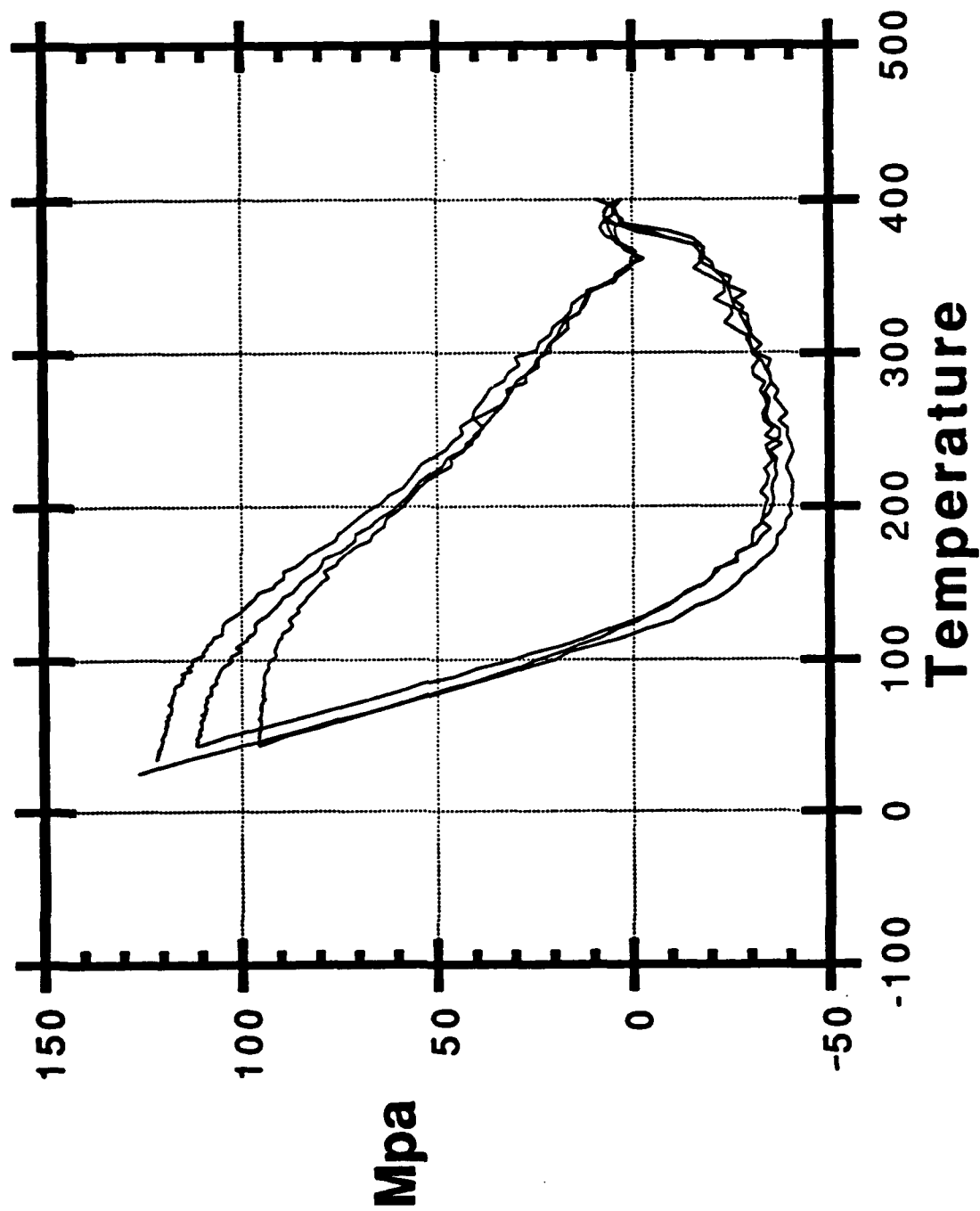


Table 2.1. Heat of Formation for a Selection of Metal Oxides

<u>Oxide</u>	<u>Heat of Formation (kcal/mol)</u>
Ta ₂ O ₅	-500
Al ₂ O ₃	-399
Cr ₂ O ₃	-270
WO ₃	-200
Cu ₂ O	-40
Au ₂ O ₃	19

Adhesion layers are required for gold, copper or silver metallization. Usually, these adhesion layers are thin films of metal(s) which easily form a stable oxide. The most effective adhesion promoting layers are transition metals (e.g. Cr and Ni). There are several problems with adhesion layers. The first problem is the interdiffusion of the adhesion layer into the gold (or copper) conductor and the resulting decrease in the electrical conductivity as the foreign atoms accumulate at grain boundaries.^(2,2) In many MCM structures, only 40-60% of the bulk conductivity of the metal (e.g. copper) is achieved. The second common problem is the processing dilemma of applying a metallic adhesion layer over the metal microstrips without having them electrically short together. The two common **unacceptable** solutions are to use an additional lithography step to pattern the adhesion metal (too costly) or to use an electroless deposition processes to encase the entire metal conductor in a material which has good adhesive properties. The electroless process is too low of a yield for this large scale step and also involves metals which interdiffuse into the copper (e.g. Ni), reducing the conductivity of the metal.

Therefore, the design criteria for an acceptable adhesion layer are (1) rapid, simple application of a thin film material, (2) no interdiffusion of the adhesion layer with the gold (or copper) causing a reduction in the metal conductivity, and (3) the adhesion material should be an electrical insulator and thermal conductor. By using gold metallization, there is no need to protect the metal from corrosion, as would be the case for copper. This is particularly important for polyimides or other relatively hygroscopic materials. Many polyimides contain 2-4% water.

2.2.1 Adhesion and Electrical Isolation Tests

Purpose:

An adhesion material comprised of thin islands of TiO_2 anchored to the conductor by titanium islands has been developed. The processing is simple, can be carried out with high yield, and uses conventional processing equipment. The goal of this portion is to examine the adhesion and insulation properties of the adhesion layer.

Approach and Results:

Adhesion:

A silicon wafer coated with a thin layer of sputtered gold (1000\AA) and photoresist was patterned and sputtered with a thin layer of titanium (10\AA) with no heat cycle during sputtering to prevent polymerization of the resist. The photoresist was then removed using acetone as the solvent, thereby exposing the covered areas of gold and obtaining on the wafer areas where no titanium is present for adhesion. The next step involved the deposition of a dielectric. In this experiment, two different dielectrics were used: silicon dioxide and polyimide. After deposition of the dielectric, the wafer was examined to observe the effects on the adhesion of the dielectric where no titanium was present.

The silicon dioxide wafer was found to have bubbled where no titanium was present. The height of these bubbles was measured using a surface profilometer and found to be approximately $800\text{\AA} \pm 100\text{\AA}$. Also noticeable was a cracking or shearing of the silicon dioxide in the areas where no titanium was present. Testing to see if the oxide could be removed in the areas with no titanium was done by placing the wafer in a beaker of water and subsequently in an ultrasonic bath. After 1 minute in the ultrasonic bath, the oxide showed no signs of lifting from the titanium-free areas.

The wafer coated with polyimide was also found to have bubbling in titanium-free areas. The bubbles on the wafer were found to have a height of 1100\AA within a range of $\pm 100\text{\AA}$ across the

wafer. The polyimide had cracking similar but not as pronounced as the oxide wafer.

Conductivity:

The conductivity of the titanium adhesion layers is important in ensuring that no short circuits exist between metal lines due to titanium adhesion layers not sufficiently oxidizing to prevent electrical connection. This experiment was designed to determine the conductivity of the thin layers of titanium deposited on a metal pattern. This was done by the following method:

1. 5 microns silicon dioxide deposited on blank silicon wafer
2. 75Å titanium/ 2000Å gold/ 75Å titanium sputtered sequentially onto wafer.
3. Metal 2 pattern (thin metal lines) patterned using photoresist.
4. 3 microns of gold plated on thin metal lines.
5. Photoresist removed using acetone, top layer of 75Å of titanium removed using EDTA etch solution, 2000Å seed layer of gold removed using iodine ($KI \& I_2$) etch solution, second 75Å layer of titanium removed using EDTA etch solution.
6. Varying layers of thickness (10Å, 50Å, 75Å) of titanium deposited on wafers - this is the adhesion layer of titanium.
7. Measurements taken across wafer to determine if conductivity exists between thin gold lines*. If conductivity exists then titanium is reason for short circuit between lines. (This measurement was taken by touching probe tips on individual metal lines spaced between 10Å and 50Å and measuring the electrical resistance between the lines. A short circuit existed if the resistance was less than 999 megaohms.)

8. If the wafer showed conductivity, the wafer was heated in a 90°C oven for 5 minutes and electrical measurements taken again. This procedure was repeated until no conductivity existed or 20 minutes in the oven had not reduced the conductivity of the titanium.

All three wafers were sputtered at the same time and left in a dry box for 17 hours before electrical measurement. The 10Å wafer was found to have no measurable resistance (>999 Mohm) between lines and therefore, the titanium layer was not conductive.

The second wafer to be measured was the 75Å sample. This sample was found to have 23 pairs of lines that showed measurable resistance and conductivity. After 20 minutes in the 90°C oven 16 of the pairs of lines no longer showed conductivity (>999 Mohm), but the seven remaining pairs showed no signs of becoming non-conductive. The 50Å sample had 10 pairs of lines that showed conductivity. After 20 minutes at 90°C, 3 pairs were still conductive and, after 30 minutes, no pairs showed conductivity.

Conclusions:

From these experiments, a critical thickness for the titanium adhesion layer can be determined. The desired thickness for the titanium adhesion layer should be between 10Å and 50Å. Less than 10Å has proved to not have good adhesion while greater than 50Å may yield a film of titanium that is conductive. The 50Å titanium layer was oxidizable after 30 minutes in the 90°C oven.

2.2.2 XPS Analysis of Adhesion Layer

Purpose:

These experiments were intended to examine the growth mechanism of titanium on gold and silicon dioxide surfaces for the purpose of understanding the method of adhesion without electrical conduction.

Approach:

The islands appear to meet the above mentioned adhesion criteria for gold and copper. X-ray Photoelectron Spectroscopy has been used to examine the nature of the adhesion layer.

Results:

The layer is an electrical insulator. The conductivity between two parallel metal lines, 2 cm long and 20 mm apart, was greater than 10^9 ohms. This test has been repeated many times over a period of about three months. Adhesion has been tested by performing three types of tests: scratch and tape pull, immersion in boiling water for one to four hours, and liquid to liquid thermal shock from 77K to 373K. Up to 100 thermal shock cycles have been performed. These tests do not exactly follow the military specifications because of time, equipment and sample size limitations. Rather, they were used simply as a process development tool. We have explored the process robustness of the adhesion layer. All adhesion and resistivity tests were passed for samples ranging from a one-half treatment (undertreated sample) to a five times overtreatment. A 30% treatment (undertreatment) failed the adhesion test.

The electrical conductivity of the gold does not appear to be affected by the adhesion layer and subsequent processing. The sheet conductivity of the gold was measured after plating. The samples were then processed and heat treated. The electrical conductivity remained about the same, within 8%, after all treatments. This fluctuation will be investigated with a larger sample set.

The structure, spatial distribution and chemical composition of the adhesion layer were analyzed by x-ray photoelectron spectroscopy (XPS). The purpose of this work is to quantify the composition and morphology of thin titanium (Ti) films. The sputtered films studied were 3 Å and a 10 Å titanium on a gold (Au) substrate. A 75 Å titanium film and a 250 Å gold film were used as pure solid standards. The films were produced with a CVC Products, Inc. DC sputtering system at a pressure of 1×10^{-5} Torr and a temperature of 50°C. The films were exposed to air at room temperature for 1 month.

The composition was studied with a X-ray Photoelectron Spectroscopy (XPS) sputter profile. XPS is a surface-sensitive technique which can obtain elemental composition information in the outermost monolayers.^(2,3) A Surface Science Laboratories SSX-100 X-Ray Photoelectron Spectrometer with aluminum Ka (1486.6 eV) x-rays was used to obtain the XPS spectra. The gold 4f_{7/2} and titanium 2p spectra were used to analyze the film. The oxidation states of Ti have been investigated^(2,4-2.6) with the Ti 2p spectra allowing easy differentiation between Ti and titanium dioxide (TiO₂). For the sputter profile, argon ion bombardment at an energy of 4 keV and a pressure of 3.7×10^{-7} Torr was used to physically remove atoms from the surface. By alternating bombardment and XPS analysis, compositional information as a function of depth is obtained. Sputter profiles are constructed by plotting the intensity verses sputter time. The intensity is measured using a gaussian fitting routine supplied by Surface Science Laboratories. The sensitivity difference for gold and titanium was corrected by measuring the XPS spectra of sputter-cleaned pure standards and forming a ratio of the pure standard intensities. Finally the sensitivity difference can be eliminated by dividing the gold intensity signal by the Au/Ti ratio.

The morphology was studied using angle-resolved XPS and scanning tunneling microscopy (STM). This report will only discuss the angle-resolved XPS results. The procedure for angle-resolved XPS is to measure the XPS signal (I_A) at various electron take-off angles (q), as illustrated in Figure 2.9.

As shown by Seah^(2.7), the XPS signal is a function of electron take-off angle (q), inelastic mean free path for an electron (l), atomic concentration, photo-electron cross-section, spectrometer detection efficiency, intensity angular asymmetry, characteristic x-ray line flux, and analyzer transmission function. Computations are greatly simplified, however, when reference spectra of pure element standards, I_A^∞ , are recorded on the same instrument. When the material analyzed can be considered homogeneous, the XPS intensity signal, I_A , can be simplified to a function of I_A^∞ , l , q , and atomic concentration.^(2.6)

Similar to the overlayer model of Seah^(2.7), a model can be developed to determine if an overlayer film (A) has island-like or

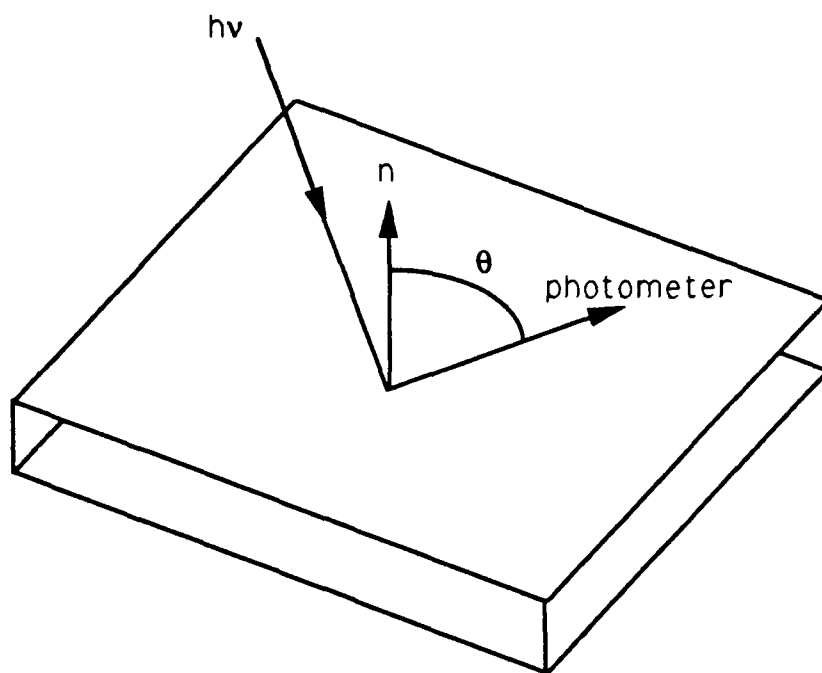


Figure 2.9: Illustration of sample orientation, $h\nu$ = inlet x-ray beam

n = normal to sample, θ = electron take-off angle, and
photometer = entrance to XPS photometer

layer-like properties. First, for layer-like films, the signal for the overlayer is given by:

$$I_A = I_A^\infty [1 - \exp(-d_A / \lambda_A \cos \theta)] \quad (2.1)$$

where d_A is the overlayer film thickness. The signal for the substrate (B) is attenuated by the overlayer:

$$I_B = I_B^\infty \exp[-d_A / \lambda_A \cos \theta] \quad (2.2)$$

For island-like overlayer films, the islands can be approximated as cubes. The height of the cube (h_A) can be calculated by d_A / j_A , where j_A is the fractional coverage. In this case, the signal from the overlayer (A) is:

$$I_A = \phi_A I_A^\infty (1 - \exp[-h_A / \lambda_A \cos \theta]) \quad (2.3)$$

The signal from the substrate (B) is found from the sum of the unattenuated emission from the surface ($1 - j_A$) and the attenuated emission:

$$I_B = I_B^\infty \{(1 - \phi_A) + \phi_A \exp[-h_A / \lambda_A \cos \theta]\} \quad (2.4)$$

Tabulated relative sensitivity factors could be used for I_A^∞ and I_B^∞ , but accuracy can be improved when experimental values of I_A^∞ / I_B^∞ are used. For the layer-like model, equations (1) and (2) can be re-organized as:

$$\frac{I_A / I_A^\infty}{I_B / I_B^\infty} = \frac{1 - \exp[-d_A / \lambda_A \cos \theta]}{\exp[-d_A / \lambda_A \cos \theta]} \quad (2.5)$$

Likewise, the island-like model, equations (2.3) and (2.4), can be re-organized to give:

$$\frac{I_A / I_A^\infty}{I_B / I_B^\infty} = \frac{\phi_A (1 - \exp[-h_A / \lambda_A \cos \theta])}{(1 - \phi_A) + \phi_A \exp[-h_A / \lambda_A \cos \theta]} \quad (2.6)$$

Notice, when $j_A = 1$, the island-like model equals the layer-like model.

The ratios $I_A/I_A^\infty/I_B/I_B^\infty$ can be measured experimentally as a function of q . The inelastic mean free path, l , can be calculated using the method of Penn⁽⁸⁾. This shows l equal to approximately 22 Å for TiO₂/Ti system at an energy of 1486.6 eV. Values for d_A and h_A are found from the sputtering deposition rate, which was calibrated by measuring the time to deposit a 3000 Å film. Some adjustments may be necessary for stoichiometry and density changes after oxidation. An estimate for d_A can also be found using the models to fit the data at low angles of q . As seen in equations (2.5) and (2.6), both models are sensitive to film thickness changes, especially at low angles of q . Lastly, for the island-like model, the fractional coverage, j_A , can be calculated by iterating to fit the experimental data at high angles of q . As shown in equation (2.6), j_A determines the island-like model's behavior when q approaches 90°.

To determine if the film has layer-like or island-like morphology, the experimental data ($I_A/I_A^\infty/I_B/I_B^\infty$) is plotted as a function of q . The theoretical models are also plotted as a function of q . At large take-off angles ($q \rightarrow 90^\circ$), the layer-like model ratio will approach infinity. Meanwhile, the island-like model becomes asymptotic. The experimental data and its behavior at large q is compared to the model predictions. Asymptotic behavior indicates island-like morphology while infinite behavior indicates layer-like morphology.

Composition:

The XPS sputter profiles are shown in Figures 2.10 through 2.12. The sensitivity sensitivity correction for Au/Ti was 8.4. The XPS intensity for gold was divided by 8.4 making direct comparison of Au and Ti intensities possible. The areas of each curve were numerically integrated to find the concentration ratio for titanium and titanium dioxide. The 3 Å film was completely oxidized as TiO₂. The 10 Å film was 53% TiO₂ and 47% Ti. The 75 Å film was 8% TiO₂ and 92% Ti. Interestingly, the amount of oxide present for the 10 Å and the 75 Å films is approximately the same (5-6 Å of Ti). Information about the film thicknesses can also be obtained from the sputter profiles. Using a silicon dioxide (SiO₂) film on a silicon substrate, the sputter rate was calibrated as 13 Å/minute (SiO₂). The film thicknesses were then calculated from Figures 2.10-2.12 and are shown in Table 2.2. Film thicknesses could also be calculated assuming a change in density and thickness upon

Figure 2.10: XPS profile of 3A Ti film.

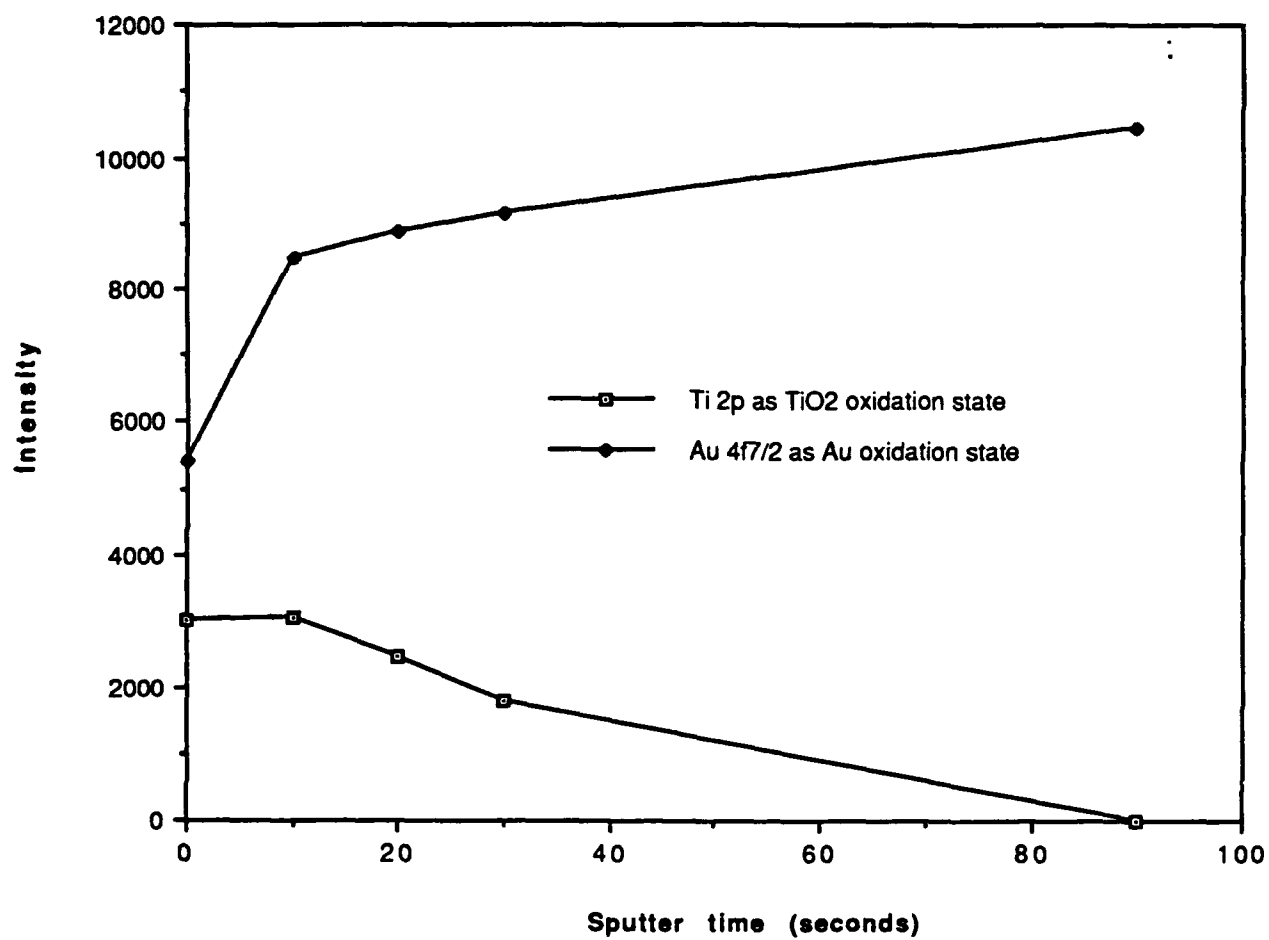


Figure 2.11: XPS sputter Profile of 10A Ti film

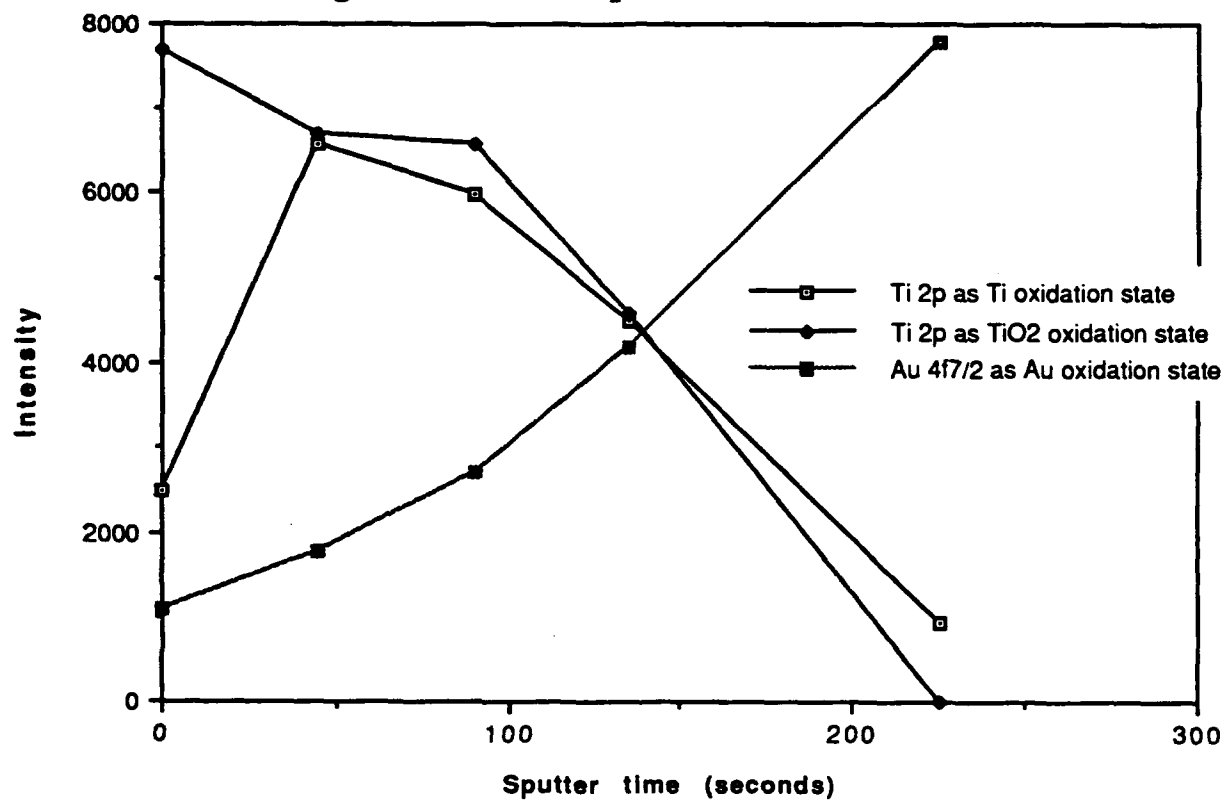
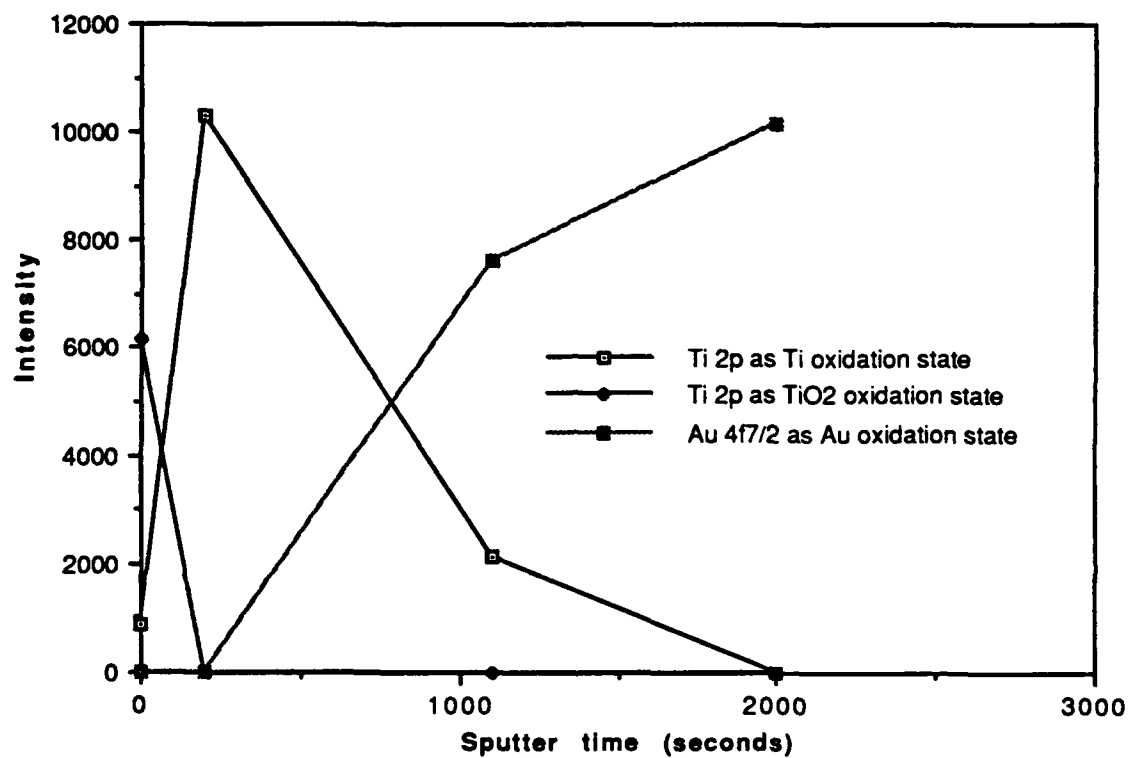


Figure 2.12: XPS profile of 75A film



oxidation. If we assume that the amorphous surface oxide has the density of anatase TiO_2 (3.84 g/cc), a 3 Å Ti (4.5 g/cc) film would have a thickness of 6 Å. Likewise the thicknesses for the 10 Å and 75 Å Ti films are calculated (see Table 2.2), accounting for the Ti/ TiO_2 concentration ratio in the calculations.

Table 2.2

<u>Film</u>	<u>Film Thickness (seconds sputtered)</u>	<u>Film Thickness (Å SiO_2)</u>	<u>Theoretical Thickness (Å)</u>	<u>Fitted Thickness Using Models (Å)</u>
3 Å Ti	30	7	6	6
10 Å Ti	130	28	15	36
75 Å Ti	700	152	81	

These values can be considered consistent within the error of the experiments. Uncertainty enters when attempting to identify the film/substrate interface from the XPS sputter profile. Also, the sputter rate can vary greatly between compounds.^(2,12) Some error also exists in the calibration of the sputter deposition rate. The sputtering rate is calibrated after long deposition times of thick films (3000 Å). This rate is used for the deposition of the 3, 10, and 75 Å films. For these thin films, it is possible for the deposition amount to vary with position in sputtering machine.

Morphology:

Angle-resolved XPS data was obtained for the 3 Å and the 10 Å Ti films and is shown in Figures 2.13 and 2.14. The method could not be used for the 75 Å film because the gold substrate could not be detected through the film. (The 75 Å Ti film was used as I_A^∞ in the calculations). The data for both the 3 Å and the 10 Å films clearly resemble the island-like model by behaving asymptotically at high angles of q . Iteration for the film thickness and fractional coverage proceeded until a good fit was obtained graphically. For the 3 Å film, the thickness was 6 ± 1 Å, and the fractional coverage was 0.5

Figure 2.13: Island/layer model for 3 Å film.
The models used $d=6$ Å, and the island model used a fractional coverage of 0.5 to fit the data.

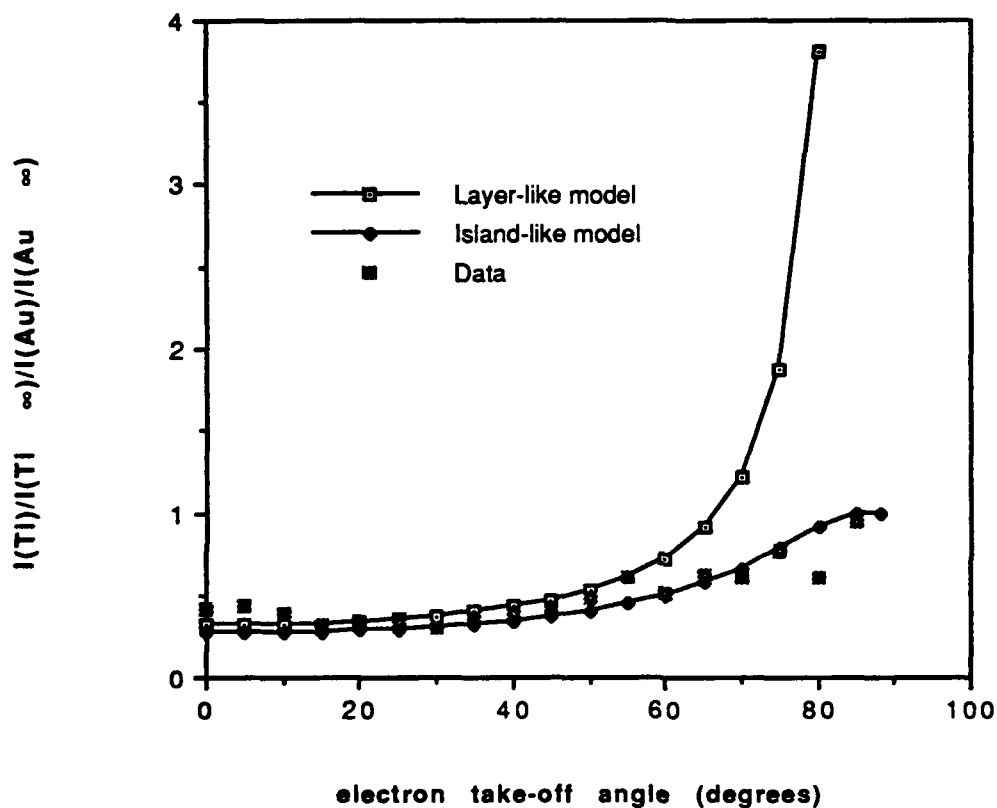
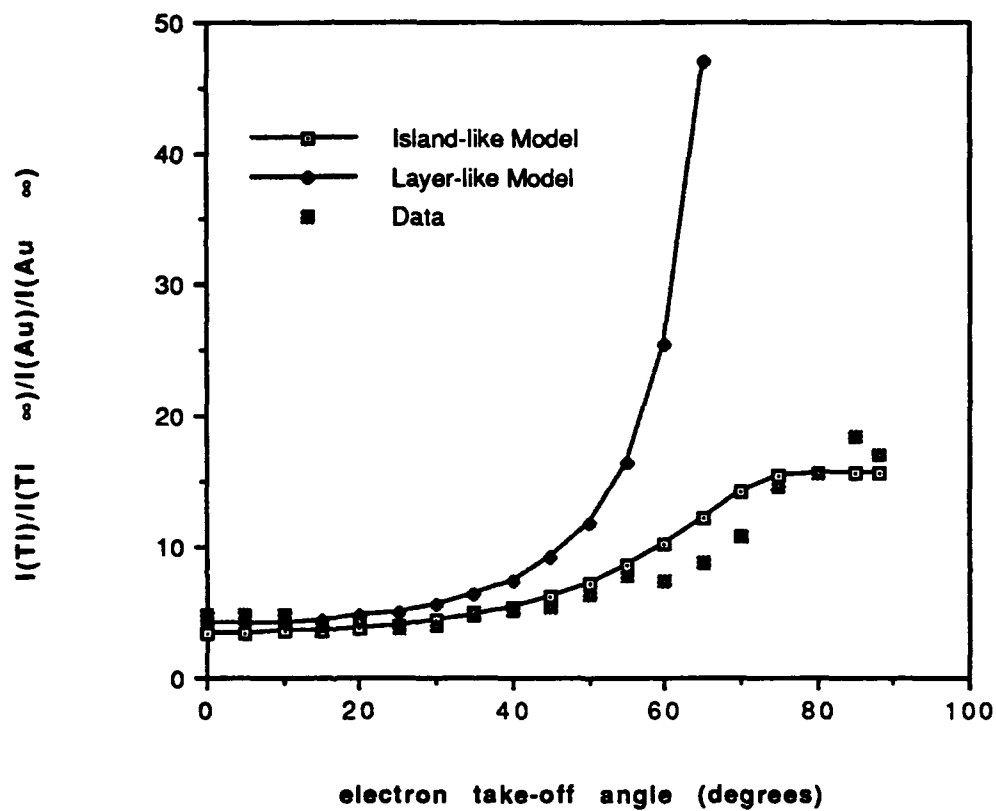


Figure 2.14: Island/layer model for 10 Å film.
The models used $d=36$ Å, and the island model used a fractional coverage of 0.94 to fit the data.



± 0.1 . For the 10 Å film, the thickness was 36 ± 6 Å, and the fractional coverage was 0.94 ± 0.01 .

Conclusion:

The composition and morphology of sputtered titanium films on gold substrates were investigated using XPS. Using a XPS sputter profile, the compositions of a 3 Å, 10 Å, and 75 Å film were 100% TiO₂, 53%/47% TiO₂/Ti, and 8%/92% TiO₂/Ti, respectively. The morphology for the 3 Å and 10 Å films was investigated using angle-resolved XPS. Both were island-like with fractional coverages of 0.5 and 0.94, respectively.

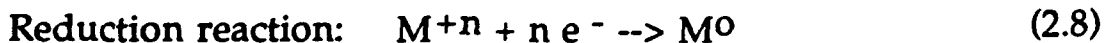
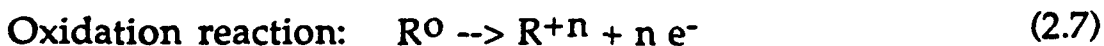
2.3 Electroless Deposition of Gold

Purpose:

The most common approach to filling level-to-level via connections in MCMs is through the use of electroless gold plating, as shown in Fig. 2.1. This study concentrates on finding an electroless method of depositing thin gold films onto gold surfaces under conditions compatible to the dielectric materials. Gold films can be electrodeposited with high purity and good electrical conductivity in addition to having high corrosion resistance; however, the only available baths are pH > 13 and > 70°C. At these conditions, all insulators of interest are oxidized. Thus, it is our goal to find suitable baths for electroless gold deposition (i.e. pH < 10 and/or < 70°C).

Approach:

Specifically, this electroless method consists of a chemical reduction of gold coupled with a chemical oxidation reaction. Here, the flow of electricity in a traditional electroplating procedure is replaced with the transfer of electrons between the oxidation reaction to the reduction reaction. In general, these reactions are:



where R^0 is the reducing agent, R^{+n} is the oxidized species, M^{+n} is the metal complex and M^0 is the metal. A necessary condition for the electrodeposition to occur is that the equilibrium potential of the reducing agent is more positive than the corresponding equilibrium potential of the metal deposition. For the filling of via holes with gold, the reduction of gold needs to occur on the gold surface only (i.e. not on other surfaces) in order to prevent gold being formed homogeneously throughout the solution. In addition, the deposition of gold needs to continue after the first layer of gold. Therefore, the electroless plating of gold must proceed as a heterogeneously catalyzed reaction, catalyzed by both the surface gold and the deposited gold.

In order for the electroless bath to autocatalytically deposit gold, a reducing agent that will reduce Au^+ to Au is necessary. In examining the feasibility of using a particular reducing agent for electroless gold deposition, the kinetics of the oxidation are investigated using potential vs. current polarization curves of the electrochemical oxidation. In addition, a measure of the driving force of the overall redox reaction and the rate of deposition can be found using the polarization curves.

Thus, current versus potential polarization curves are first obtained for the oxidation of a possible reducing agent. The mixed potential, E_{mp} , is found where the oxidation and reduction current densities are equal. The value of this current density, i_{pl} , will approximate the plating rate. Plus, the driving force for the gold deposition reaction is indicated by the potential difference between the gold reduction and the oxidation. To confirm how successful a reducing agent may be, an electroless bath can be prepared and tested for its actual deposition rate.

Given the success of Okinaka's^(2,12) electroless bath consisting of $KAu(CN)_2$ and KBH_4 , this investigation begins with the study of the oxidation of KBH_4 under the conditions necessary for depositing gold onto gold/polymer multilayer interconnects. In addition, other possible reducing agents are considered including hydroxylamine sulfate and hydroxylamine hydrochloride. The polarization curves for the oxidation of these reducing agents are obtained using a Pine Instrument AFASR Rotator and either a gold disk or platinum ring working electrode with rotating capabilities, a saturated calomel reference electrode and a platinum counter

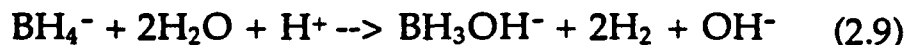
electrode. The current - potential data is obtained using a EG&G PARC Model 366 Bi-potentiostat, EG&G PARC Model 175 Universal Programmer, Nicolet 4500 Oscilloscope and/or a HP7090A X-Y recorder. The electrolytic cell is a 250 mL jacketed beaker with a VWR 1165 Refrigerated Constant Temperature Circulator to maintain a constant temperature.

In testing an electroless bath for its gold deposition rate, a gold covered glass slide is partly masked with black wax and the entire slide is cleaned using deionized water and KCN. The electroless bath solution is prepared and placed in the 250 mL water-jacketed beaker and kept at a constant temperature with the circulating bath. The slide is then placed in the bath for a specific period of time, generally over 45 minutes. Next, the black wax is removed using acetone. The height of the deposited gold is measured with a Dektak surface profilometer.

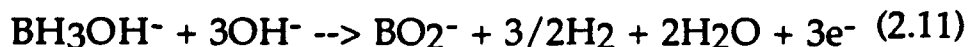
Results:

As mentioned, a useful technique of studying oxidation kinetics of an electrochemical reaction is to measure the potential versus current polarization curves using linear sweep voltammetry. Since potassium borohydride has been found successful at reducing gold in an electroless bath by Okinaka^(2,12), the oxidation of borohydride under different conditions is being investigated using polarization curves. The kinetics of the borohydride oxidation can be investigated as a function of concentration of KBH_4 , surface material of the electrode, mass transfer limitations, pH, and temperature of the solution.

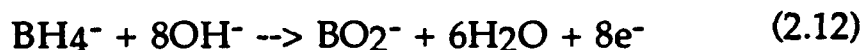
In solution, BH_4^- hydrolyzes as follows:



As the pH increases, the equilibrium is shifted to the right. According to Okinaka^(2,12), it is the hydrolysis intermediate, BH_3OH^- , that is responsible for electroless deposition of gold. At a high pH, the oxidation of BH_3OH^- is very small compared to the oxidation of BH_4^- and proceeds as:



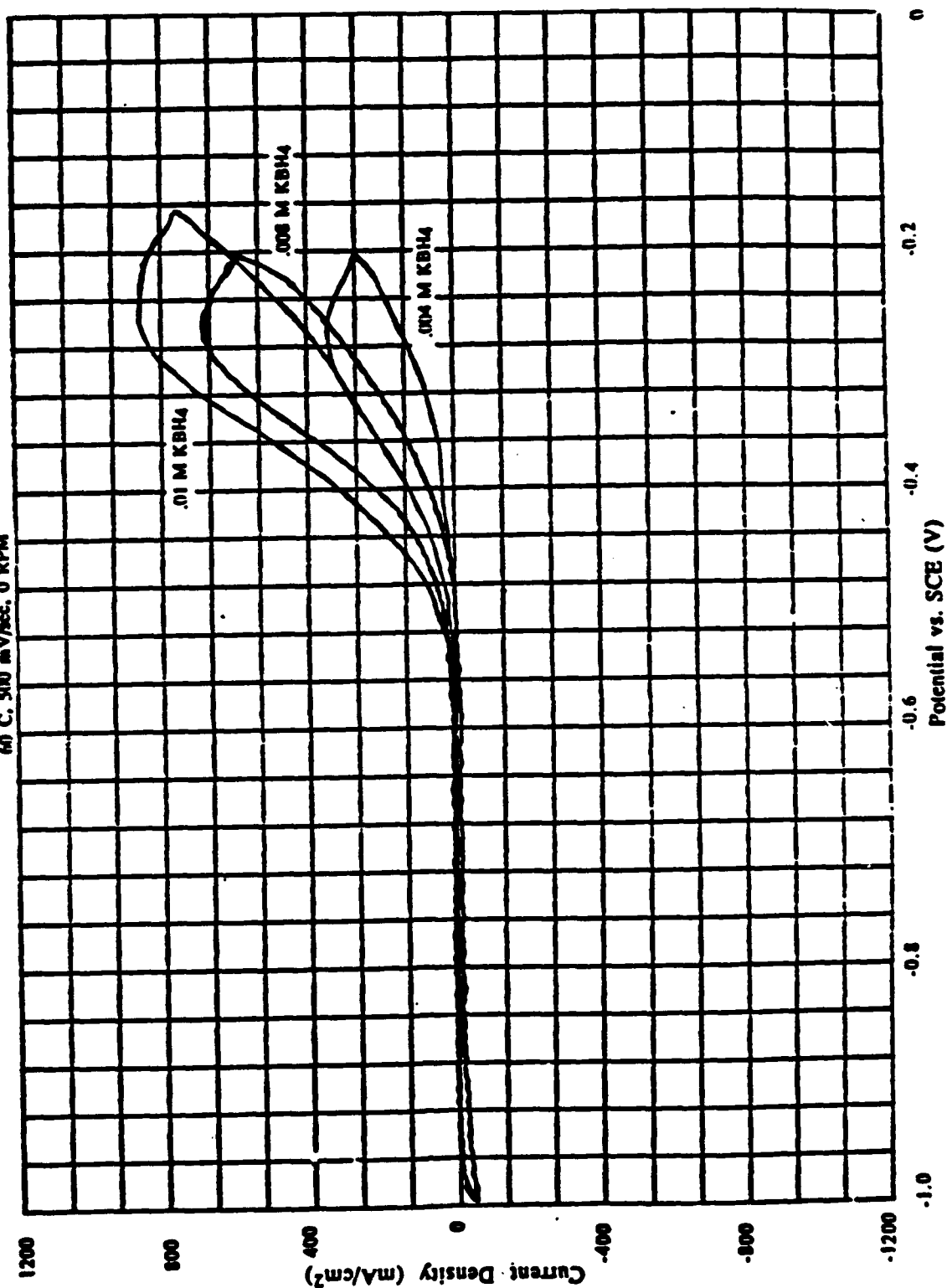
Whereas, the oxidation of BH_4^- dominates at high pH, eq. 2.12, and occurs at a more positive potential :



The oxidation of KBH_4 on a gold surface and at high pH appears as a single anodic peak in the current density as the potential is scanned in the positive direction. Figure 2.15 shows how this peak current density varies with increasing concentration of KBH_4 . This oxidation of KBH_4 at high pH is performed at 60°C in a stationary solution at a gold electrode. When the concentration of KBH_4 is increased, the peak current density increases proportionally. Increasing the temperature of the solution will increase the kinetics of the oxidation. In Figure 2.16, this temperature effect is evident with the larger peak current density at the highest temperature. Here .004 M KBH_4 is oxidized at a stationary gold electrode in a high pH buffer solution. If the concentration and temperature are constant, the oxidation of KBH_4 at a high pH on a gold electrode can still be altered by decreasing the mass transfer of the system. By rotating the electrode, the mass transfer rate increases and more KBH_4 reaches the electrode for oxidation. As a result, the polarization curve of the oxidation of borohydride shows a higher anodic peak. Figure 2.17 compares the oxidation of .004 M KBH_4 at high pH, 60°C , at a gold electrode that is stationary to the oxidation at a rotating electrode. When the electrode is rotating, the anodic current levels out at the limiting current rather than peak at the peak current. Another significant observation of the oxidation of KBH_4 is seen in Figure 2.18. This shows the effect of the electrode material on the oxidation kinetics. At the platinum electrode, .004 M KBH_4 is oxidized at a more negative potential than if it is oxidized on a gold electrode. In other words, KBH_4 is more easily oxidized on a platinum surface than a gold surface. To examine the effect of pH on the oxidation of borohydride, the following experiments are performed at 25°C on a gold stationary electrode with surface area of .196 cm^2 , approximately 20 to 30 minutes after adding borohydride to the solution. Figure 2.10 shows the polarization curve of the oxidation of 0.01 M KBH_4 at $\text{pH} = 12.9$. The large anodic peak represents the oxidation of BH_4^- . The oxidation of BH_3OH^- is indistinguishable next the oxidation of BH_4^- . In a pH

Figure 2.15

OXIDATION OF KBH₄
 in .2 M NaOH, on Au Electrode
 60 C, 500 mV/sec, 0 RPM



OXIDATION OF .004 M KBH_4
in 2 M NaOH, on Au Electrode
500 mV/sec, 0 RPM

Figure 2.16

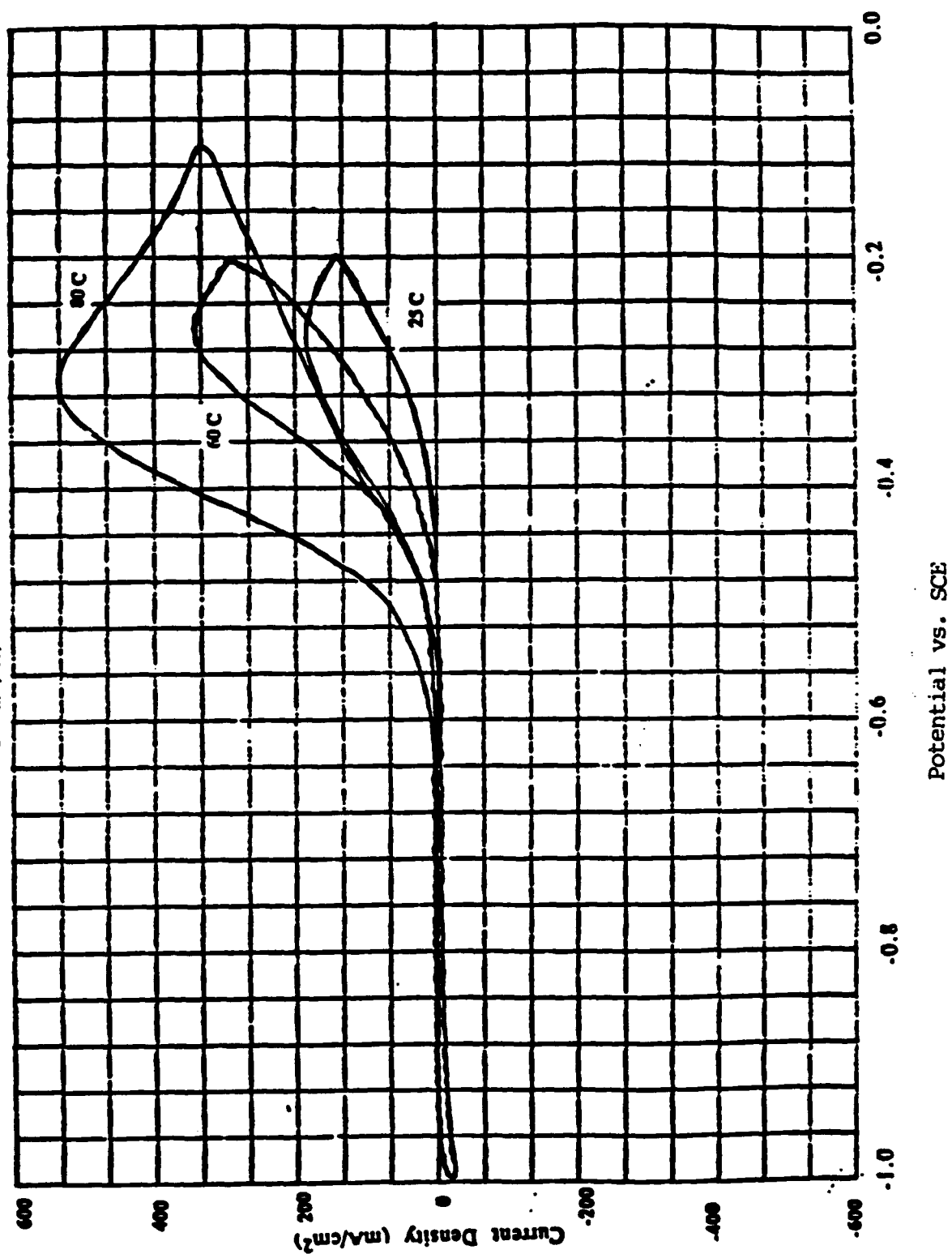


Figure 2.17

OXIDATION OF .004 M KBH₄
 in .2 M NaOH, on Au Electrode,
 60 C, 500 mV/sec

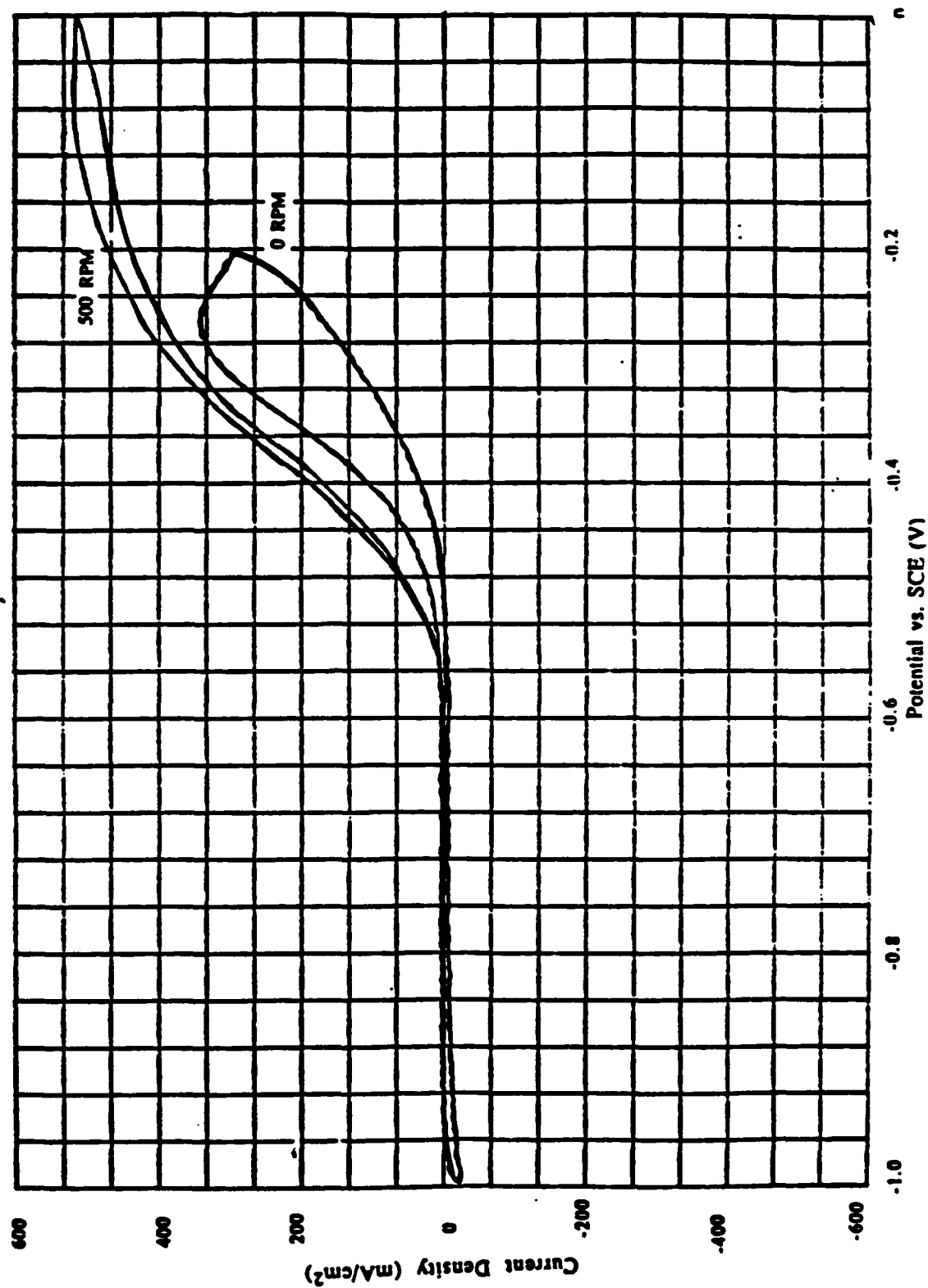
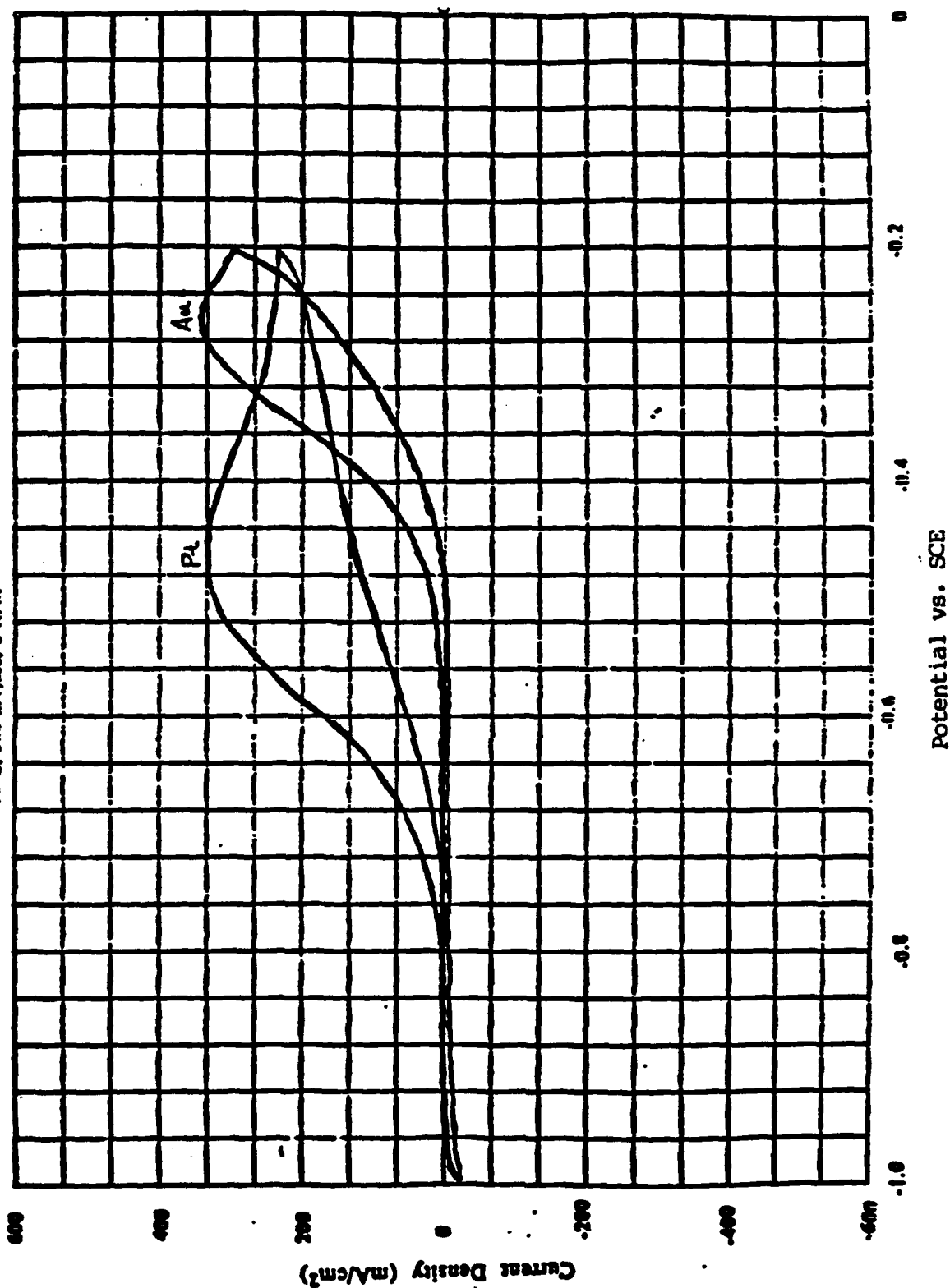


Figure 2.18

OXIDATION OF .004 M KBH₄

in .2 M NaOH

60 C, 500 mV/sec, 0 RPM



11.0 buffer solution, the oxidation of BH_3OH^- is seen in Figure 2.19 is still negligible. In addition, Figure 2.20 shows the oxidation of .01 M KBH_4 occurring over a larger potential range with the peak current being slightly less than at the higher pH. When the oxidation of borohydride is performed in pH 9.1, two distinct oxidation peaks appear. With the same borohydride concentration, Figure 2.21 shows the oxidation of BH_3OH^- occurring 0.2V more negative than the oxidation of BH_4^- . The peak current of BH_4^- is significantly less at this lower pH. Whereas, the oxidation of BH_3OH^- is now identifiable. However, lowering the pH to 7.8 catalyzes the hydrolysis of borohydride. At this pH, the only boron species present in solution after about 20 minutes is BO_2^- . Figure 2.22 shows the small anodic wave. From figures 2.19-2.22, it is apparent that as the pH is lowered, there is a positive shift in the potential corresponding to the peak current. In addition, the lowest pH at which BH_3OH^- ions are present in the solution is pH 9. Figure 2.23 shows the oxidation of BH_3OH^- after one hour.

In searching for a reducing agent that will reduce gold at a lower pH, hydroxylamine sulfate and hydroxylamine hydrochloride were investigated. The oxidation of hydroxylamine compounds are less understood because of its complex mechanism. According to Rao and Meites^(2,13), the principal oxidation products are nitrous oxide, nitrogen and nitrite with occasional traces of oxygen and nitrate. It is known that hydroxylamine will oxidize in the same general potential range necessary to reduce gold. At pH=3, 0.07 M hydroxylamine sulfate will have a zero current potential of 0.1 V vs. SCE at 70°C. Figure 2.24 shows the oxidation of hydroxylamine sulfate on a gold stationary electrode with a 100 mV/sec potential sweep rate. This figure shows only the beginning of the hydroxylamine oxidation. At pH 4, the .07 M hydroxylamine sulfate solution will have a zero current potential around 0 V vs. SCE at 80°C, seen in Figure 2.25. Comparing Figures 2.24 and 2.25, the effect of an increase in pH is seen in the negative potential shift. By increasing the concentration of hydroxylamine sulfate to .25 M, Figure 2.26, the current density is seen to increase significantly as compared to Figure 2.25.

When hydroxylamine hydrochloride is oxidized, there is very similar behavior to hydroxylamine sulfate. Figure 2.27 shows the oxidation of .1 M hydroxylamine hydrochloride at pH 3, 80 C on a gold stationary electrode with a scan rate of 100 mV/sec. Figure

Figure 2.19

**.01 M KBH₄ at GOLD ELECTRODE
BUFFER pH = 12.89, 25 C, 100 mV/sec**

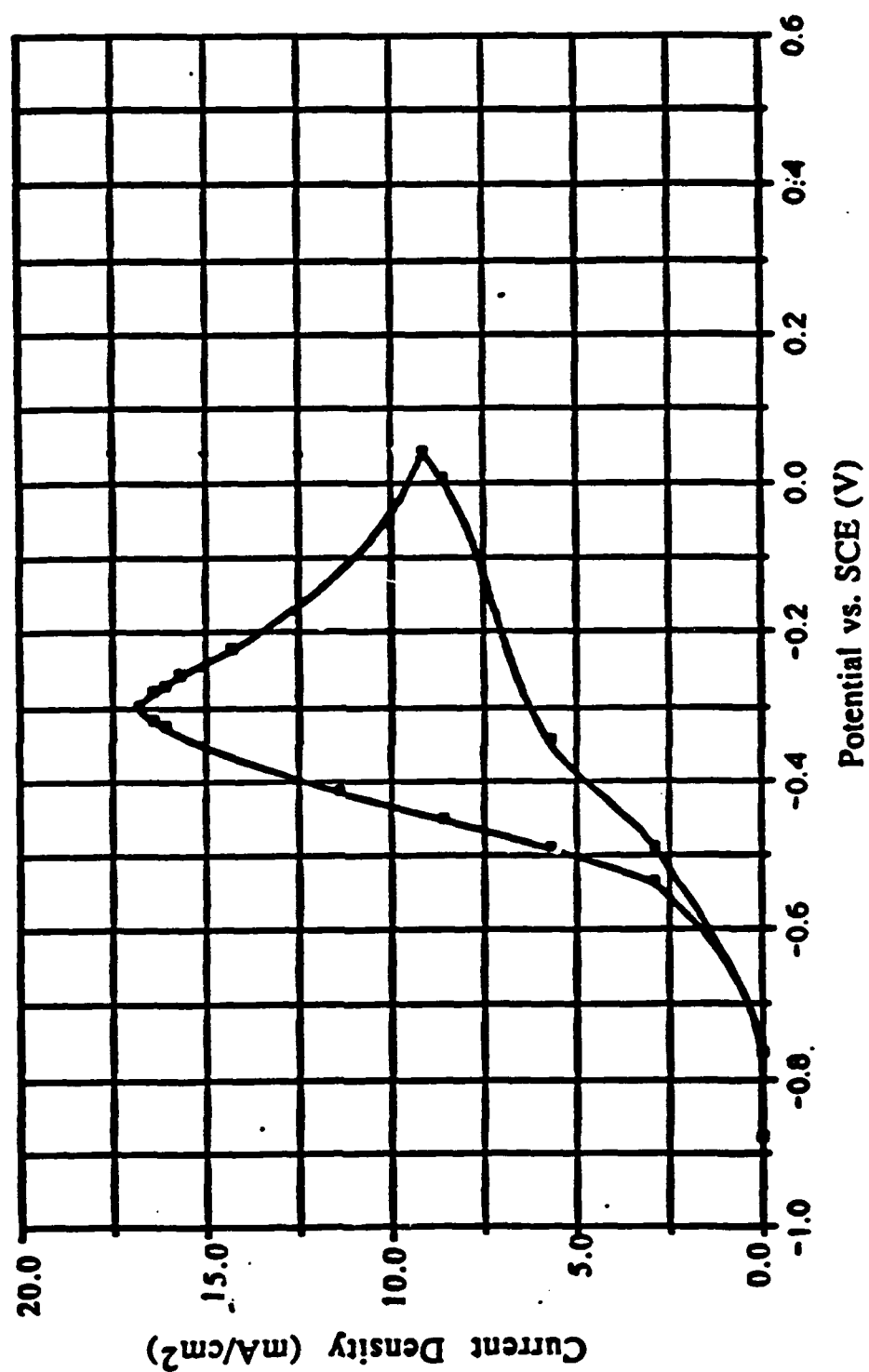


Figure 2.20

**.01 M KBH₄ at GOLD ELECTRODE
BUFFER pH = 10.96, 25 C, 100 mV/sec**

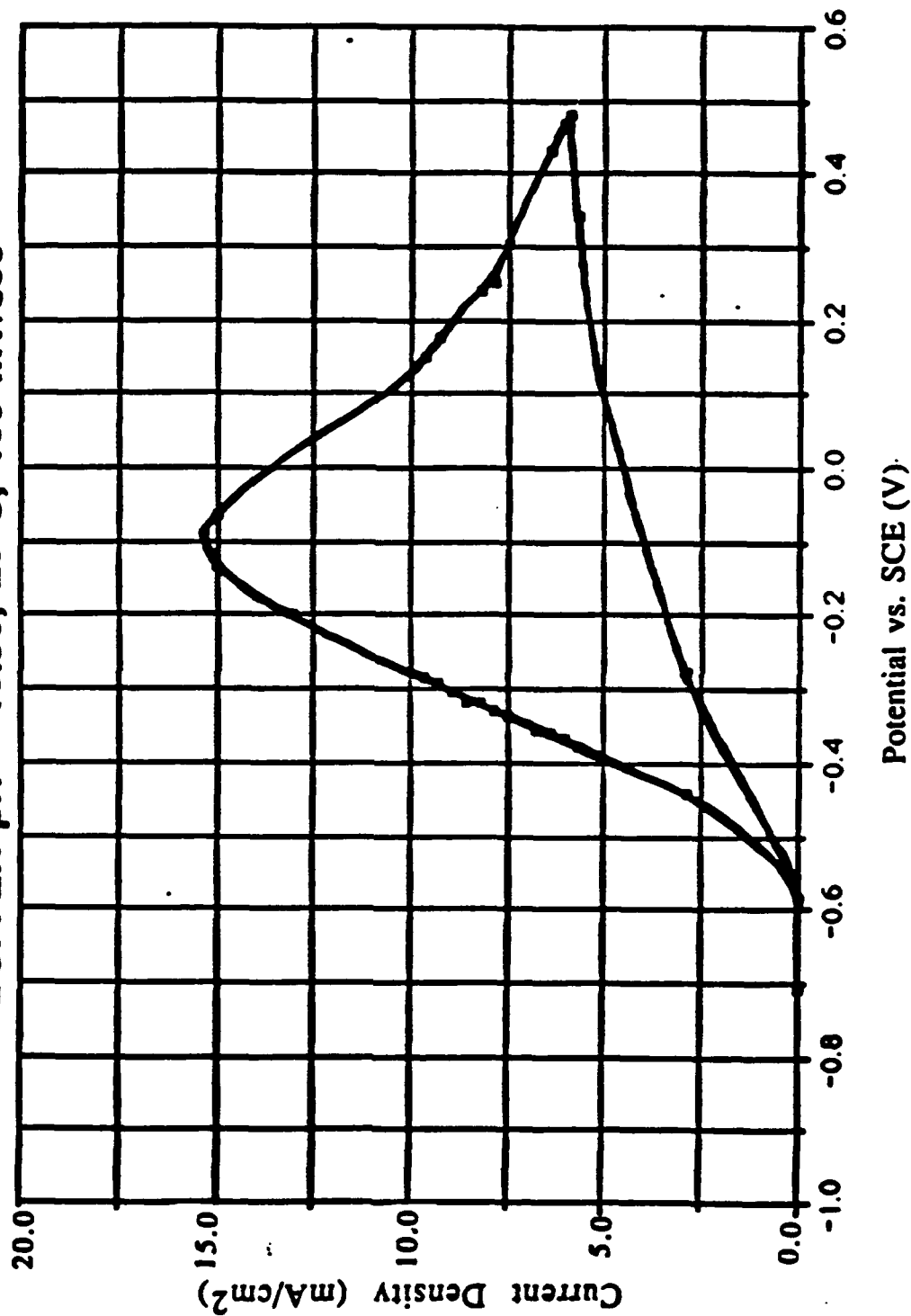


Figure 2.21

**.01 M KBH₄ at GOLD ELECTRODE
BUFFER pH = 9.14, 25 C, 100 mV/sec**

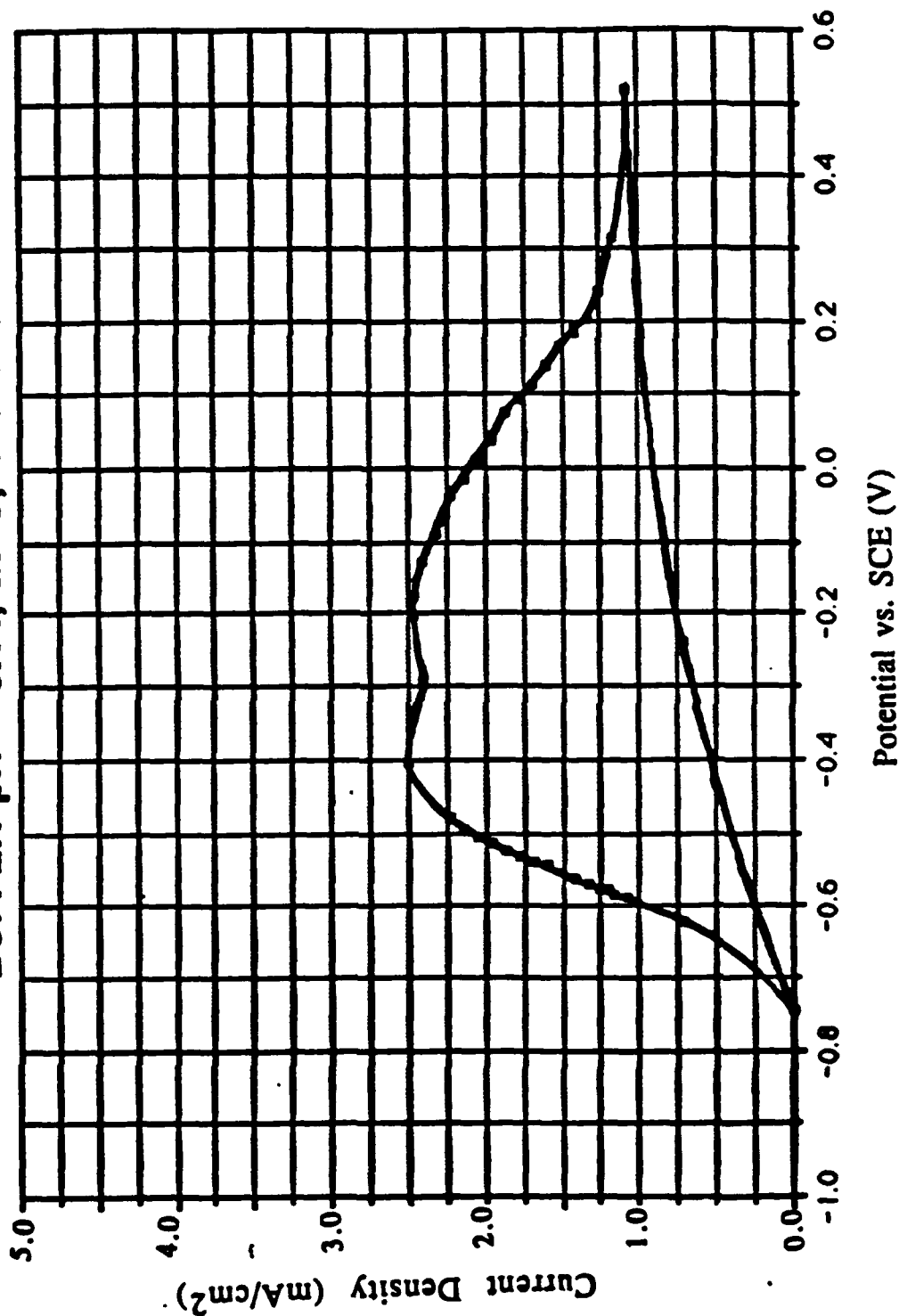


Figure 2.22

**.01 M KBH₄ at GOLD ELECTRODE
BUFFER pH = 7.78, 25 C, 100 mV/sec**

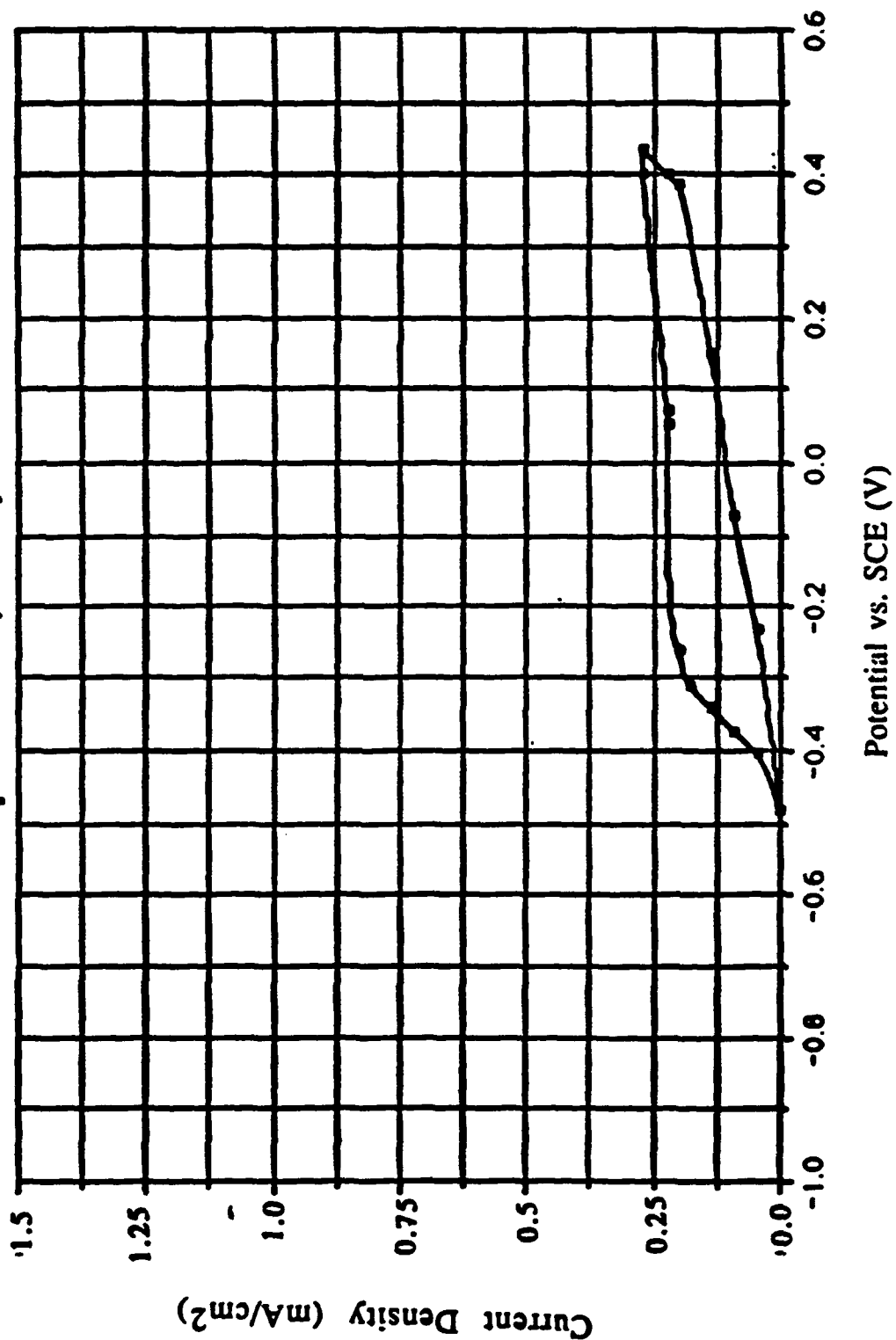


Figure 2.23

**.01 M KBH₄ at GOLD ELECTRODE
BUFFER pH = 9.14, 25 C, 100 mV/sec**

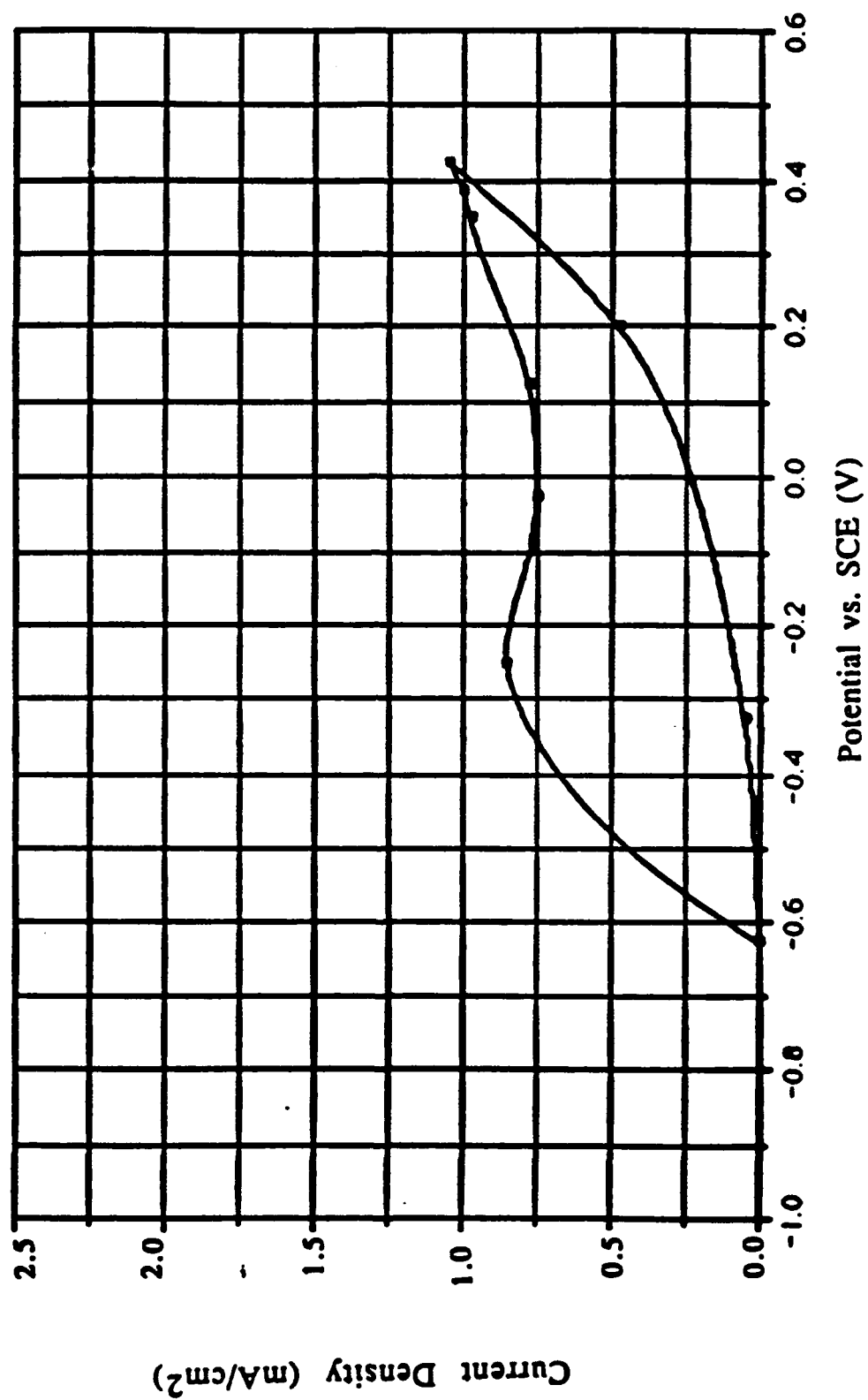


Figure 2.24

OXIDATION OF .07M HYDROXYLAMINE SULFATE

70 C, 100 mV/sec, pH = 3

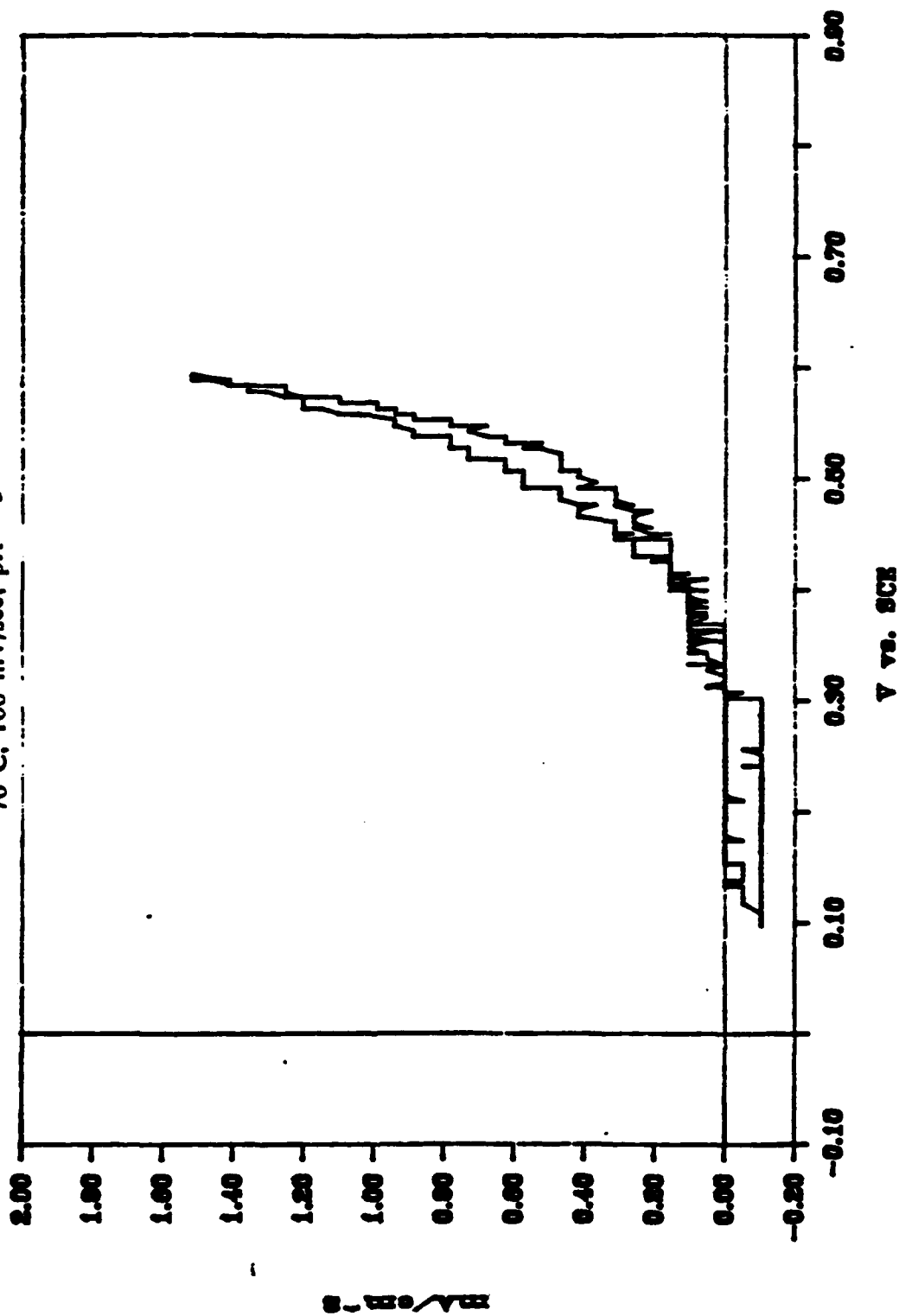


Figure 2.25

OXIDATION OF .068 M HYDROXYLAMINE SULFATE

80 C. 100 mV/sec, pH = 4

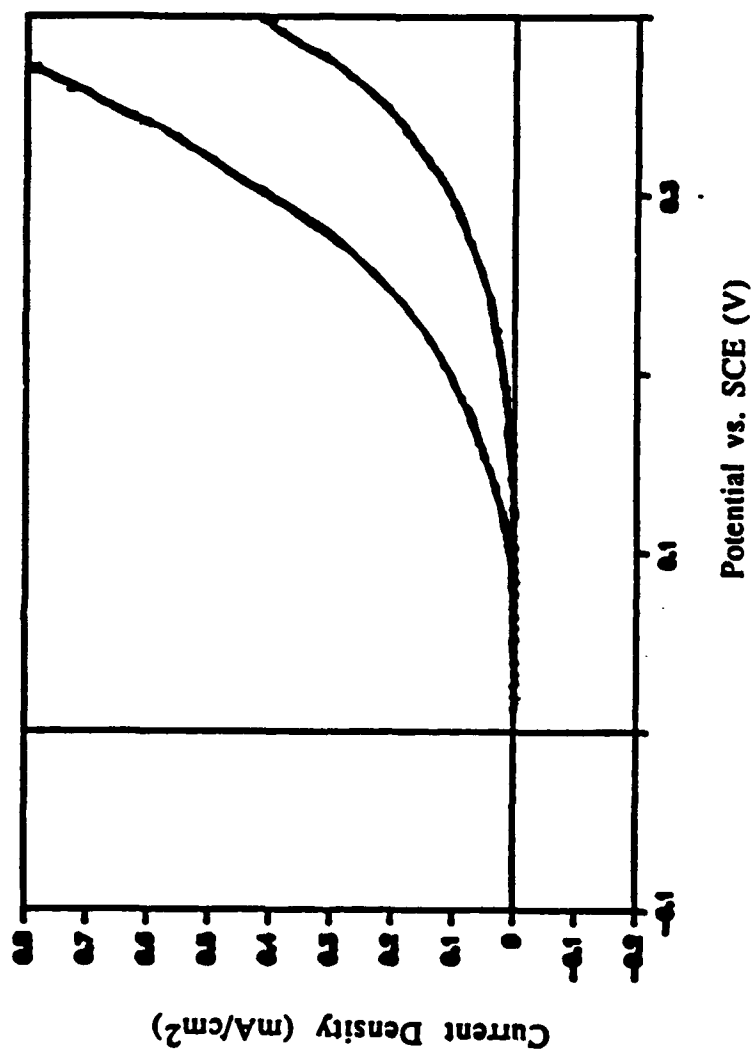


Figure 2.26

OXIDATION OF .25M HYDROXYLAMINE SULFATE

80 C, 100 mV/sec, pH = 4

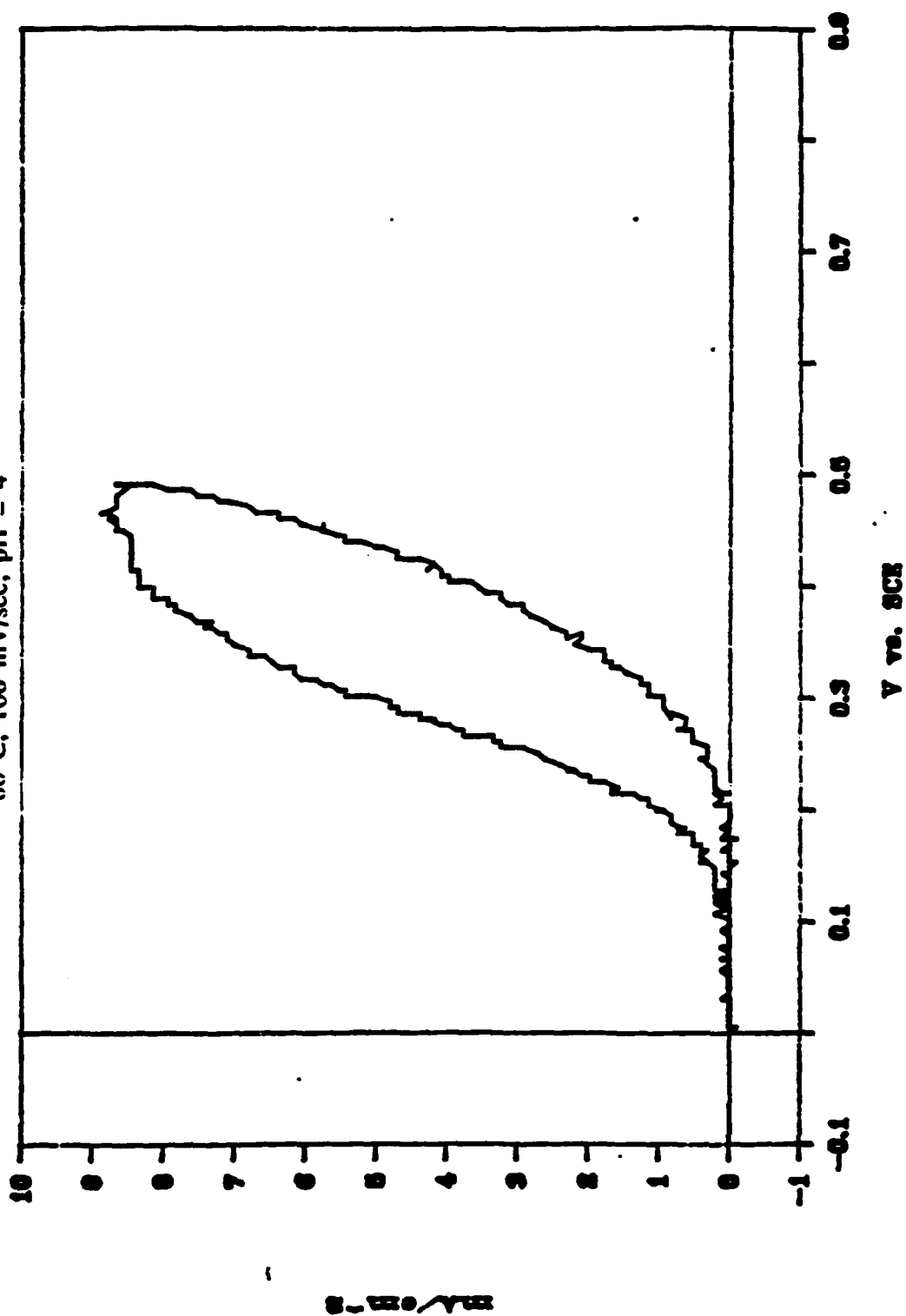
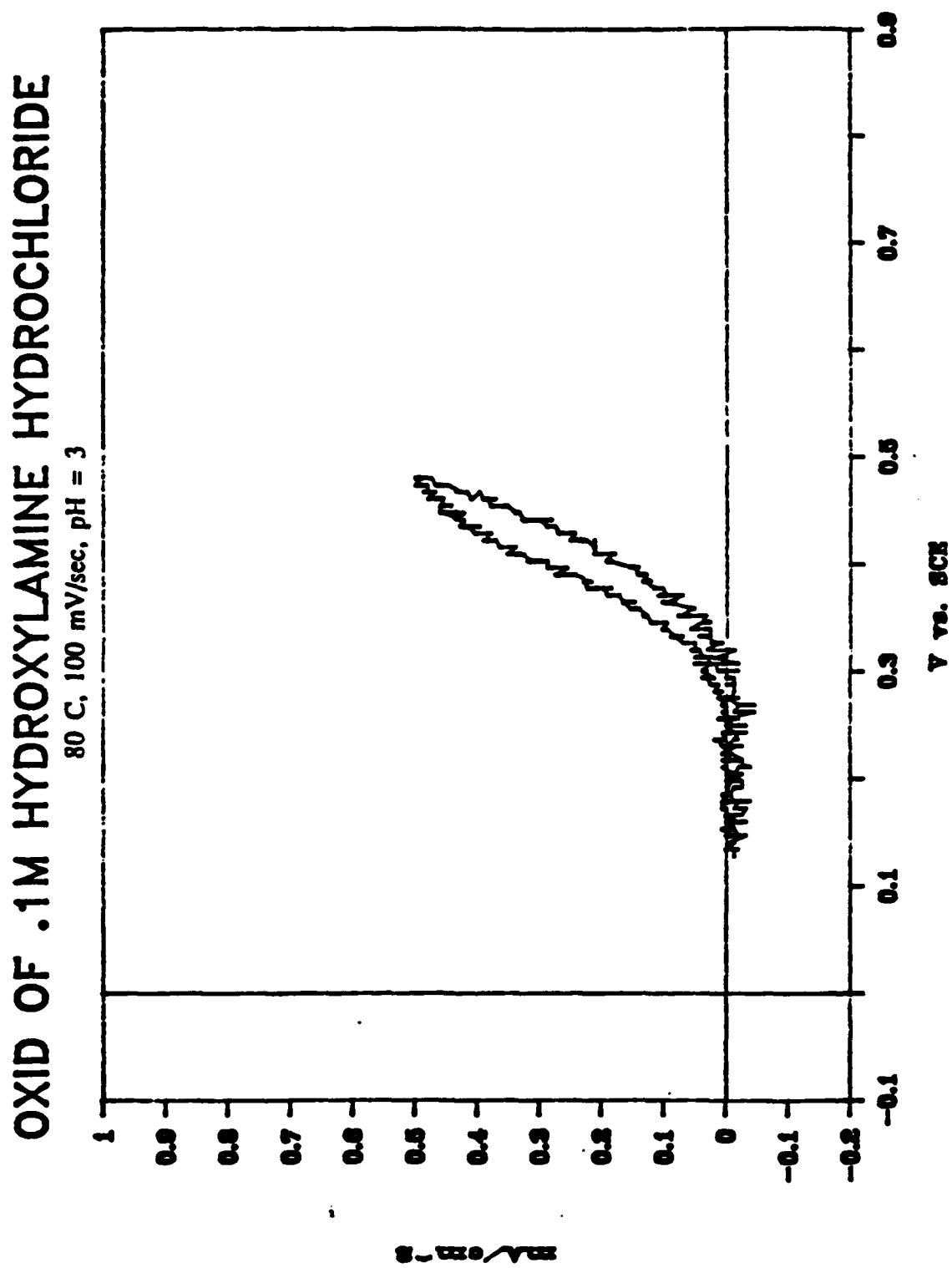
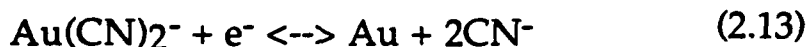


Figure 2.27



2.19 shows the oxidation of 0.2 M hydroxylamine hydrochloride at pH 4.7. The result of an increase in pH, Figures 2.27 and 2.28, is the shift of the zero current potential to more negative values. Figure 2.29 shows the oxidation of 0.25 M hydroxylamine sulfate in a 4.7 pH buffer solution at 80°C and 100 mV/sec.

The reduction of $\text{KAu}(\text{CN})_2$ is being investigated at low pH's and compared to the oxidation potential of the reducing agent. The reduction of gold proceeds as follows:



In Figure 2.30, the reduction of .14 M $\text{KAu}(\text{CN})_2$ is shown at 80°C and pH 3. The zero current potential is 0.26V versus SCE. The reduction of 0.1 M $\text{KAu}(\text{CN})_2$ at 80°C and pH 4.7 is seen in Figure 2.31. The zero current potential shifts to a more negative value of 0.17 V vs. SCE, with the increase in pH. Both figures suggest that the reduction of gold at low to medium pH's will occur in the same potential range as the oxidation of hydroxylamine.

Therefore, obtaining the voltammograms of the oxidation of hydroxylamine sulfate and the reduction of $\text{KAu}(\text{CN})_2$ separately but under the exact same conditions and in the same buffer solution is the next step. These curves can be compared to find the mixed potential where electroless plating will occur and to predict the deposition rate of the gold. Figures 2.32 a and b show the oxidation of 0.068 M hydroxylamine sulfate and the reduction of 0.037 M $\text{KAu}(\text{CN})_2$ at 80°C and pH 1.8 on a gold electrode. The anodic current equals the cathodic current at 0.19V vs. SCE. The corresponding current density is very small, .005 mA/cm². The calculated deposition rate from this current density is 3100 A/hr. Figures 2.33 a and b show the oxidation of .068 M hydroxylamine sulfate and the reduction of .037 M $\text{KAu}(\text{CN})_2$ at 80°C and pH 4 on a gold electrode. The mixed potential at this higher pH is .14 V vs. SCE, with a corresponding current density of .025 mA/cm². This current density suggests a gold deposition rate of 15500 A/hr. This deposition rate is better, yet still low.

In Table 2.3, the various electroless baths and their deposition rate are shown. The first three electroless baths have the same concentrations: 0.05 M hydroxylamine sulfate, 0.02 M potassium gold cyanide, 0.075 M citric acid, and 0.5 M sodium chloride. The pH is constant and the temperature varies. At 55°C, the deposition rate is 1180 A/hr. The deposition rate increases with

Figure 2.28

OXID OF .2M HYDROXYLAMINE HYDROCHLORIDE

80 C, 100 mV/sec, pH = 4.7

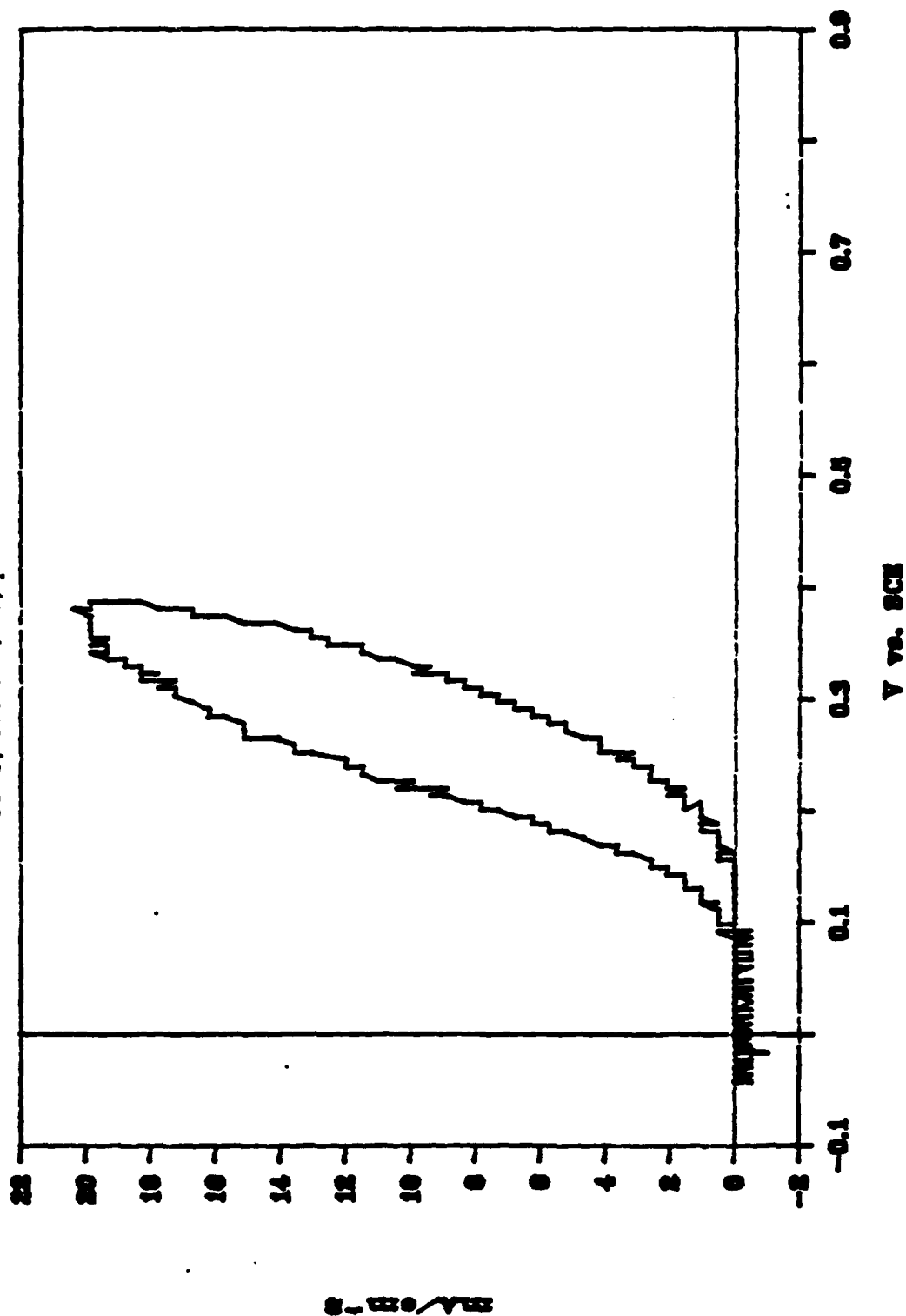


Figure 2.29

OXIDATION OF .25M HYDROXYLAMINE SULFATE

80 C, 100 mV/sec, pH = 4.7

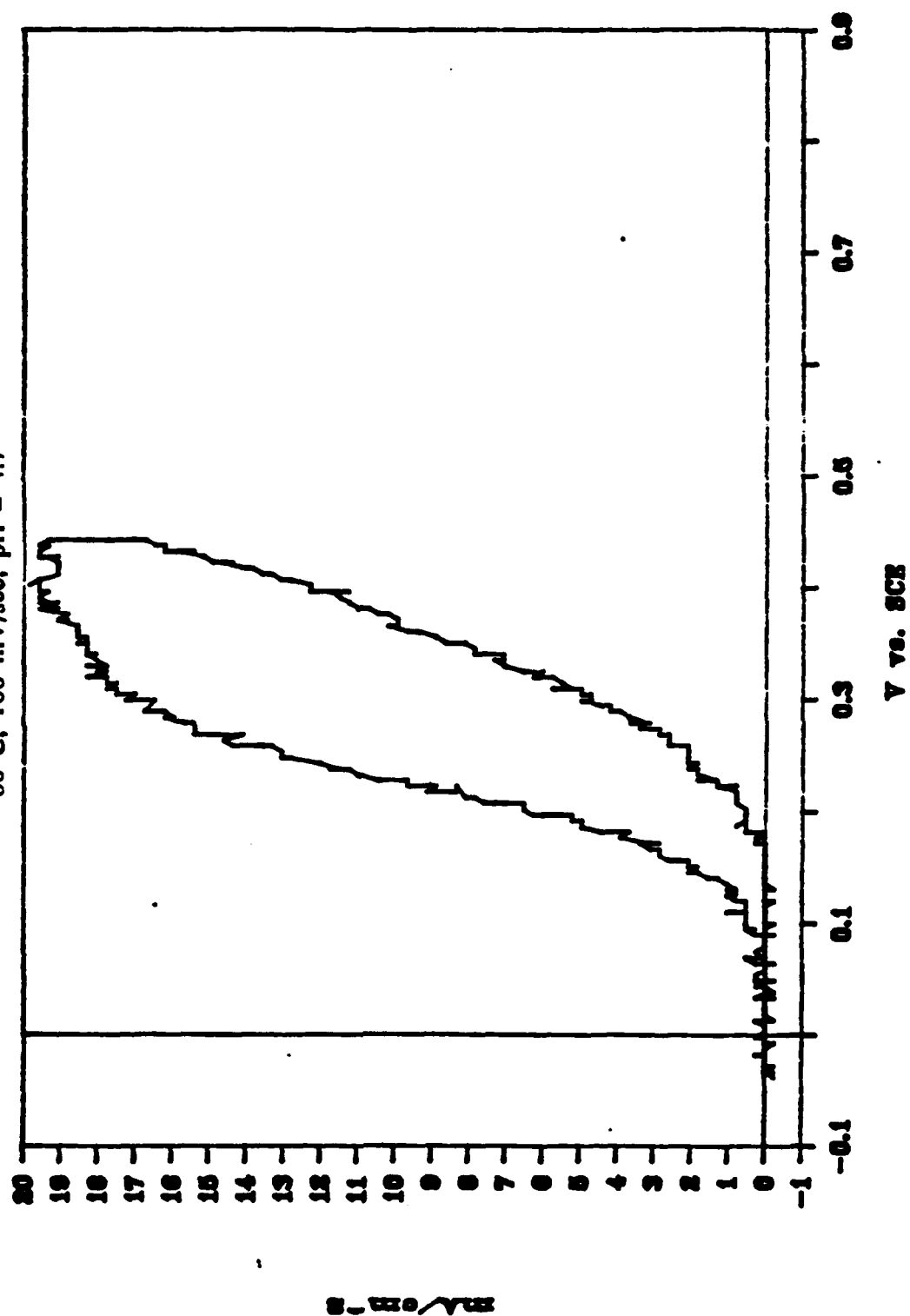


Figure 2.30

REDUCTION OF .14 M $\text{KAu}(\text{CN})_2$
50 C, 100 mV/sec, pH = 3

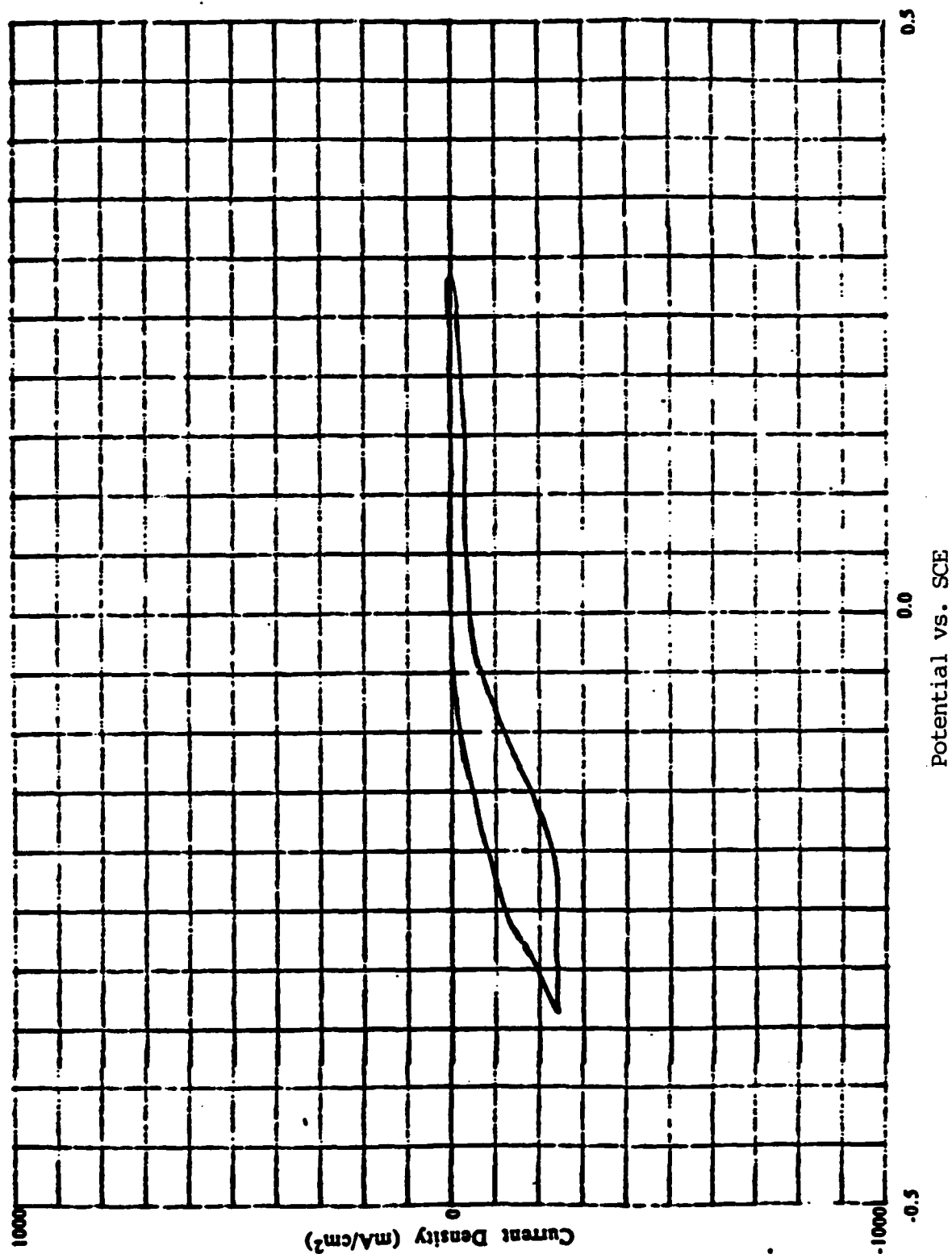
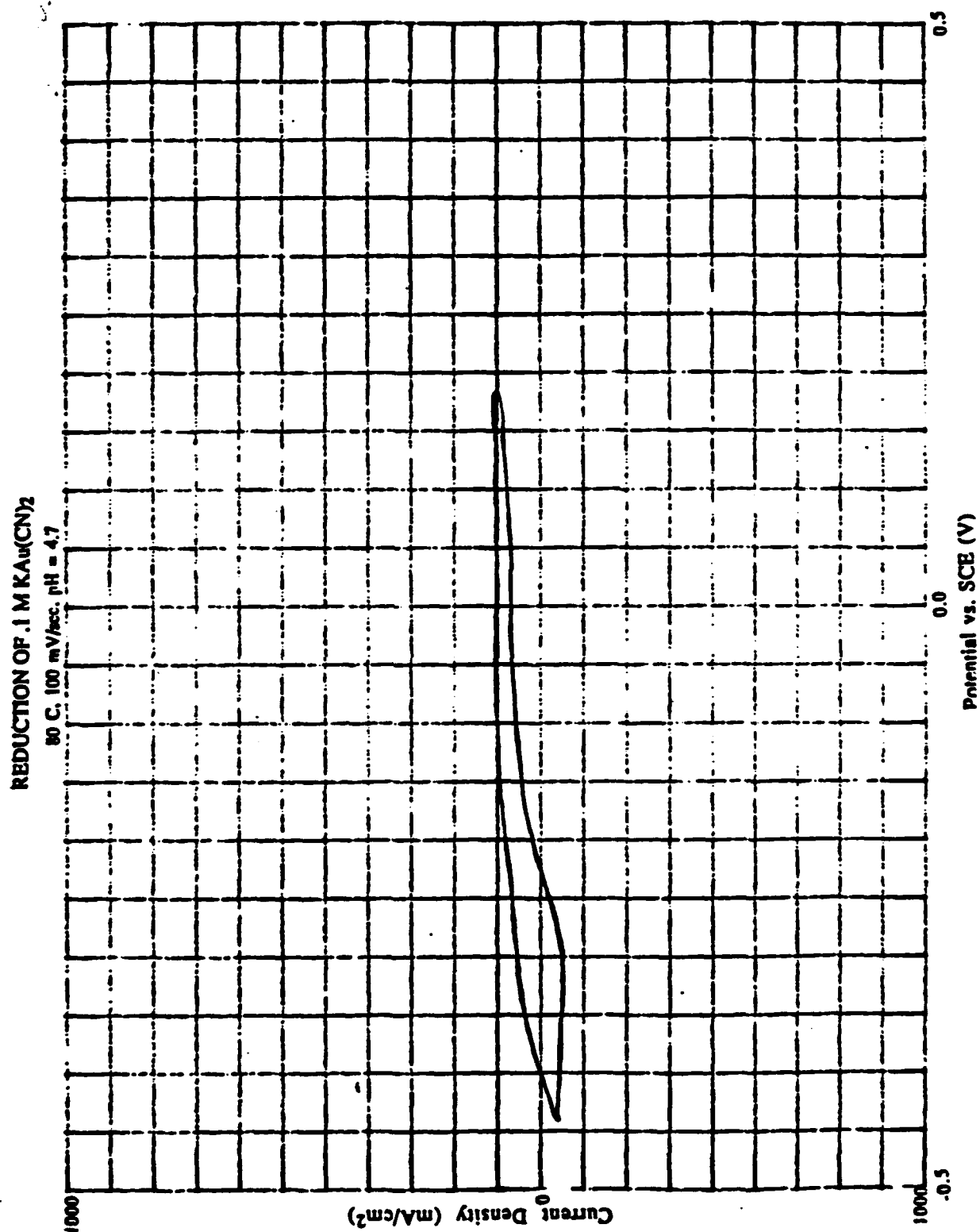


Figure 2.31



OXIDATION OF .068 M HYDROXYLAMINE SULFATE

80 C, 100 mV/sec, pH = 1.8

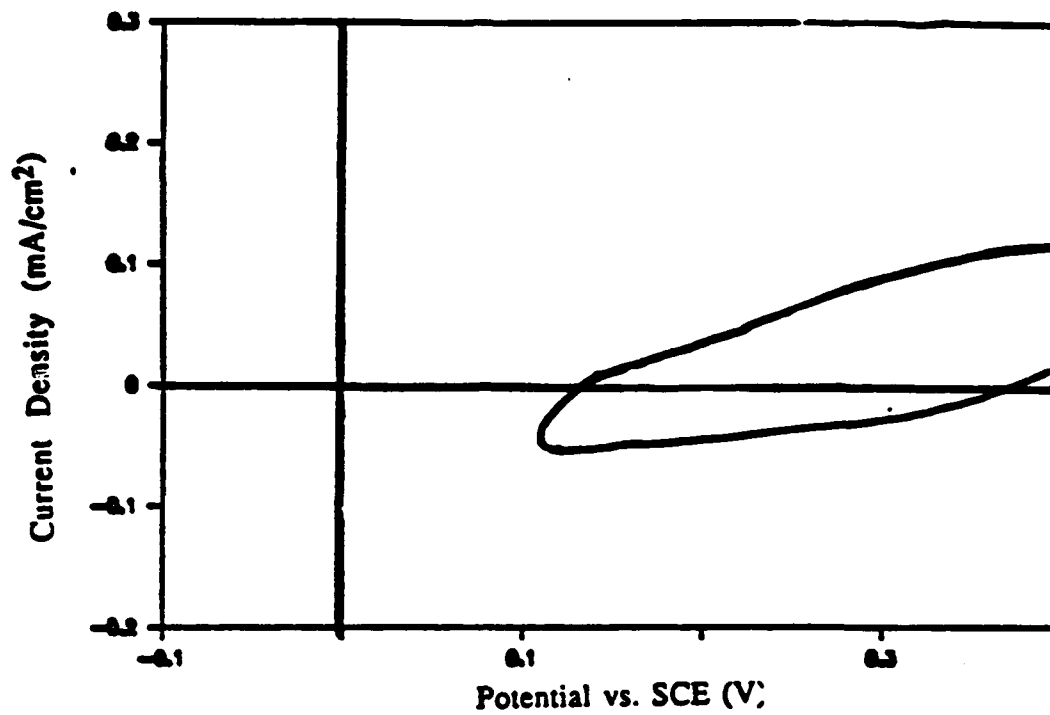


Figure 2.32 b

REDUCTION OF .037 M KAu(CN)₂

80 C, 100 mV/sec, pH = 1.8

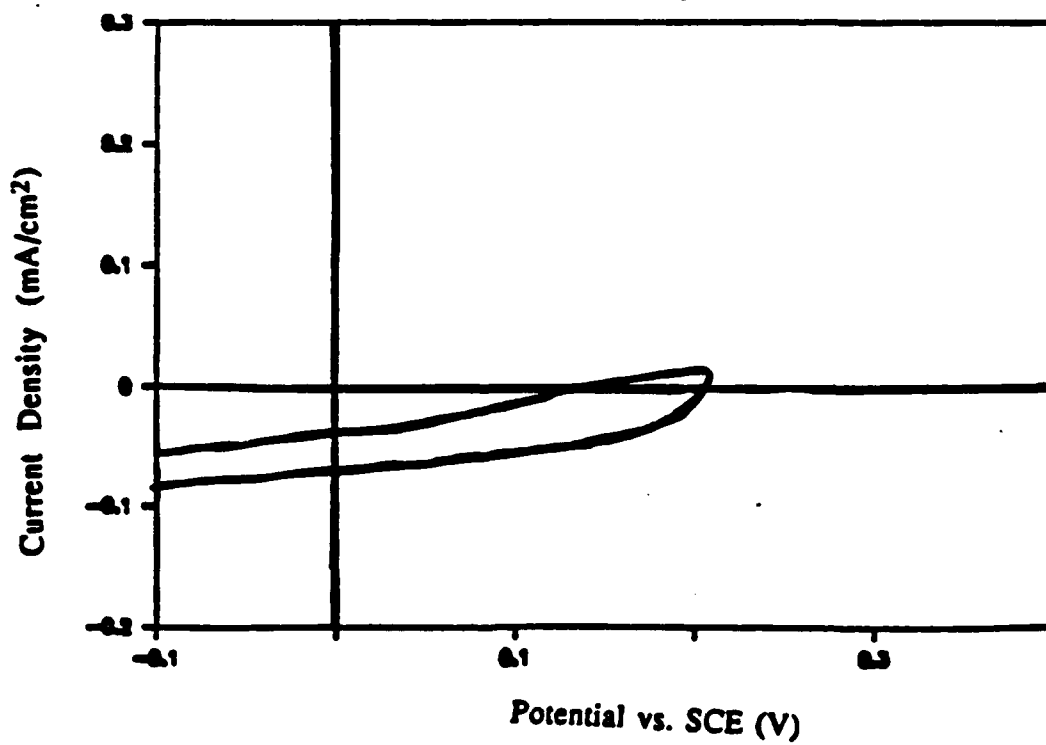


Figure 2.33 a

OXIDATION OF .068 M HYDROXYLAMINE SULFATE

80 C, 100 mV/sec, pH = 4

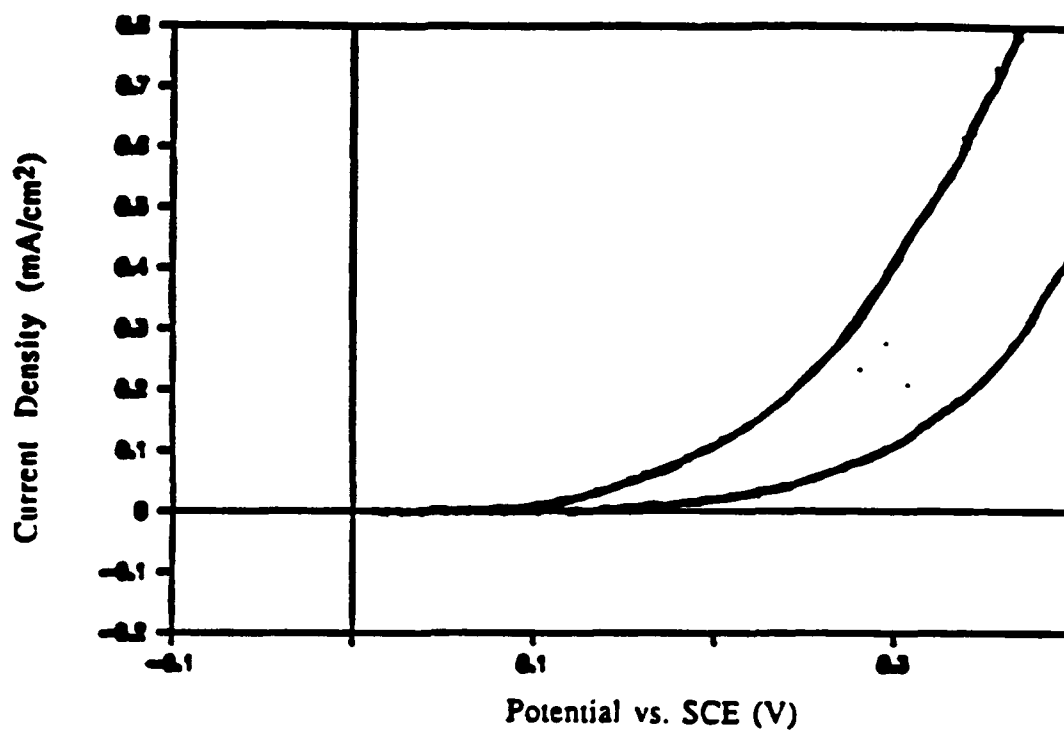


Figure 2.33 b

REDUCTION OF .037 M KAu(CN)₂

80 C, 100 mV/sec, pH = 4

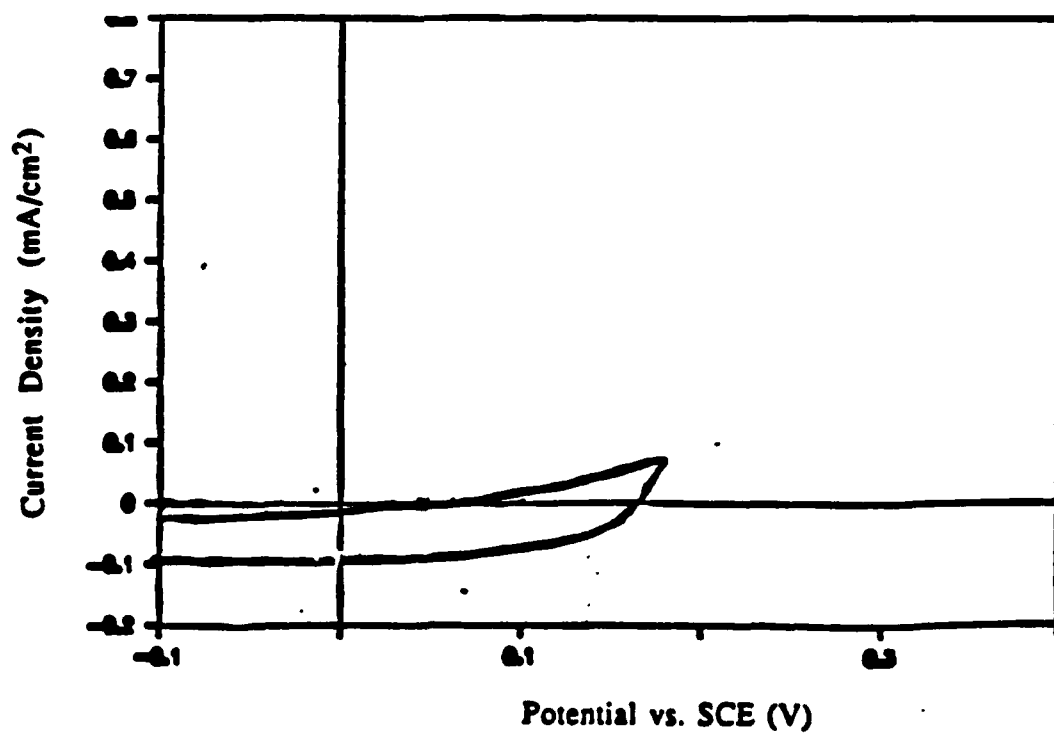


TABLE 2.3

Electroless Bath	Reducing Agent	Oxidizing Agent	Buffer and Supporting Electrolyte	Temperature (C)	pH	Deposition Rate (A/hr)
1	.05 M HYDROXYLAMINE SULFATE	.02 M KAu(CN) ₂	.075 M CITRIC ACID .5 M KCl	55	1.7	1180 +/- 200
2	.05 M HYDROXYLAMINE SULFATE	.02 M KAu(CN) ₂	.075 M CITRIC ACID .5 M KCl	66	1.7	1240 +/- 200
3	.05 M HYDROXYLAMINE SULFATE	.02 M KAu(CN) ₂	.075 M CITRIC ACID .5 M KCl	76	1.7	1460 +/- 200
4	.05 M HYDROXYLAMINE SULFATE	.02 M KAu(CN) ₂	.15 M CITRIC ACID .076 M NaOH .5 M KCl	85	2.4	1260 +/- 200
5	.05 M HYDROXYLAMINE SULFATE	.02 M KAu(CN) ₂	.15 M CITRIC ACID .076 M NaOH .5 M KCl	87	2.4	1380 +/- 200
6	.05 M HYDROXYLAMINE SULFATE	.02 M KAu(CN) ₂	.15 M CITRIC ACID .076 M NaOH .5 M KCl	92	2.4	1500 +/- 200
7	.05 M HYDROXYLAMINE O-SULFONIC ACID	.02 M KAu(CN) ₂	.15 M CITRIC ACID .076 M NaOH .5 M KCl	84	2.2	480 +/- 200

temperature slightly to 1240 A/hr at 66°C and 1460 A/hr at 76°C. All three deposition rates are very low. Electroless baths 4, 5 and 6 are similar to 1, 2 and 3 but at a higher pH. The bath compositions are: 0.05 M hydroxylamine sulfate, 0.02 M potassium gold cyanide, 0.15 M citric acid, 0.076 M NaOH and 0.5 M sodium chloride. An increase in deposition rates with temperature is evident here as well with 1260 A/hr at 85°C, 1380 A/hr at 87°C and 1500 A/hr at 92°C. Electroless bath 7 uses 0.05 M hydroxylamine ortho-sulfonic acid instead of hydroxylamine sulfate. Comparing electroless bath 4 and 7, at similar compositions, temperatures and pH's, it is clear by the 480 A/hr deposition rate, that hydroxylamine o-sulfonic acid is even less effective as a gold reducing agent. Further experiments showed that at temperatures higher than 50°C, hydroxylamine o-sulfonic acid begins to decompose.

Conclusions:

By studying the oxidation kinetics of potassium borohydride at various conditions, it can be concluded that potassium borohydride is unsuccessful at lower pH's. This is due to the fact that complete hydrolysis of BH_4^- to borohydride's highest oxidized form, BO_2^- , occurs at pH's lower than 9. Using voltammograms of the oxidation of hydroxylamine, it is apparent that the oxidation kinetics of hydroxylamine sulfate are very similar to the oxidation kinetics of hydroxylamine hydrochloride. By examining the potential range, it appears that at low to medium pH's hydroxylamine may reduce gold electrolessly. However, the predicted deposition rates are low, ranging from 0.3 mm/hr to 1.5 mm/hr.

Presently, hydrazine sulfate and phosphorous acid are being considered. As before, their oxidation kinetics on a gold surface will be studied using linear sweep voltammetry. Comparison of their oxidation with the reduction of potassium gold cyanide will give an indication of their possible use in an electroless bath.

3. Low Dielectric Constant Insulators

Three approaches are being taken in developing low dielectric constant insulators for GHz MCMs. The first is to match the properties of existing materials to those properties necessary for MCMs (see Table 3.1). The second approach is to work with companies/organizations who may have materials which could be of interest to MCMs and help them develop/characterize properties and processes. The third approach is to develop or apply new materials to MCM ourselves. These three approaches have been given in order of importance and in order of level of work.

Along with this effort to develop and characterize materials is the need to develop in-situ test methods where they do not exist. Thermal cure history, fabrication environment, and type of substrate upon which the pre-polymer is cast all can have a significant effect on the final film properties. Therefore, a polymer film cured on a particular surface may have significantly different properties than a film of the same material cured free of the substrate. In order that the characterization test results actually reflect the behavior of the polymer in a MCM performance environment, it is necessary to measure the critical film properties directly on the substrate. A list of insulator attributes which will be examined in this study is given in Table 3.1.

Table 3.1
INSULATOR ATTRIBUTES

- (1) Dielectric constant and loss tangent
- (2) Mechanical properties
- (3) Coefficient of thermal expansion
- (4) Insulator to insulator adhesion
- (5) Metal to insulator adhesion
- (6) Processing temperature
- (7) Moisture content
- (8) Photosensitive
- (9) Thermal stability
- (10) Deposition method and rate
- (11) Degree of Planarization
- (12) Chemical properties
- (13) Anisotropic nature of properties
- (14) Potential for future MCM growth

- (15) Projected lifetime
- (16) Thermal conductivity
- (17) Cost

3.1 Polyimides and Bis-Benzocyclobutenes

Purpose:

The purpose of this work is to evaluate commercially available polymers for use as interlevel dielectrics in gigahertz-frequency multi-chip modules. Our approach is to develop a series of in-situ, non-destructive test methods to evaluate the critical performance properties of a select group of polymeric thin films. In-situ measurements are necessary because the film on the wafer will lose the inherent stress caused by the CTE mismatch between the film and the substrate if removed from the wafer. The stress causes the polymer molecules to be oriented in the plane of the film. As a result, the in-plane properties for many polymers are different than the out-of-plane properties. In multi-layer structure applications (i.e. MCMs), the polymer properties normal to the plane are as crucial to the performance as polymer properties in the plane. Hence, in-situ characterization techniques must be developed to measure properties in both dimensions. The measurements should be non-destructive so that the materials can be tested during processing. Non-destructive tests can also be useful for quality control on production parts during fabrication.

In this study, thin dielectric films will be evaluated in the gigahertz-frequency region (see section 5); currently, most of the available dielectric data on these materials is from testing in the megahertz-frequency region. The effect of film anisotropy on electrical, mechanical and thermal performance properties will be evaluated quantitatively. Comprehensive evaluation of polymer properties as a function of processing parameters and material chemistry will be performed.

In summary, our goals are:

- To evaluate the dielectric properties of various polymers at gigahertz frequencies.

- To determine the effect of film anisotropy on the properties related to MCMs.
- To characterize the residual stress and coefficient of thermal expansion as they relate to MCM manufacture and use.
- To study the degree of moisture absorption of a given polymer and how the moisture affects the dielectric properties.
- To characterize commercial polymers to permit selection of the best material and processing conditions for a given MCM design.

Approach:

High Frequency Electrical Property Measurements:

A test structure consisting of a 3-metal layer/2 polymer layer structure will be used to evaluate the gigahertz-frequency dielectric performance of the polymer. This test structure contains sets of transmission lines in the same plane at varying separations (Figure 3.1a), transmission lines above a zig-zag signal lines (Figure 3.1b), transmission lines that step between levels through a via (Figure 3.1c), and transmission lines that bend in one plane (Figure 3.1d). Dielectric properties will be evaluated by transmitting a signal from each end of a line at the same time. Measurement of the signal transmission and reflection of the two signals provides information about a particular feature such that a characteristic impedance, capacitance and resistance for each particular type of signal line can be determined. The capacitance of a line will be a direct result of the dielectric constant of the surrounding dielectric material, while the resistance and inductance are a function of the metal line and the losses in the dielectric. By using several different line configurations (Figure 3.1a-d), a library of transmission characteristics may be compiled for a given line feature and dielectric material. Using this information, a future MCM designer may then use an appropriate sum of the electrical contributions of a length of signal line, a line crossing over (or under) another line, a step through a via, or a bend in the same plane and predict what the electrical properties of a design are before fabrication.

Figure 3.1

Electrical Properties -- High Frequency

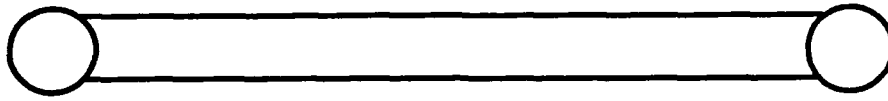


Figure 3.1a. Straight line in one plane

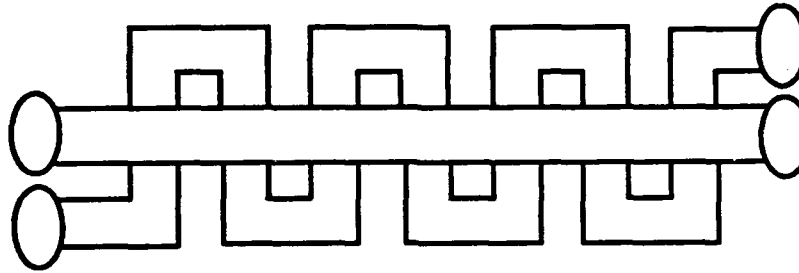


Figure 3.1b. Cross Talk between Layers

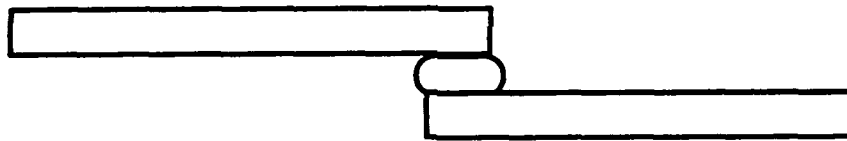


Figure 3.1c. Step through a via

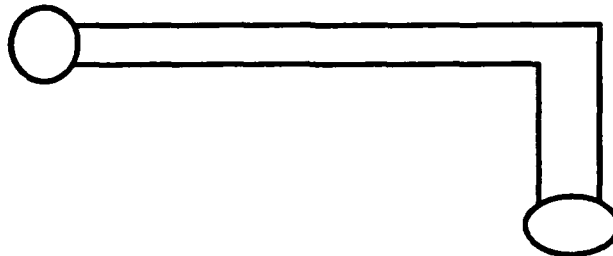


Figure 3.1d. Bend in one plane

Fabrication details for this test structure can be found in section 2.1, and details concerning measurement of the GHz frequency electrical properties can be found in section 5.

Low Frequency Dielectric Measurements:

Work by Linda Lin, et al.^(3.1) has demonstrated that polyimides develop a high amount of film anisotropy during processing. This anisotropy has been translated to a large difference in the electrical properties in-the-plane and through-the-plane of the polymer film. (Yoon, et al.^(3.2)) Characterization of the dielectric properties of the film in each of the two directions is critical to MCM design.

The degree of anisotropy can be quantified by using Metricon Model Prism Coupler. The Metricon focuses plane-polarized laser light on the surface of the film while varying the angle of incidence of the light. The angles at which the light is absorbed into the film is characteristic of the index of refraction of the material. Using this method twice, once with the polarizer parallel with the surface of the film and once with it perpendicular to the surface, the in-plane and through-plane refractive indices may be determined for the film. The difference between the in-plane and through-plane refractive indices, also known as the birefringence, is characteristic of the degree of anisotropy of the film, i.e. the larger the birefringence, the larger the amount of film orientation.

At low frequencies, a parallel-plate capacitor structure will be used to measure the through-plane dielectric constant (Figure 3.2a). An interdigitated electrode structure (Figure 3.2 b) will be used to determine the in-plane dielectric constant by measuring the gain and phase of the signal on the undriven half of the electrode structure and using a computer simulation of the electric fields to back calculate the dielectric constant and loss tangent of the polymer.

Thermal and Mechanical Properties:

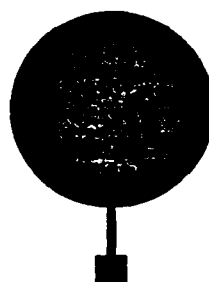
A number of in-situ test methods for measuring mechanical properties of thin polymer have been developed, including substrate curvature^(3.3), load-deflection of polymer membranes^(3.4), bending beam techniques^(3.5) and resonance of polymer strings^(3.6). In this

Figure 3.2

Top View

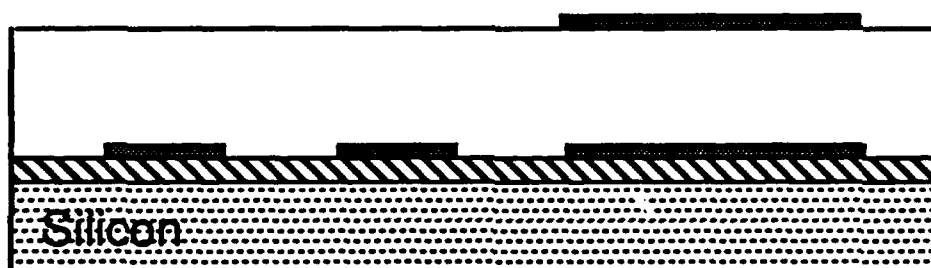


**a. Interdigitated
(Comb) electrode**



**b. Parallel-Plate
Capacitor**

Side View



study, each of these techniques will be used for characterizing the dependency of in-plane mechanical and thermal properties on the type of chemical system and processing conditions for the polymer dielectrics.

During the first year of funding, work has been focused on using the wafer curvature method for determining in-plane residual stress and coefficient of thermal expansion. The curvature of a bare silicon wafer is measured by a Flexus Laser Curvature Scanner. This wafer is then coated with polymer and is cured. The curvature of the coated wafer is then determined. The difference in curvature before and after coating is directly related to the residual stress in the polymer film. In-plane coefficient of thermal expansion is determined by coating two substrates with different CTE's with polymer. By measuring the wafer curvature of each substrate at two different temperatures, the film in-plane CTE can be extracted.

The wafer curvature technique described above is restricted to the measurement of in-situ mechanical properties. The spin coat processing of polymer films may lead to polymers which are oriented in the plane of the film; this orientation will cause the mechanical and thermal properties in the plane of the film to be different from those properties through the plane of the film. Currently, there is no test method for measuring mechanical and thermal properties normal to the plane of the film.

In this study, the use of microfabricated electrodes will be used to determine through plane modulus and residual stress of thin polymer films. The basic concept for this test device is that the measurement of polymer permittivity and loss factor depends on the spacing between the electrodes in a parallel plate capacitor whereas the dielectric properties of a polymer film on a comb (interdigitated) electrodes do not depend on the thickness of film above the electrode surface (providing that the coating is greater than twice the spacing between the electrodes). A comb electrode and a parallel plate capacitor (optionally combined with field effect transistors for signal amplification) will both be fabricated on the surface of a silicon wafer as shown in Figure 3.2.

Operation of the comb electrode device is as follow: a sinusoidal voltage applied to the driven comb electrodes causes a time-varying current (both conduction and displacement current) to flow through the polymer sample to the other comb electrode. An

admittance bridge or gain-phase meter is then used to determine the magnitude and phase of the current through the comb capacitor. This capacitor current depends on the dielectric properties (i.e. permittivity ϵ' and loss factor ϵ'') of the polymer film covering the surface of the electrodes. These dielectric properties can thus be determined from the amplitude and phase measurements combined with information on the electrode geometry^{3,7}. This calculation of the electrical properties of the polymer is independent of the film thickness when the comb electrode geometry is used.

In contrast, the determination of the dielectric properties of the film between the plates of the parallel plate capacitor is directly dependent on the spacing between the electrodes (i.e. the thickness of the polymer). For parallel plate electrodes, with a cross-sectional area A and a spacing between the electrodes of L , the capacitance C can be approximated by:

$$C = \frac{\epsilon' \epsilon_0 A}{L} \quad (3.1)$$

and the resistance R by:

$$R = \frac{L}{\omega \epsilon'' \epsilon_0 A} \quad (3.2)$$

where ω is the measurement frequency, and ϵ_0 is the permittivity of free space. Small changes in the film thickness (L) can therefore be determined by measuring the dielectric properties of the film using the comb electrodes (measurement independent of film thickness) and using this information together with the parallel plate results (measurement dependent on film thickness). Any changes in dielectric properties will be normalized out in this fashion. For example, to measure the modulus of a polymer film, both comb and parallel plate electrodes will be fabricated on a silicon wafer coated with a polymer film. The wafer will be placed in a pressure chamber, and the gain and phase measurements from both electrodes will be collected as the pressure is increased at constant temperature. As the pressure increases, the polymer film will compress. Using the gain-phase measurements obtained on the comb electrode, we can determine the film dielectric properties. The parallel plate capacitor will then be calibrated with the

dielectric properties to determine the spacing between the electrodes. Knowing the applied pressure and the polymer film thickness, the out-of-plane modulus of the polymer can be determine in-situ.

The coefficient of thermal expansion normal to the film surface can be measured in a similar fashion. A silicon wafer with both types of electrodes will be placed in an oven. The gain and phase measurements for both devices will be obtained as a function of temperature. Since the comb electrodes are fixed on a silicon dioxide substrate, the spacing changed between the electrodes due to temperature variations will be insignificant in comparison with the changes in spacing between the parallel plate electrodes. Therefore, the dielectric properties of the polymer film can be determined from the comb electrodes as described above and used in combination with the parallel plate measurement to obtain the spacing between the electrodes. The coefficient of thermal expansion normal to the film surface can then be calculated from changes in polymer film thickness as a function of temperature.

Moisture Barrier Properties:

Two different moisture tests will be performed as part of this work. The first test is to determine the amount of moisture a given film can absorb. This testing will be performed by a suspending a spin-coated polymer film from the pan of a Cahn microbalance into a humidity controlled chamber. Moisture uptake is then measured gravimetrically during exposure to different levels of relative humidity. This technique is described in more detail in Section 3.5.

The second test involves determining the effect of moisture on parallel-plate electrical property measurements. An electrically packaged parallel-plate capacitor fabricated on a thin polymer film is temperature cycled from $\sim 25^{\circ}\text{C}$ to 200°C in both dry and moist environments. Differences between the two experiments demonstrate the effect of moisture on the dielectric constant at a given temperature.

Materials for Evaluation:

Seven different materials have been chosen for evaluation. Table 3.2 lists the polymers to be tested. DuPont PI-2555 is chosen

Table 3.2 Polymers for Evaluation

<u>Company</u>	<u>Name</u>	<u>Chemistry</u>	<u>Comments</u>
DuPont	PI-2555	BTDA/ODA/MPDA	Standard
	PI-2566	6FDA/ODA	Fluorinated
National Standard	EL-5010	Acetylene-Terminated	Low dielectric constant
		Isoimide	
Hitachi	PI-2611D	BPDA/PPD	Low Stress
	EL-5512	Acetylene-Terminated	Low dielectric constant,
		Isoimide	Fluorinated
Dow	PIQ-L100	Polyisindoloquinazolinedione	Low stress
	XU13005.01	Benzocyclobutene	Non-polyimide

as a baseline material for this study. It is an older polyimide which has been well-characterized in a number of studies.

DuPont PI-2566 is chosen as an example of a fluorinated polyimide. The fluorination in the structure should give superior moisture properties compared with the PI-2555, as well as lowering the dielectric constant.

DuPont PI-2611D is an example of a low-stress, rigid-rod polyimide. This material should give a much lower CTE and residual stress than the standard PMDA-ODA polyimides. The rigidity of the backbone causes the material to be highly oriented, on the level of an order of magnitude higher anisotropy than PI-2555 or PI-2566.

Two National Starch materials, EL-5010 and EL-5512, will be evaluated to look at film chemistry. EL-5010 is a standard-type, low dielectric constant polyimide while EL-5512 is a fluorinated, low dielectric constant polyimide. These materials will be compared with PI-2555 and PI-2566.

Hitachi PIQ-L100 has been chosen as a second low stress material to compare to PI-2611D. The chemistries of the two materials are different and will allow determination of relationships of properties with polyimide chemistry.

Lastly, a developmental material XU13005.01 benzocyclobutene (BCB), from Dow is being evaluated as a non-polyimide dielectric material. BCB has low dielectric constant, low moisture absorption and little to no anisotropy. This material will give a low orientation comparison to standard polyimide measurements.

Results:

Processing:

PI-2555, PI-2566, PI-2611D, BCB, and EL-5010 have all been successfully spin-coated on silicon, 50 Å Ti/2000 Å Au/10 Å Ti coated silicon and plated gold coated with 10 Å Ti. Each of these polymers adheres well to each of these substrate materials.

Low Frequency Dielectric Properties:

Parallel-plate capacitance measurements can be dramatically affected by moisture, and fringing effects. Moisture absorption of the polymer film causes significant increase in the measured value of the dielectric constant. Initial dielectric measurements were performed in the Georgia Tech Microelectronic Research cleanroom facility. This facility has humidity control of $\pm 5\%$ RH with a setpoint of 45% RH. This 5% variation in the relative humidity can cause significant variations in the dielectric constant. Table 3.3 shows capacitance data from three different days and the associated relative humidity measured ~5 minutes after the capacitance reading. The relative humidity value does not necessarily reflect the equilibrium moisture content of the polymer since the humidity varies in the cleanroom, and moisture requires time to diffuse in or out of the film.

Further study of the effect of moisture was performed by measuring the temperature dependence of the dielectric constant in ambient and dry conditions. Figure 3.3 shows dielectric constant versus temperature for three temperature cycles, performed in ambient air. The diffusion of moisture within the film causes a hysteresis effect on the dielectric constant. A similar experiment performed in a dry environment is shown in Figure 3.4. The results of all three temperature cycles overlay one another and no hysteresis is observed.

From these experiments, the importance to perform dielectric constant measurements in a controlled humidity environment has been demonstrated. For future work dielectric measurements will be made on a dry nitrogen-filled glove box.

The second problem with parallel-plate capacitor measurements is the error caused by edge fringing of the capacitor. Figure 3.5 shows the original parallel-plate capacitor design which was used for testing. Results from this structure showed a variation of dielectric constant as a function of capacitor size. Table 3.4 lists data for a typical measurement of a parallel-plate capacitor test structure. Capacitors numbered 1 are the smallest and number 7s are the largest. The higher dielectric constant measurement on the smaller capacitors is due to the effect of edge fringing. The smallest capacitor has the highest ratio of capacitor area to probe pad area and is therefore the most in error. To remove the effect of fringing, a correlation from ASTM standard

Table 3.3
Effect of Humidity on Measured Dielectric Constant

Humidity	Dielectric Constant
37.7%	3.2784
43.9%	3.4497
44.3%	4.0006

Figure 3.3
Dielectric Constant versus Temperature
Performed in Ambient Conditions

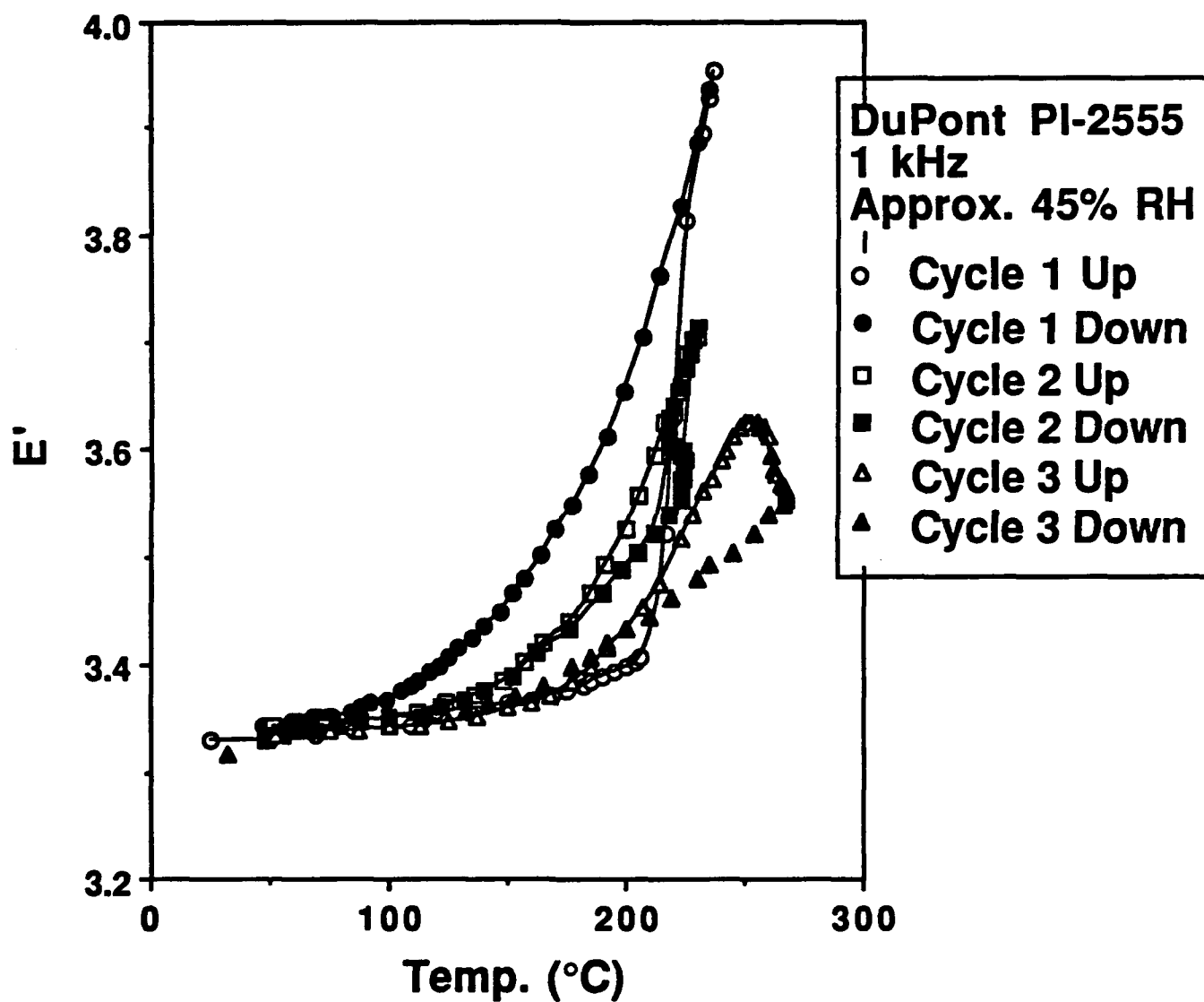
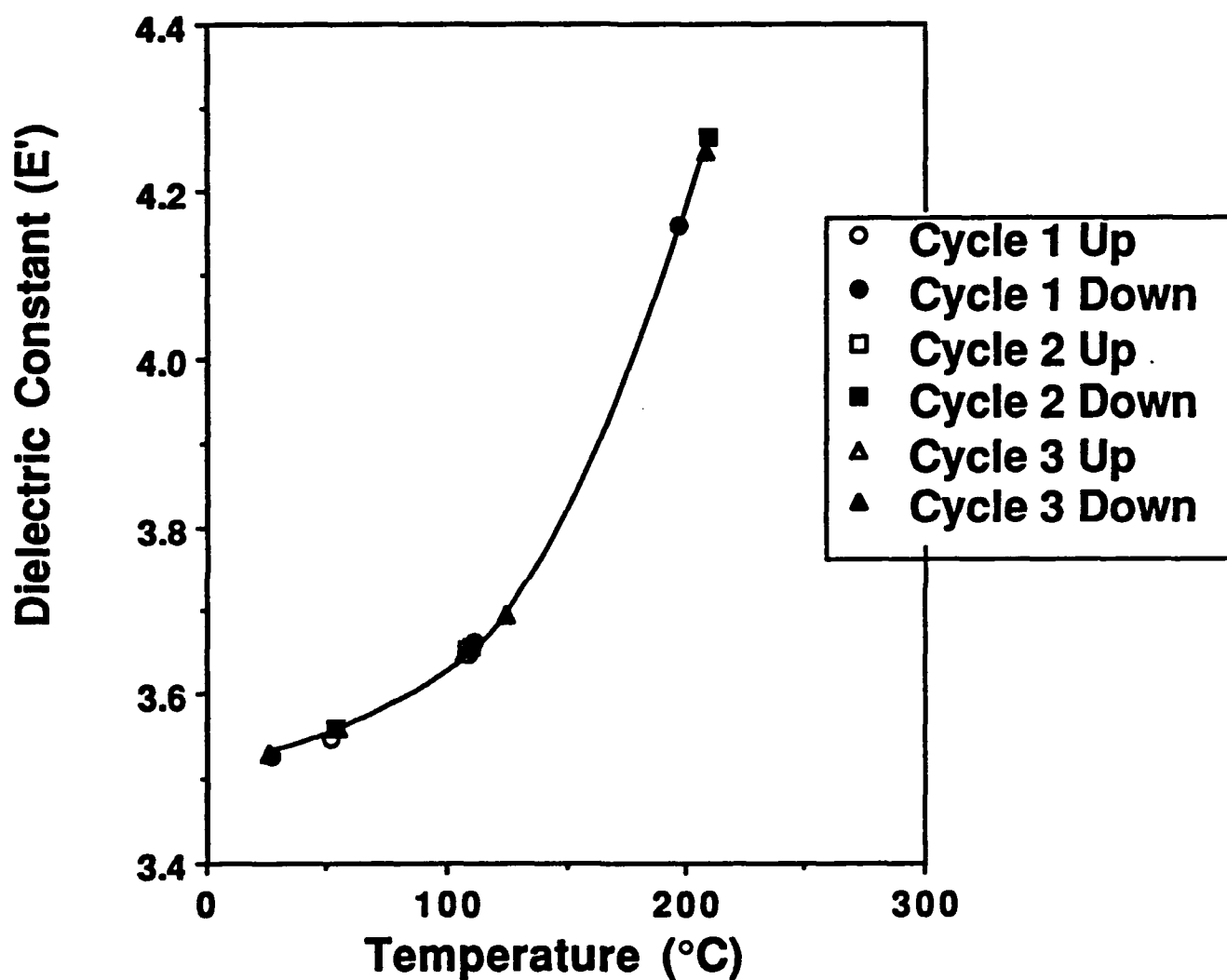


Figure 3.4
Dielectric Constant Versus Temperature
Performed in Moisture-Free Environment



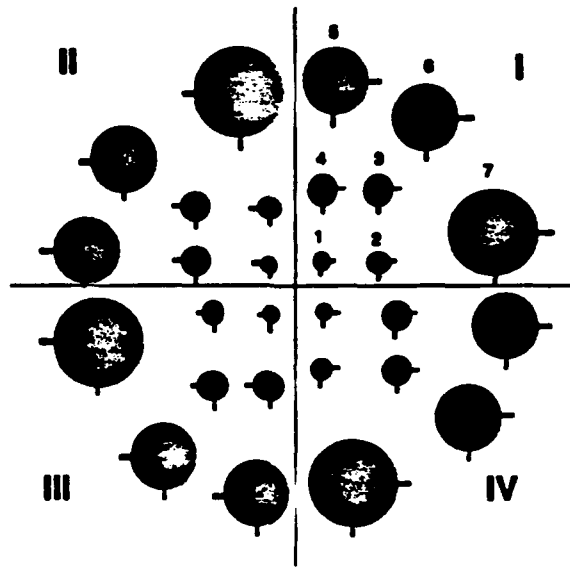


Figure 3.5 Old-Style Capacitor Mask

Table 3.4 Capacitor Data for PI-2545				
LOT 10B	PI-2545	RH=44.3%		
QUAD	POSITION	Capac.	AREA	DIELECTRIC
	(#)	(pF)	(cm ^2)	CONSTANT
1	1	-	0.0288	-
	2	57.2	0.0579	3.8455
	3	103	0.1070	3.7529
	4	99.9	0.1031	3.7972
	5	568.5	0.5869	3.8084
	6	564.5	0.5857	3.7642
	7	1088.4	1.0595	4.0006
2	1	30.5	0.0290	4.0750
	2	57.63	0.0589	3.8241
	3	103.4	0.1029	3.9157
	4	-	0.1074	-
	5	567.6	0.5647	3.8869
	6	577.8	0.5638	3.9537
	7	1086.9	1.0507	4.0340
3	1	29.2	0.0293	3.8621
	2	56.1	0.0548	3.9707
	3	102.6	0.1031	3.8545
	4	-	0.1088	-
	5	563.3	0.5678	3.8613
	6	574.2	0.5652	3.9436
	7	1094	1.0505	4.0450
4	1	29.5	0.0309	3.6984
	2	54	0.0544	3.8574
	3	106.1	0.1077	3.8128
	4	105.5	0.1088	3.7808
	5	566.8	0.5715	3.8241
	6	567.4	0.5793	3.7719
	7	1101.4	1.0578	4.0322

D150-70 for circular parallel-plate capacitors was used. Table 3.5 lists values of the corrected and uncorrected capacitances and dielectric constants. The correction did not eliminate the effect of the sharp corners on the probe pad sufficiently to successfully correct the data.

To eliminate the fringing problems a new structure without probe was made. Figure 3.6 shows this new structure. Testing of this structure is ongoing, but preliminary results for a single capacitor size show good correlation to literature values.

Fabrication of an interdigitated electrode structure first required that the optimum geometry be determined. To perform this optimization, a computer program developed by Huan Lee at Micromet Instruments, Inc. was obtained on a proprietary basis. The geometry variables within this program are the line width, the height of the IDE above the ground plane, the line thickness, the meander length between the combs, and the separation between lines. Figure 3.7 shows the geometry graphically. Relative change in gain of the response per change in dielectric constant was determined for each of the five varying line width. Calculations were done between a dielectric constant of 2.5 and 4. Table 3.6 lists typical data and calculated values for optimization of the line width.

Figure 3.8 shows the effect of line width on the relative change in gain per change in dielectric constant. The results show that the thinner the line width, the higher variation with dielectric constant. Two microns have been taken as the optimum value for fabrication as this is the minimum feature size available at Georgia Tech. The two micron line width requires four micron thick film above the IDE, that is, the film thickness must be two times the line width to prevent fringing into the air.

Figure 3.9 shows the effect of the thickness of the oxide layer on the gain per dielectric constant. There is a plateau in this graph and the optimum value is between 1mm and 1.5 mm. The maximum in this figure is the result of two competing electrical effects. At low heights above the ground plane, the electric field is primarily running through the ground plane and the gain is very low. At large heights above the ground plane, resonance with the ground plane decreases such that the value of the absolute gain of the signal decreases. This decrease causes the relative change in

**Table 3.5 Capacitor Data for PI-2545
with Correction for Edge Capacitance**

LOT 10B	PI-2545	RH=44.3%			
QUAD	POSITION	Capac.	DIELECTRIC	Edge	Dielectric
	(#)	(pF)	CONSTANT	Capacitance(pF)	Constant
	1	-	-	-	-
	2	57.2	3.8455	0.630652173	3.8031
	3	103	3.7529	0.808691892	3.7235
1	4	99.9	3.7972	0.798283256	3.7669
	5	568.5	3.8084	1.884612544	3.7958
	6	564.5	3.7642	1.888576768	3.7516
	7	1088.4	4.0006	2.522074761	3.9914
	1	30.5	4.0750	0.500885531	4.0080
	2	57.63	3.8241	0.639061944	3.7817
	3	103.4	3.9157	0.837916756	3.8840
2	4	-	-	-	-
	5	567.6	3.8869	1.84913474	3.8742
	6	577.8	3.9537	1.824620244	3.9412
	7	1086.9	4.0340	2.47390429	4.0248
	1	29.2	3.8621	0.485634535	3.7979
	2	56.1	3.9707	0.633579079	3.9259
	3	102.6	3.8545	0.843664891	3.8228
3	4	-	-	-	-
	5	563.3	3.8613	1.810013307	3.8489
	6	574.2	3.9436	1.816714362	3.9311
	7	1094	4.0450	2.473756255	4.0358
	1	29.5	3.6984	0.46038749	3.6406
	2	54	3.8574	0.60514204	3.8142
	3	106.1	3.8128	0.814064774	3.7836
4	4	105.5	3.7808	0.816106038	3.7516
	5	566.8	3.8241	1.84791353	3.8117
	6	567.4	3.7719	1.861453419	3.7595
	7	1101.4	4.0322	2.496616873	4.0231

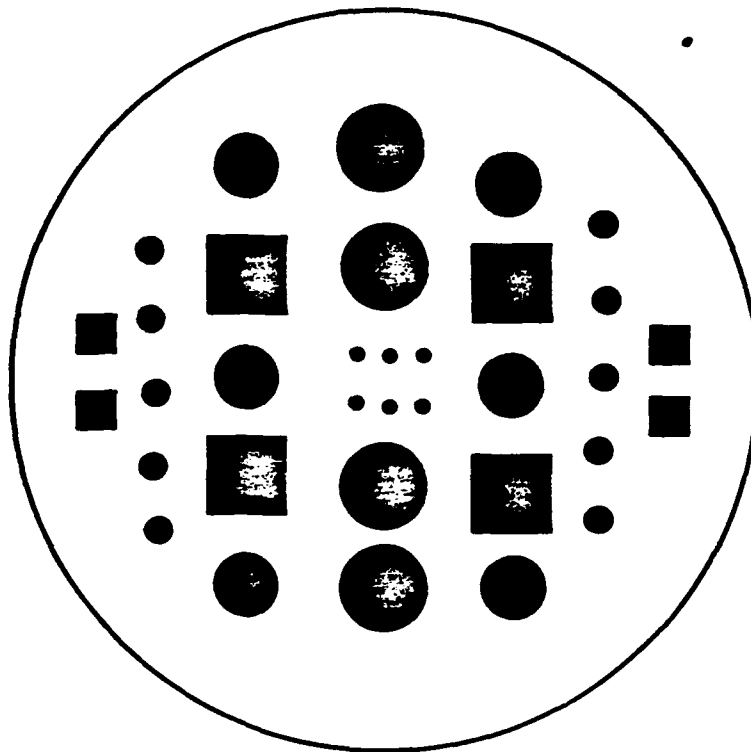
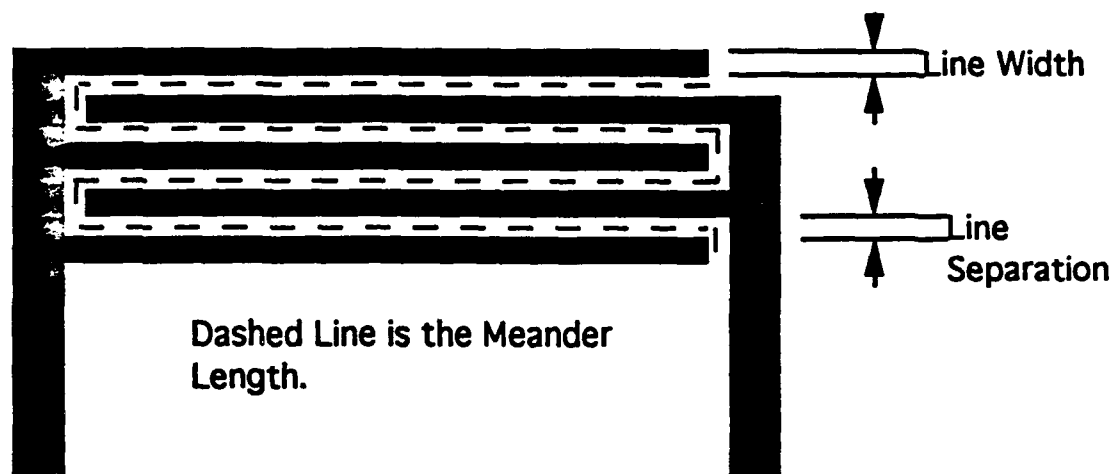
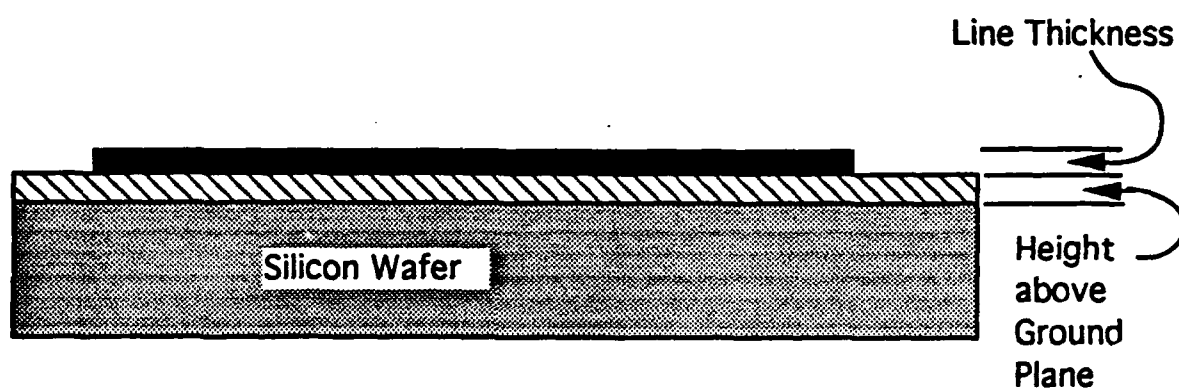


Figure 3.6 New-Style Capacitor Mask



Top View



Side View

Figure 3.7
Geometry of Interdigitated Electrode

Table 3.6 Effect of Line Width on Relative Gain

Width (μm)	Height (μm)	Thickness (μm)	Meander (cm)	E'	E''	Gain (dB)	Phase (deg)	Change in Gain per Change in E' (dB)	Avg. $\partial\text{Gain}/\partial\text{E}'$ (dB)	Avg. Gain (dB)	Relative ∂Gain per $\partial\text{E}'$ (dlm'less)
2.0	0.5	0.5	25	2.5	0	-22.89668	0	-3.10602	-2.63929	-20.69509	0.12753
				3.0	0	-21.34367	0	-2.59432			
				3.5	0	-20.04651	0	-2.21754			
				4.0	0	-18.93774	0				
2.5	0.5	0.5	25	2.5	0	-25.38147	0	-3.22870	-2.75099	-23.09139	0.11913
				3.0	0	-23.76712	0	-2.70292			
				3.5	0	-22.41566	0	-2.32134			
				4.0	0	-21.25499	0				
3.0	0.5	0.5	25	2.5	0	-27.41434	0	-3.30048	-2.81687	-25.07257	0.11235
				3.0	0	-25.76410	0	-2.76614			
				3.5	0	-24.38103	0	-2.38398			
				4.0	0	-23.18904	0				
3.5	0.5	0.5	25	2.5	0	-29.12899	0	-3.35308	-2.85955	-26.75170	0.10689
				3.0	0	-27.45245	0	-2.80302			
				3.5	0	-26.05094	0	-2.42254			
				4.0	0	-24.88397	0				
4.0	0.5	0.5	25	2.5	0	-30.60146	0	-3.38444	-2.88517	-28.20303	0.10230
				3.0	0	-28.90924	0	-2.82486			
				3.5	0	-27.49681	0	-2.44620			
				4.0	0	-26.27371	0				
4.5	0.5	0.5	25	2.5	0	-31.89038	0	-3.36736	-2.89337	-29.48778	0.09812
				3.0	0	-30.20670	0	-2.87570			
				3.5	0	-28.76885	0	-2.43706			
				4.0	0	-27.55032	0				
5.0	0.5	0.5	25	2.5	0	-33.03431	0	-3.37488	-2.91186	-30.63389	0.09505
				3.0	0	-31.34687	0	-2.85194			
				3.5	0	-29.92090	0	-2.50876			
				4.0	0	-28.66520	0				

Figure 3.8
Effect of Line Width on Relative Change
in Gain from Computer Simulation

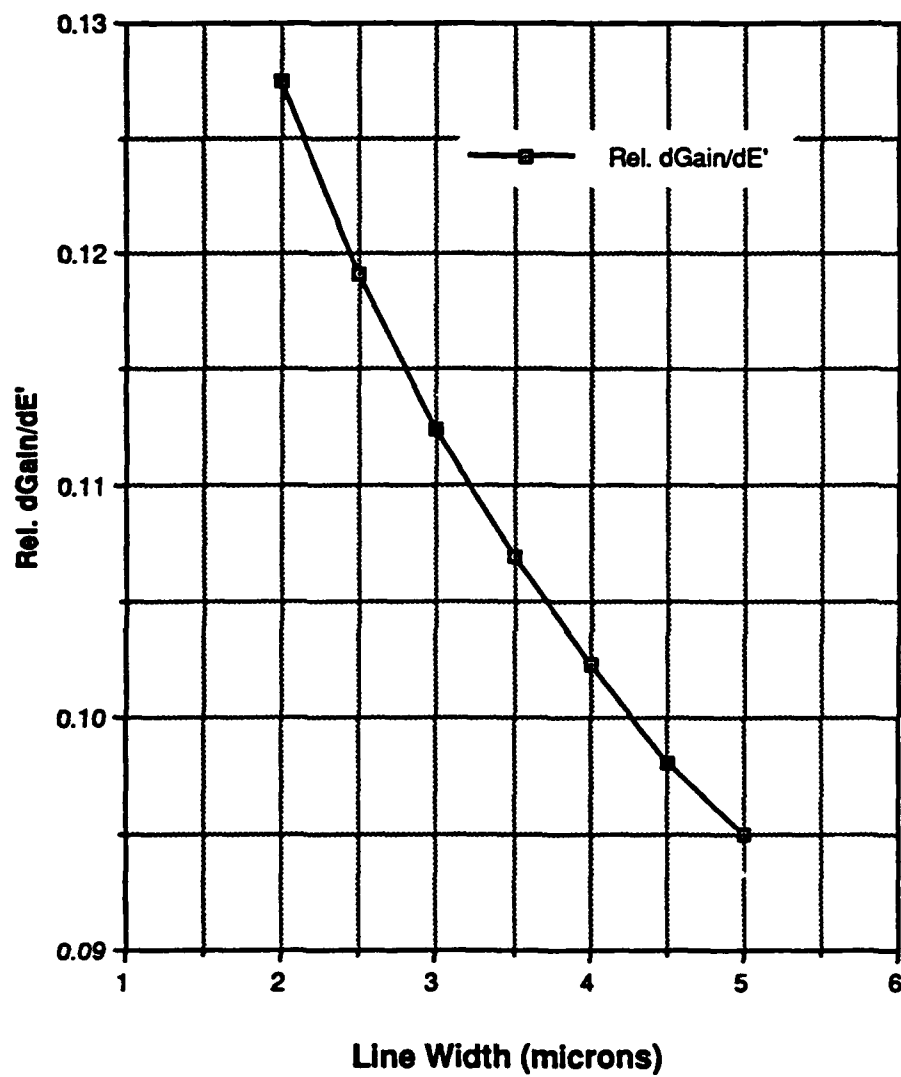
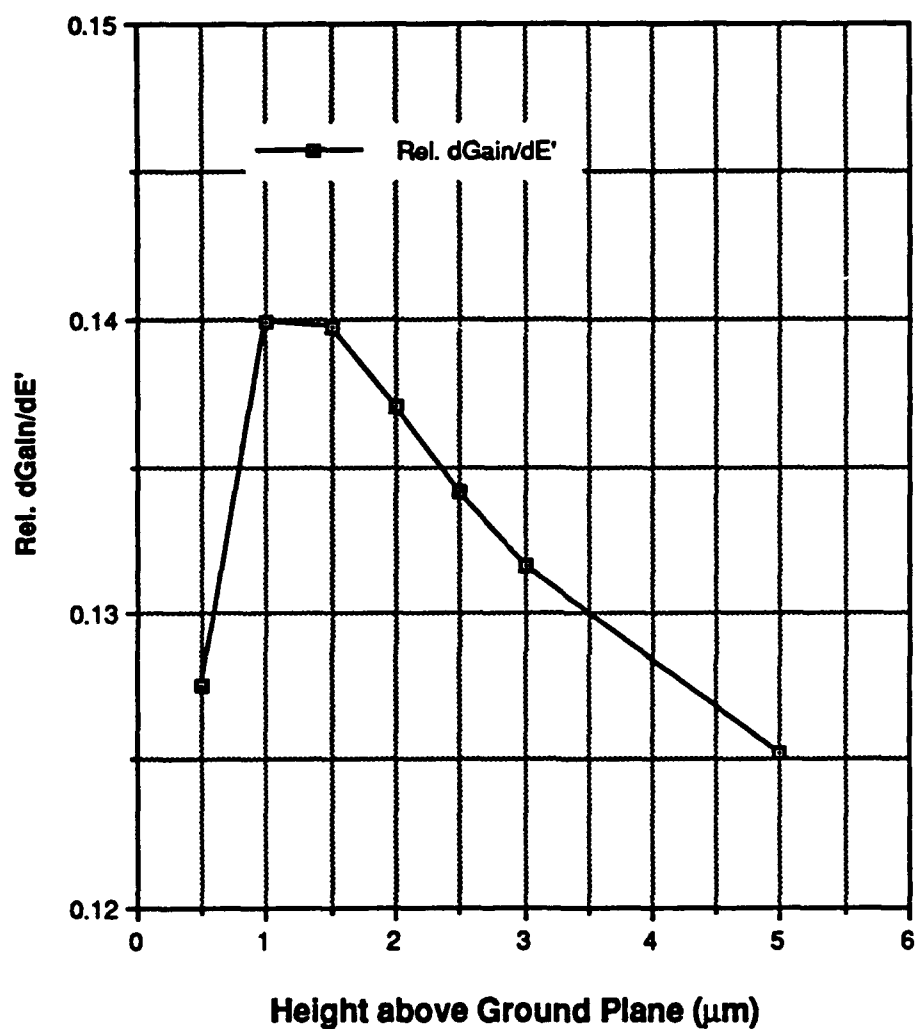


Figure 3.9
Effect of Oxide Layer Thickness on Relative
Change in Gain from Computer Simulation



gain with dielectric constant to decrease as the size of the gain decreases.

Figure 3.10 demonstrates the effect of the thickness of the lines on the relative change in gain with dielectric constant. The results show that the thicker the lines, the better the response. A maximum response occurs at the set maximum thickness of three microns. Three microns is the maximum thickness at which plating uniformity can be achieved. Therefore, optimum thickness is set at three microns.

Figure 3.11 shows the effect of meander length or IDE size. The response asymptotes at about 800 cm of meander. Increasing the meander length beyond 800 cm will increase the response only slightly while drastically increasing the size of the IDE. The optimum meander length is, therefore, set at 800 cm.

Figure 3.12 shows the effect of line separation on the response. The maximum occurs at about 0.7 microns, however such submicron features are impossible for fabrication at the Georgia Tech facility. At approximately two microns, there is a relatively flat area with increased response if slightly wider or narrower. Therefore, the line spacing is chosen to be the same as the line width at two microns.

From this optimization, an IDE structure is being fabricated, along with a parallel-plate capacitor, on masks by Microphase Laboratories in Albuquerque, NM. Fabrication of IDEs will begin on arrival of the masks.

Birefringence:

Use of the Metricon prism coupler to determine birefringence has been performed on five polymer materials. Figure 3.13 a shows birefringence for the five polymers. The first thing to notice is the much higher birefringence of the PI-2611D. This value is the result of the PI-2611D being a rigid rod polyimide which has a much higher orientation along the rods length than across the diameter. Interestingly, the PI-2611D has a higher birefringence than even liquid crystalline polymers. Figure 3.13 b shows the four polymers excluding PI-2611D. Of these four, PI-2555 has the highest birefringence, while the BCB has the lowest birefringence. PI-2555 and PI-2566 are expected to be more highly orientated than

Figure 3.10
Effect of Line Thickness on Relative Change
in Gain from Computer Simulation

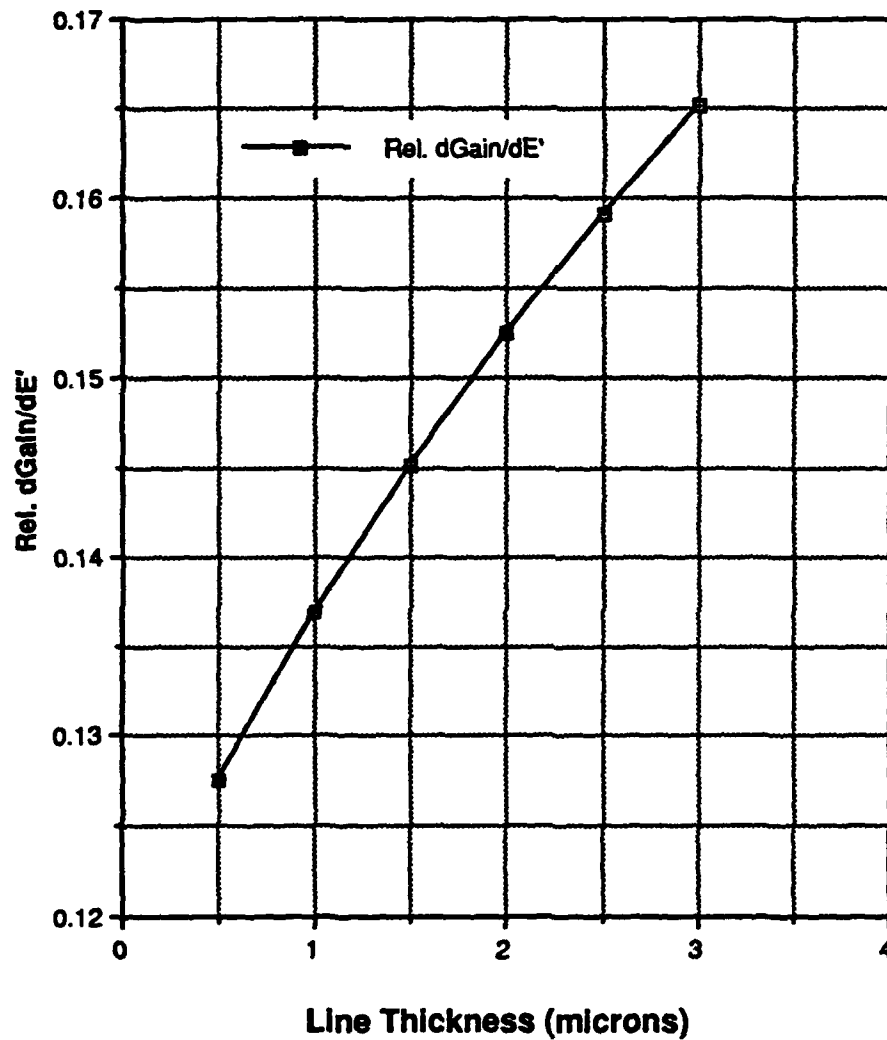


Figure 3.11
Effect of Meander Length on Relative
Change in Gain from Computer Simulation

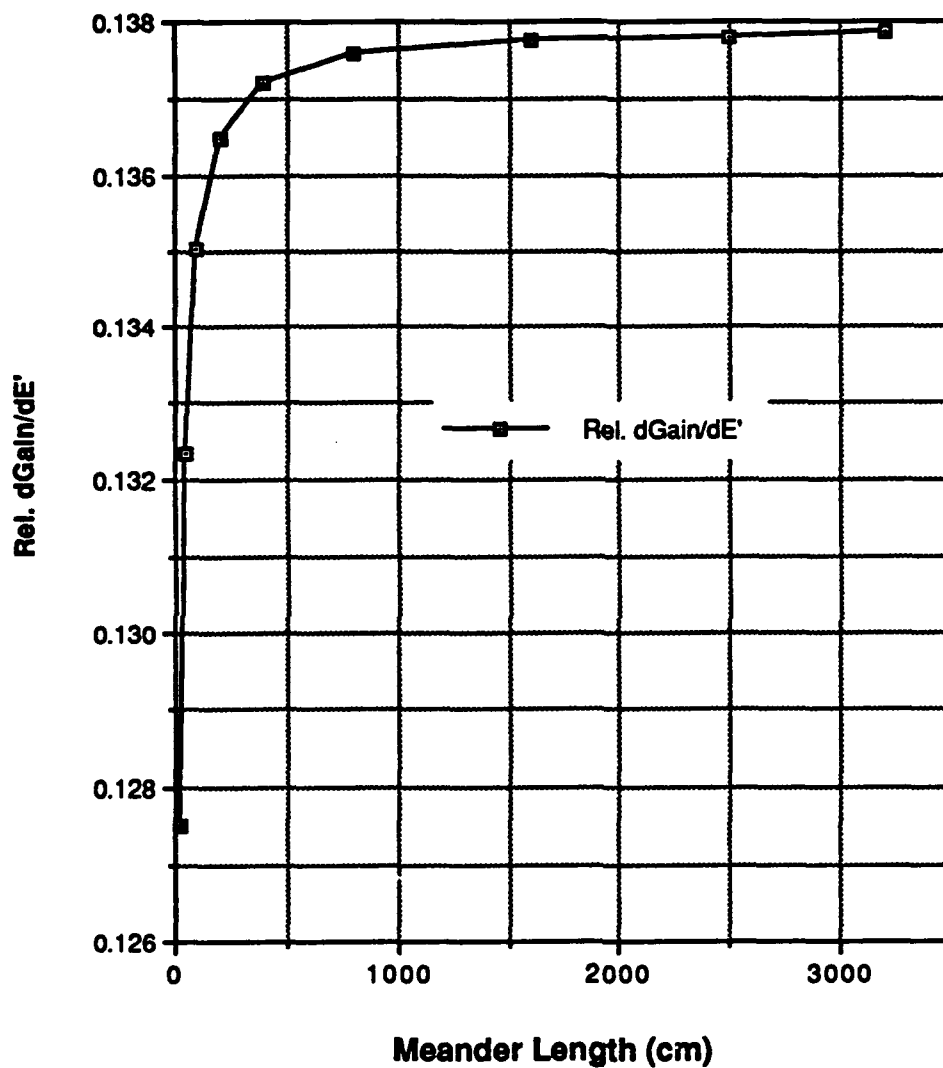


Figure 3.12
Effect of Finger Separation on Relative
Change In Gain from Computer Simulation

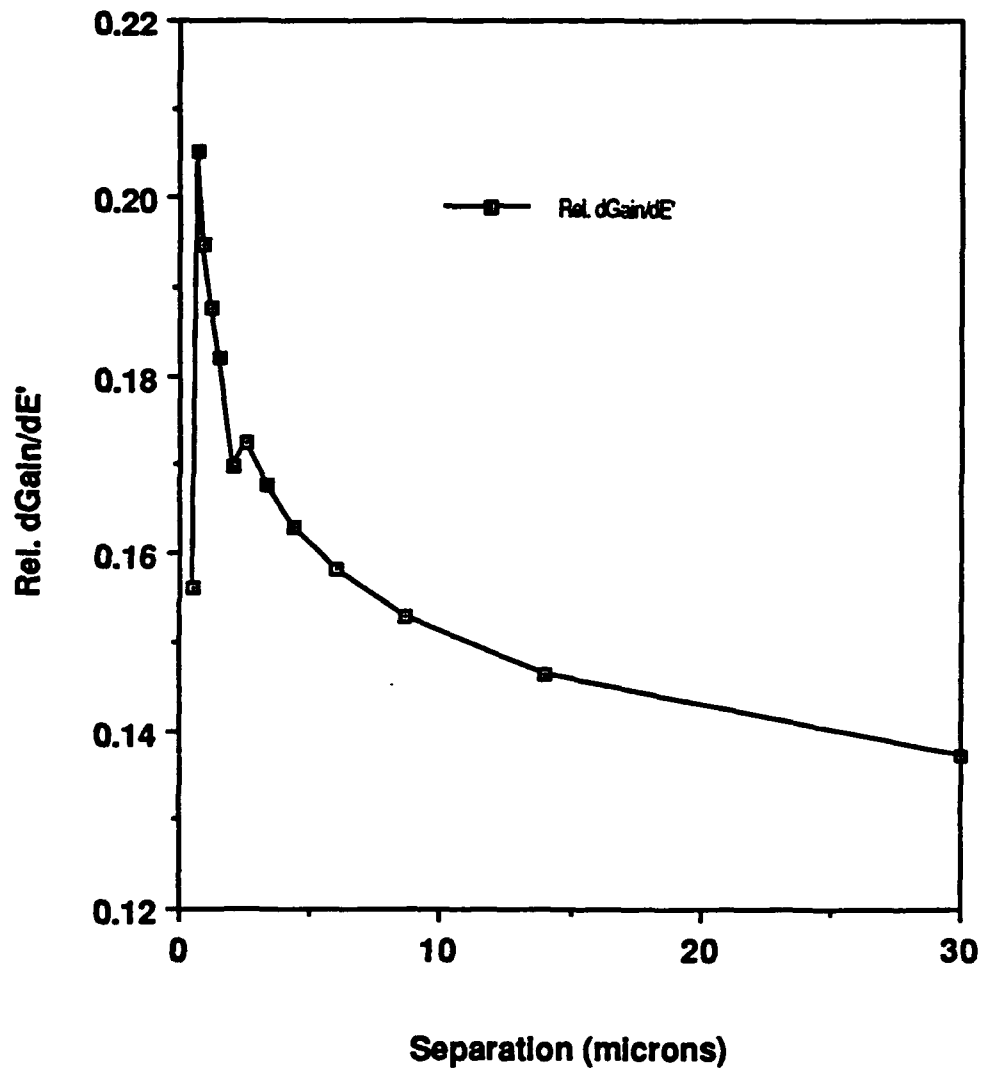


Figure 3.13 a. Birefringence of Five Polymers

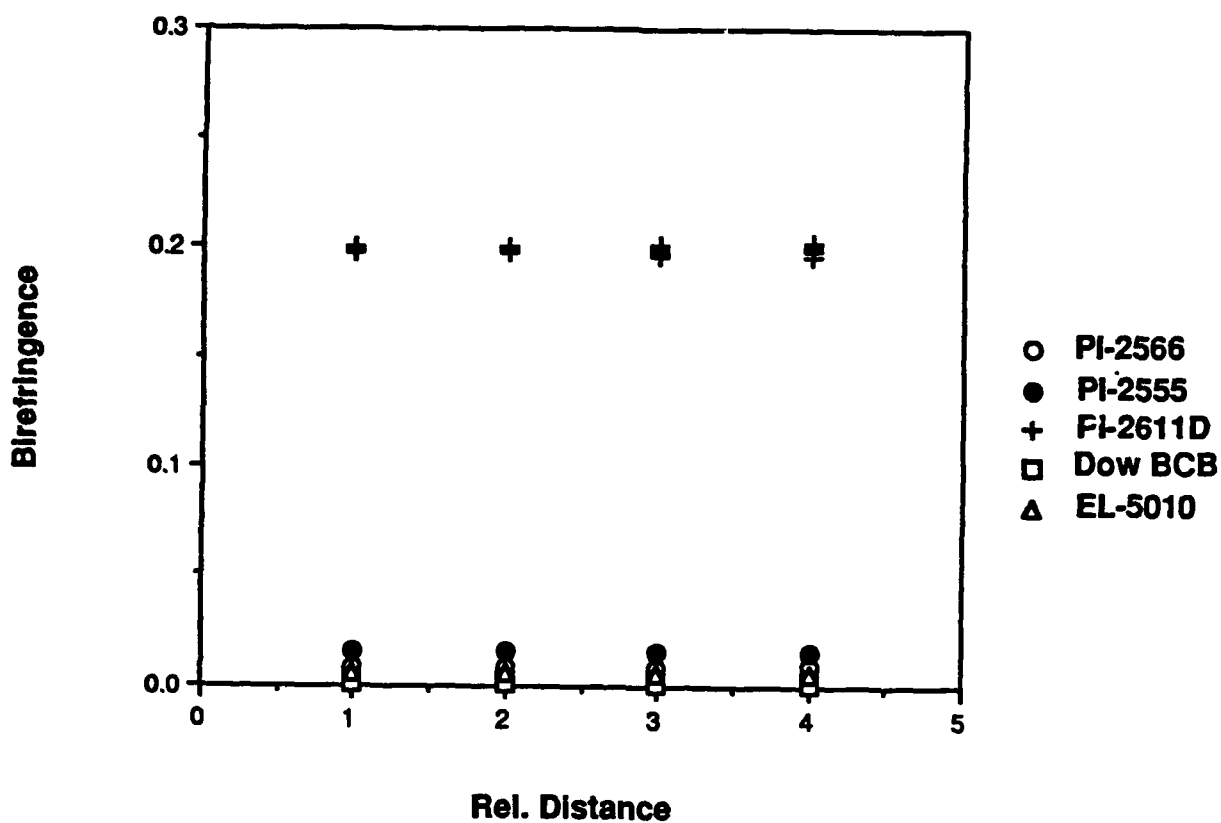
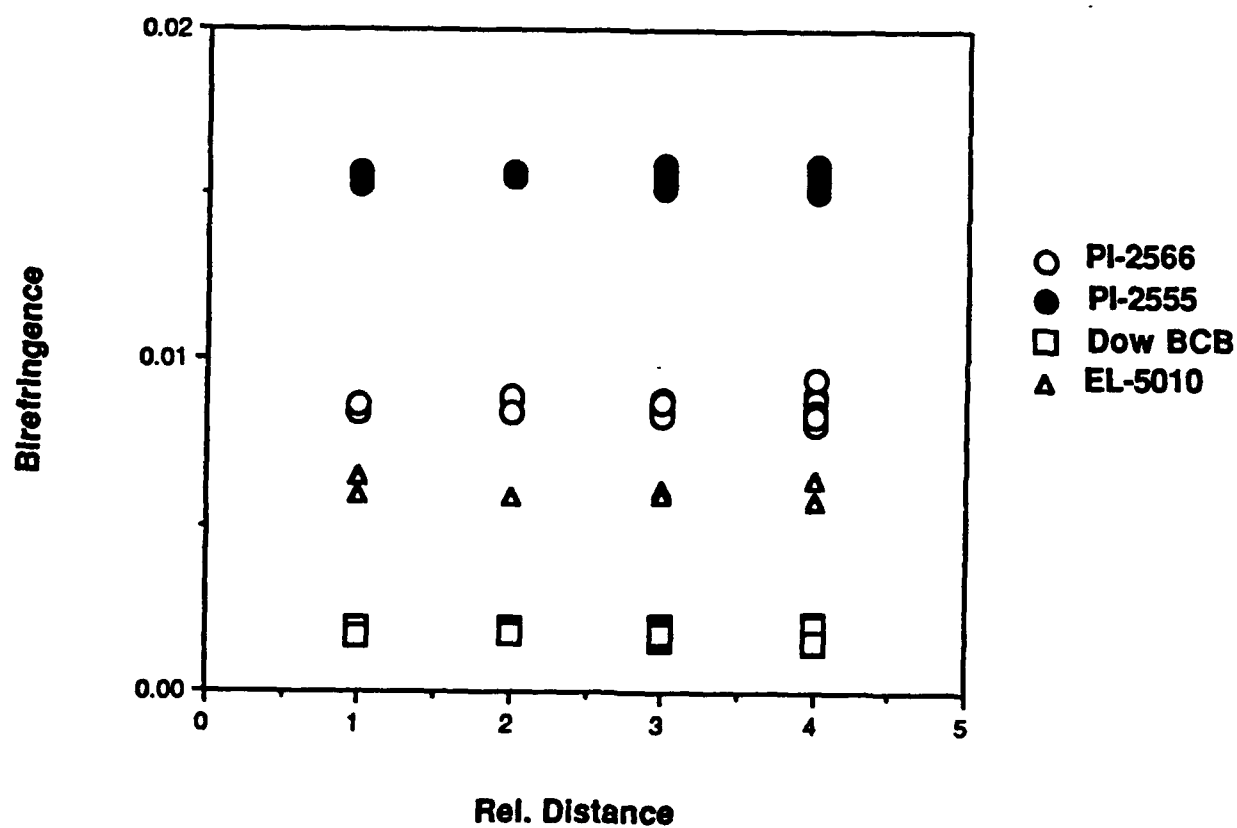


Figure 3.13 b. Birefringence of Polymers excluding PI-2611D



the other polymers because of the chemistry of the polyimide. Benzocyclobutene should be essentially unoriented and the birefringence data concurs with this statement.

Another item of interest is shown in Figure 3.14. This figure shows the consistency of the in-plane and out-of-plane refractive indices across the wafer at various points. This consistency indicates that the film is uniform on the wafer in all directions.

Mechanical Properties

The Flexus wafer curvature measurement system has been used to determine the film stress for BCB. The stress for 5.6 microns of BCB on silicon is 31.1 MPa. This value agrees with the statement that BCB has a lower residual stress than standard polyimides. A typical value for polyimide residual stress is about 40 MPa. Further data for the other polymers will be available in the very near future. CTE measurements using the Flexus are in progress, using silicon and aluminum as the two substrates. The through-plane mechanical property test structure will be fabricated on arrival of the masks.

3.2 Polyquinolines

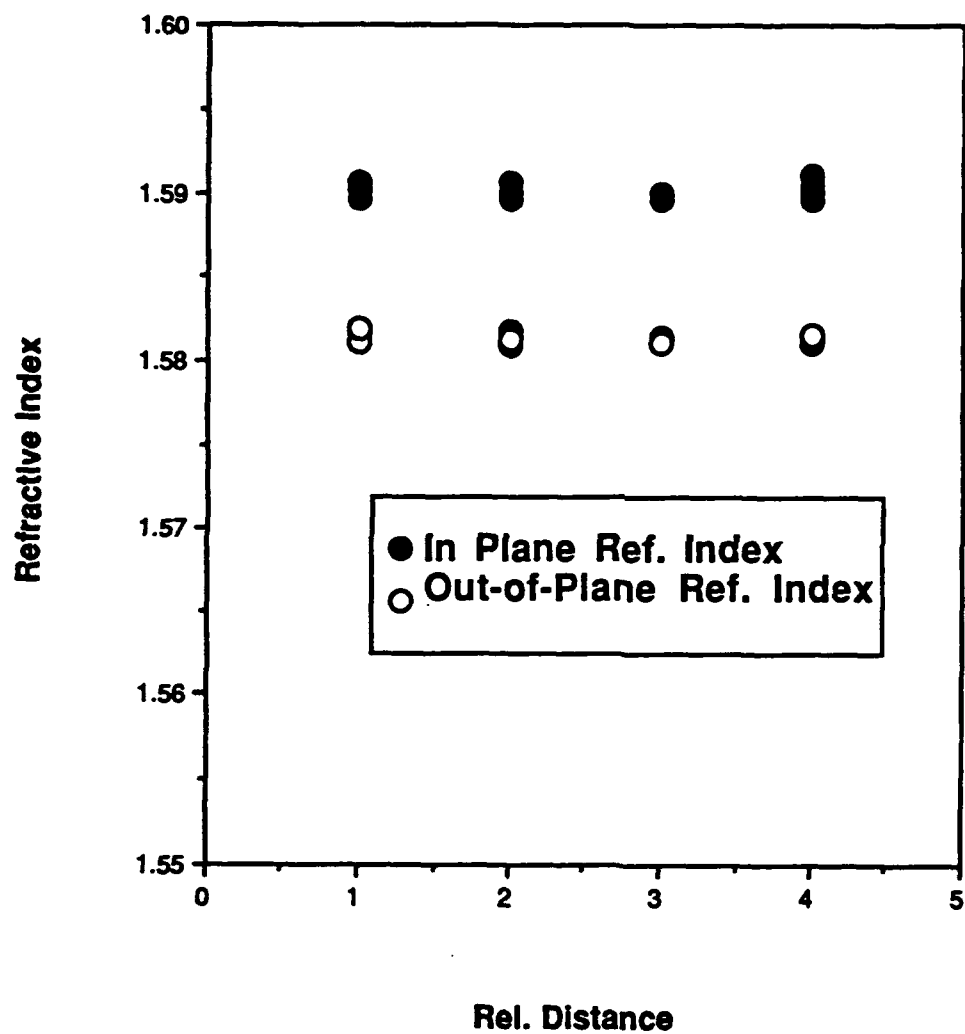
Purpose:

Polyquinoline is a low dielectric constant polymer with some desirable moisture and chemical properties. However, it has not been used previously in MCMs. The purpose of this study is to investigate its suitability for high performance MCMs.

Approach:

The electrical properties of the polymers at high frequencies will be measured by fabricating test structures that contain several sets of metal lines. These lines will be in the plane of the wafer as well as through the polymer film. Parallel plate capacitors will be used to measure the dielectric constant of the polymers at low frequencies. Residual stress and in-plane coefficient of thermal expansion stress are measured on a Flexus (F2320), which uses the wafer curvature to infer the stress in the wafer. These stress

Figure 3.14 In-Plane and Out-of-Plane Index of Refraction for PI-2566



measurements were carried out over a range of temperatures. The thickness of the polymer films were measured using a Metricon prism coupler.

Results and Conclusions:

Polyquinolines are reported to have a low dielectric constant, low residual stress and low water absorption. Thus, the first step is to produce capacitor test wafers. These are made by sputtering a layer of gold on a 4 inch silicon wafer, followed by spin coating the polymer and curing it. Then, the top plate of the parallel plate capacitor is patterned from gold deposited above the polymer layer. The surface area of the top plate of the capacitor as well as the thickness of the polymer film near the capacitor are measured. The capacitors are then electrically probed. The measured dielectric constant is 2.94 (see table 3.7), which is slightly higher than the 2.8 value that was reported by Maxdem.

The stress of the polyquinoline film is also measured. The uncured wafer was first taken from 24°C to the recommended cure temperature of 350°C, held at this temperature for one hour and then brought back down to 24°C. Stress measurements were taken throughout the whole cycle. From Figure 3.15 we can see that the final stress after curing is higher than before curing. The final value for the stress at 24°C is 40.7 MPa which is twice as high as that reported by the manufacturers. This source of this discrepancy is currently under investigation.

Future Work:

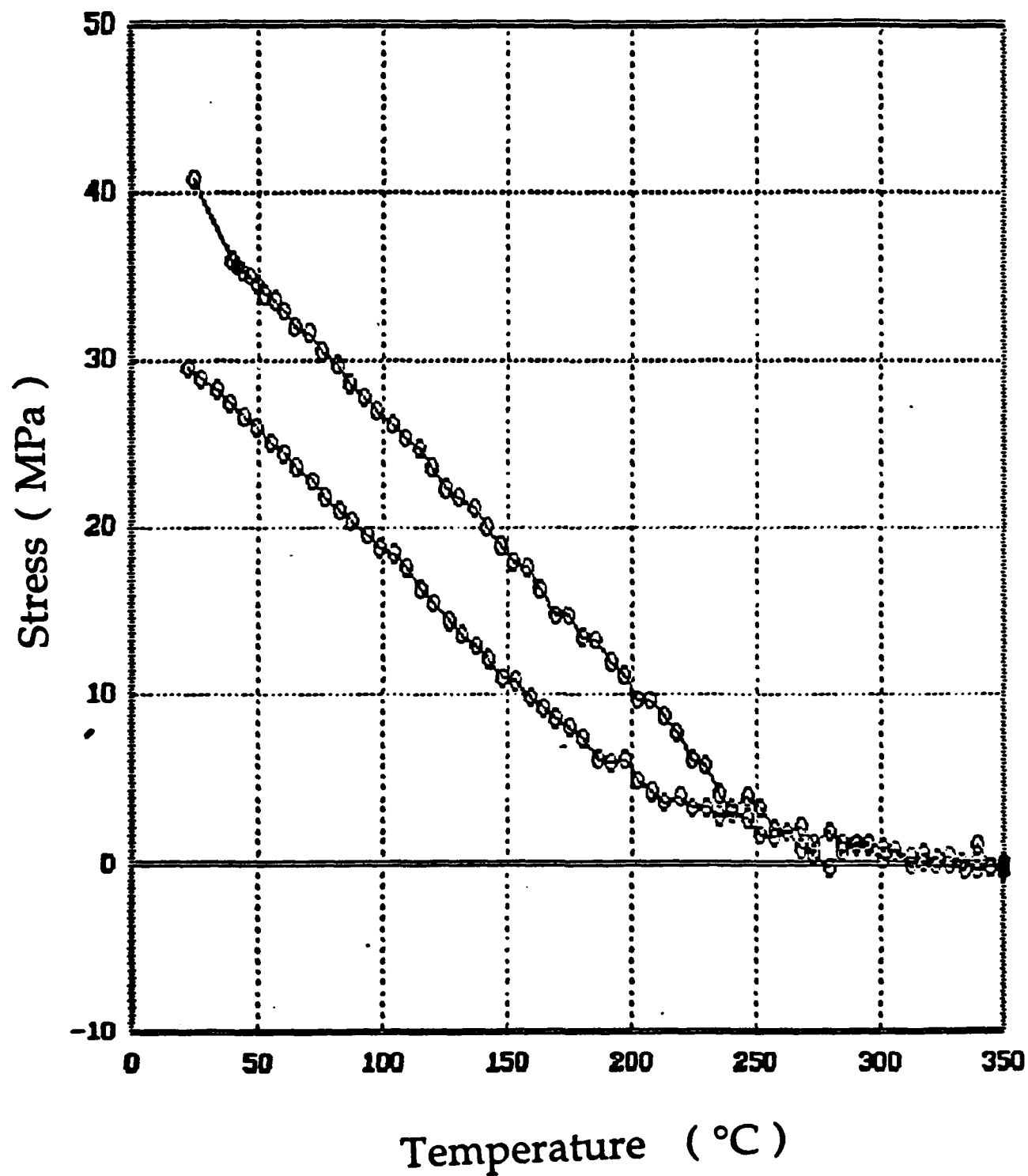
Future experiments include:

- to quantitatively measure the effects of moisture on the electrical properties in the polymer films.
- to measure the effect on final cure temperature on the residual stress and electrical properties.
- to measure the electrical properties at high frequencies.

Table 3.7 Dielectric Constant for Polyquinoline.

Diameter μm	Sides μm	Area μm^2	Capacitance nF	Thickness μm	Dielectric	Average
1807		2.565E+06	0.0152	4.90	3.28	
1900		2.835E+06	0.0164	4.90	3.20	
1813		2.582E+06	0.0152	4.90	3.26	
1816		2.590E+06	0.0152	4.90	3.25	
1813		2.582E+06	0.0158	4.90	3.39	
						3.28
3552		9.909E+06	0.0529	5.24	3.16	
3660		1.052E+07	0.0548	4.99	2.94	
3612		1.025E+07	0.0551	5.02	3.05	
3681		1.064E+07	0.0542	5.24	3.02	
3634		1.037E+07	0.0496	5.08	2.75	
3590		1.012E+07	0.0509	5.08	2.89	
3602		1.019E+07	0.0489	5.24	2.84	
3694		1.072E+07	0.0502	5.25	2.78	
						2.93
8534		5.720E+07	0.2945	5.08	2.96	
8551		5.743E+07	0.3042	4.90	2.93	
8452		5.611E+07	0.2910	5.08	2.98	
8427		5.577E+07	0.2680	5.25	2.85	
8451		5.609E+07	0.2997	4.89	2.95	
						2.93
11529		1.044E+08	0.5285	5.08	2.91	
11617		1.060E+08	0.5600	4.91	2.93	
11587		1.054E+08	0.5586	4.91	2.94	
11588		1.055E+08	0.5513	4.98	2.94	
						2.93
5182	5203	2.696E+07	0.1330	5.37	2.99	
5305	5235	2.777E+07	0.1356	5.37	2.96	
5202	5217	2.714E+07	0.1281	5.50	2.93	
5293	5224	2.765E+07	0.1308	5.50	2.94	
						2.96
10467	10496	1.099E+08	0.5789	4.98	2.97	
10526	10526	1.108E+08	0.5807	4.91	2.91	
10482	10467	1.097E+08	0.5809	4.91	2.94	
10496	10496	1.102E+08	0.5821	4.98	2.97	
						2.95

Figure 3.15 Curing Cycle for Polyquinoline PQ100/350.



3.3 Photodefinable Polyimides

Purpose:

Photosensitive polyimides are the simplest insulators to process for interlayer dielectrics in MCMs. Since a majority of the cost of an MCM is in processing, they are often viewed as the low cost alternative. However, photodefinable materials are expensive and a number of the desirable properties of insulators (Table 3.1) are sacrifices. The purpose of this study is to investigate the processing-performance trade-offs. Photodefinable polyimides can be classified into two major groups: those that require a high temperature cure to convert the photocrosslinked intermediate to the fully imidized final product, and those that are preimidized as well as photosensitive and do not require a high temperature cure. Three separate commercially available products were evaluated for superior processing, mechanical, and electrical characteristics. Of the three products, two were of the non-preimidized class (Amoco Ultradel 7501, Ciba-Geigy Probimide 349), and one was of the preimidized class (Ciba-Geigy Probimide 412).

Approach:

The evaluation of each of the three commercial products was organized under three main criteria: processing performance, mechanical performance, and electrical performance. In terms of processing performance, the figures of merit included shelf-life, cost, physical ease and reproducibility of processing, percent shrinkage upon final cure, and via hole wall profiles. In terms of mechanical performance, the figures of merit included the residual stress upon cure, adhesion to gold metallization, degree of planarization, and the percent moisture uptake. Finally, in electrical performance, the figure of merit was mainly the dielectric constant of the material. In every single criteria listed above, the cure cycle played a dominant role in the resulting film properties.

Results:

The preliminary results obtained indicate that very little, if any, sacrifices in material performance are endured in return for the convenience of photodefinability. Immediately below will be found

individual summaries on each product's strengths and weaknesses, and Tables 3.8-3.10 summarize the data collected over the past year. The dielectric constant and residual stress are summarized in Figures 3.16 and 3.17.

Ciba-Geigy Probimide 349

In terms of processing performance, the Ciba-Geigy Probimide 349 ranked as the least desirable product. Soft bake times were on the order of two hours, and the soft baked film was very susceptible to damage during the soft contact on the mask aligner. In addition, the wall profiles displayed heavily rounded corners and edges, and wall slopes of better than 60° could not be obtained due to the 55% shrinkage that occurred during the cure. Perhaps the worst attribute was the opaqueness upon final cure. Even curing the film in a nitrogen atmosphere could not prevent the film from turning such a dark color as to preclude this product from any applications where pattern alignments are required. For this reason, the evaluation of the mechanical and electrical performance of this material was not pursued.

Amoco Ultradel 7501

In terms of overall material performance, the Amoco Ultradel 7501 delivered all the advantages of photodefinability in conjunction with superb processing, mechanical, and electrical characteristics. The spin coatings were effortless and produced very uniform and reproducible films. The shelf-life of this material is indefinitely at 4°C, and six months at room temperature. The soft bake times were under twenty minutes, the material displayed excellent adhesion to the gold metallization, and the wall profiles and slopes were sharp and nearly vertical. The sharp, vertical wall profiles were possible due to the less than 10% shrinkage the film experienced during the cure. Above approximately 200°C, the percent shrinkage and wall profiles became independent of the final cure temperature. The residual stress proved to be a function of the final cure temperature, with the fully cured, transparent film displaying a residual stress of 42.0 MPa. In addition, upon subsequent reheating cycles the film displayed complete elasticity as long as the highest temperature the film was previously processed at was not exceeded. The dielectric constant of the material also proved to be a function of the final cure temperature with the fully cured, transparent film displaying a dielectric constant of 3.15.

Data Table 3.8: Residual Stress

Ultradel 7501	
Cure Temp (°C)	Residual Stress (MPa)
100	29.8
150	31.3
250	35.0
300	38.9
350	42.0
400	42.0

Probimide 412	
Cure Temp (°C)	Residual Stress (MPa)
100	25.5
150	32.4
250	33.8
300	35.3
350	34.7
400	34.9

**Data Table 3.9: Dielectric Constant
Ciba-Geigy Probimide 412**

Cure Temp:	Capacitan ce	Thickness	E'		
150 °C	(nF)	(mm)			
1	0.2672	10.10	3.22261		
2	0.2662	10.00	3.17876		
3	0.2657	10.10	3.20452	Avg	3.19106
4	0.2656	9.95	3.15574		
5	0.2648	10.10	3.19366		
Cure Temp:	Capacitan ce	Thickness	E'		
250 °C	(nF)	(mm)			
1	0.2576	10.42	3.20526		
2	0.2572	10.40	3.19414		
3	0.2584	10.35	3.19361	Avg	3.20006
4	0.2572	10.42	3.20028		
5	0.2570	10.45	3.20700		
Cure Temp:	Capacitan ce	Thickness	E'		
300 °C	(nF)	(mm)			
1	0.3084	8.47	3.11923		
2	0.3083	8.47	3.11822		
3	0.3148	8.40	3.15765	Avg	3.12666
4	0.3072	8.50	3.11810		
5	0.3074	8.50	3.12013		
Cure Temp:	Capacitan ce	Thickness	E'		
350 °C	(nF)	(mm)			
1	0.3122	8.40	3.13157		
2	0.3125	8.40	3.13458		
3	0.3133	8.50	3.18001	Avg	3.14911
4	0.3120	8.45	3.14819		
5	0.3123	8.45	3.15122		

**Data Table 3.10: Dielectric Constant
Amoco Ultradel 7501**

Cure Temp:	Capacitan	Thickness	E'		
150 °C	ce	(mm)			
	(nF)				
1	0.3035	9.70	3.51544		
2	0.3033	9.65	3.49502		
3	0.3037	9.70	3.51776	Avg	3.49927
4	0.3031	9.65	3.49271		
5	0.3016	9.65	3.47543		
Cure Temp:	Capacitan	Thickness	E'		
250 °C	ce	(mm)			
	(nF)				
1	0.2943	9.56	3.35968		
2	0.2958	9.56	3.37680		
3	0.2981	9.50	3.38170	Avg	3.37147
4	0.2954	9.56	3.37224		
5	0.2968	9.50	3.36695		
Cure Temp:	Capacitan	Thickness	E'		
300 °C	ce	(mm)			
	(nF)				
1	0.2786	9.65	3.21039		
2	0.2785	9.60	3.19261		
3	0.2794	9.65	3.21961	Avg	3.20042
4	0.2785	9.60	3.19261		
5	0.2780	9.60	3.18688		
Cure Temp:	Capacitan	Thickness	E'		
350 °C	ce	(mm)			
	(nF)				
1	0.2683	9.70	3.10772		
2	0.2680	9.80	3.13625		
3	0.2691	9.90	3.18125	Avg	3.15221
4	0.2690	9.90	3.18007		
5	0.2683	9.85	3.15578		

Figure 3.16

E' vs. Final Cure Temperature

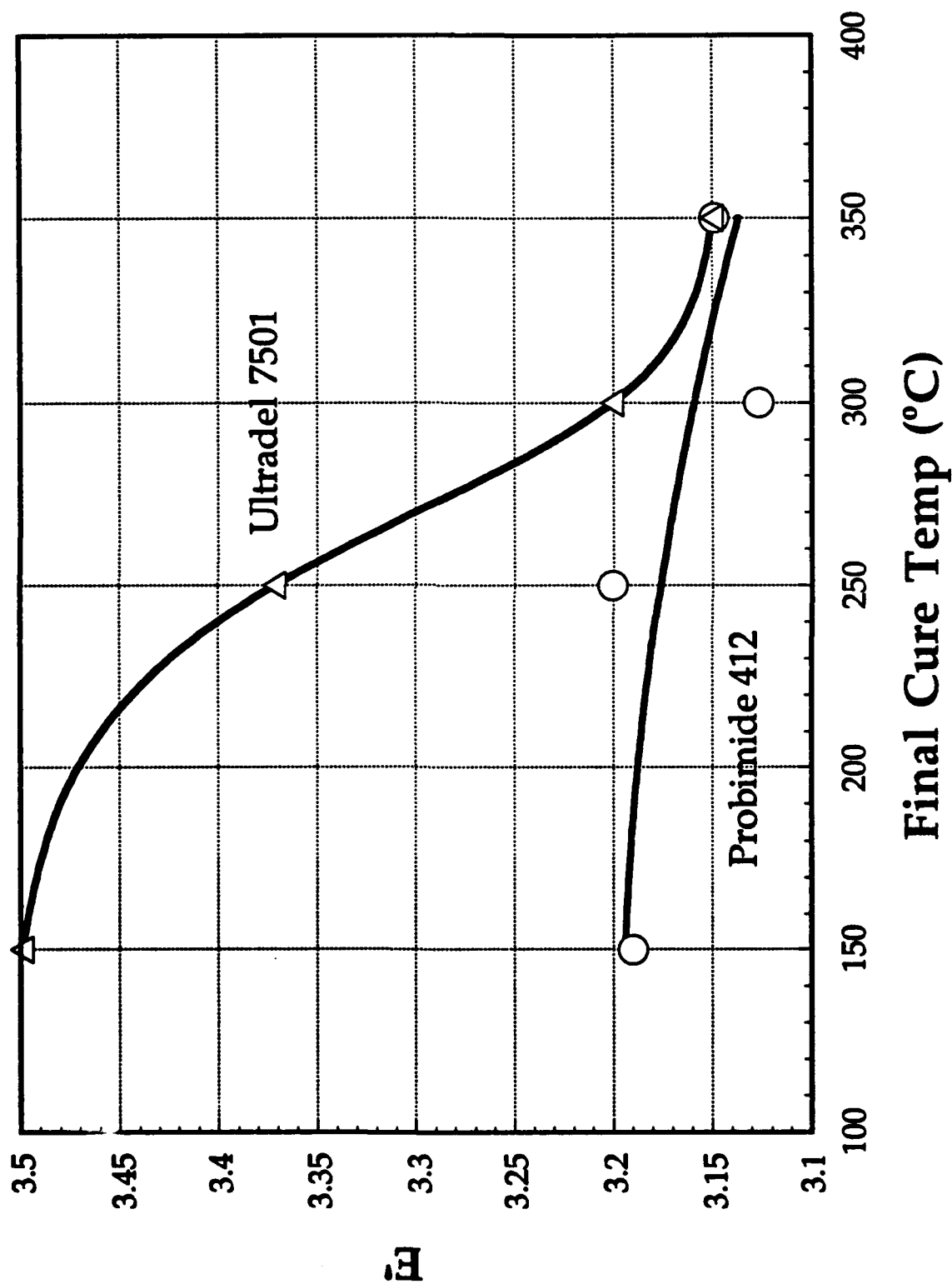
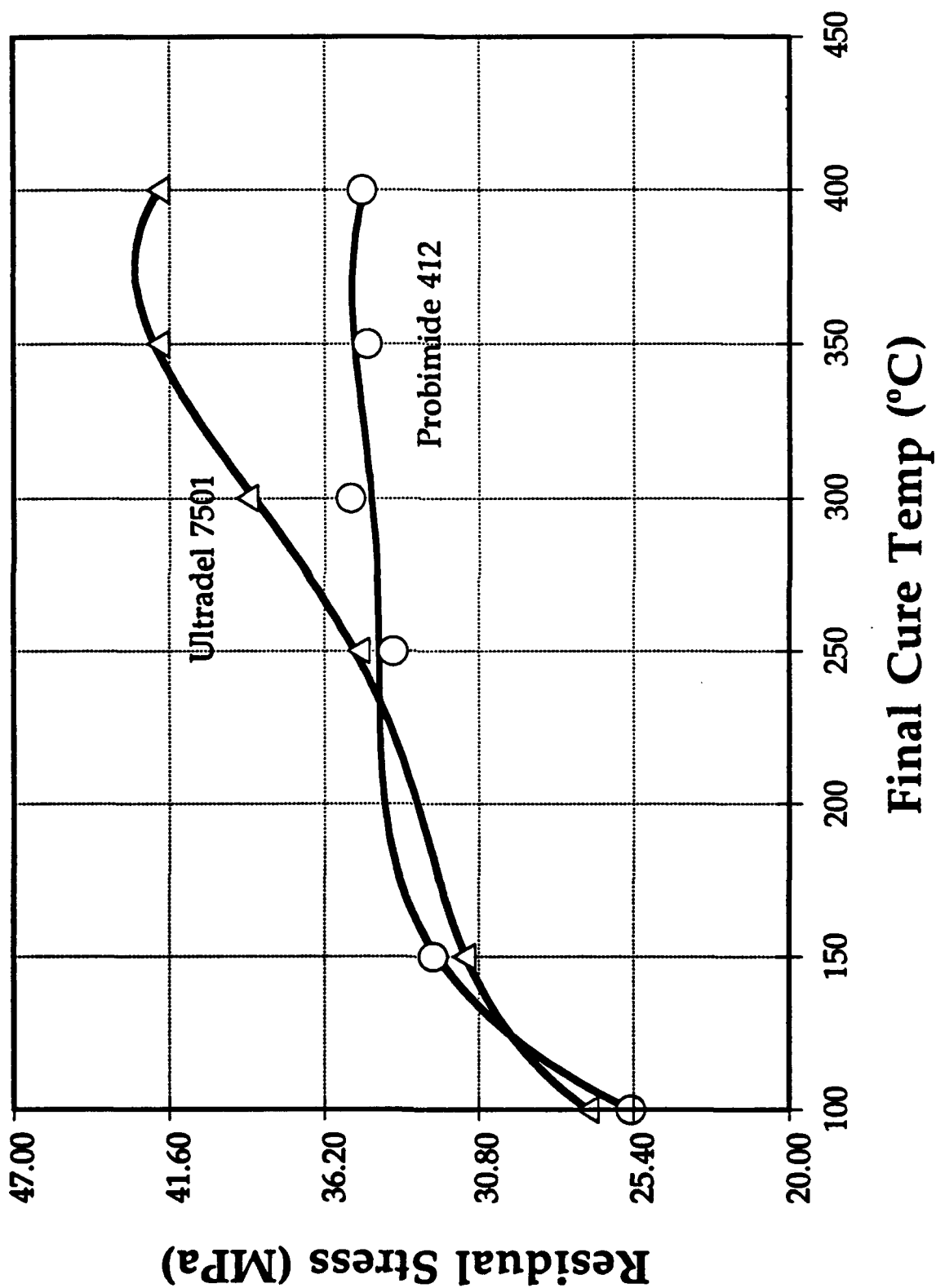


Figure 3.17

Residual Stress vs. Final Cure Temp



Ciba-Geigy Probimide 412

In terms of overall material performance, the Ciba-Geigy Probimide 412 also delivered all the advantages of photodefinability in conjunction with superb processing, mechanical, and electrical characteristics. In addition, the preimidized attribute of the product resulted in some very advantageous low temperature processing capabilities. The spin coatings were also effortless and produced uniform and reproducible films. Since the product is preimidized, the shelf-life of this material is indefinitely at room temperature. The soft bake times were also under twenty minutes, the material displayed excellent adhesion to the gold metallization, and the wall profiles and slopes were also sharp and nearly vertical. The sharp, vertical wall profiles were possible due to the less than 10% shrinkage the film experienced in the cure. Above approximately 200°C, the percent shrinkage and wall profiles become independent of the final cure temperature. Unlike the Amoco product, the residual stress proved to be nearly independent of the final cure temperature and was measured to be 35.0 MPa. In addition, upon subsequent reheating cycles the film displayed complete elasticity as long as the highest temperature the film was previously processed at was not exceeded. The dielectric constant of the material also proved to be nearly independent of the final cure temperature, and was measured to be 3.15. The fact that the residual stress and dielectric constant were nearly independent of the final cure temperature introduces the possibility of low temperature processing with this material that is simply not an option with the non-preimidized materials.

Conclusions and Unresolved Questions:

The Ciba-Geigy Probimide 349 is not a suitable material for multi-chip modules due to its opaqueness upon final cure. The manufacturer stated that curing in a good vacuum might alleviate this problem, but even if a transparent film could be obtained the poor wall profiles and slopes, as well as the temperamental processing characteristics, preclude its recommendation. The Amoco Ultradel 7501 and the Ciba-Geigy Probimide 412 both represent all the advantages of a photodefinable product and can match nearly any non-photosensitive product in their processing, mechanical, and electrical properties. However, the preimidized Ciba-Geigy Probimide 412 holds the added dimension of possible low temperature processing, and thus it receives the highest recommendation of the three.

A few questions remain unresolved. First of all, the degree of planarization and percent moisture uptake have yet to be investigated. The percent moisture uptake will be investigated using the films already prepared for the residual stress measurements, and the very low percent shrinkage of the two recommended products almost assures a degree of planarization of nearly 100%. Secondly, residual stress curves for all the materials need to be investigated at low temperatures (around 77K) for applications in high-temperature superconducting devices. Thirdly, complete multi-chip module test structures should be fabricated to explore the electrical properties of the materials in more detail, including the dielectric constant of the materials as a function of water uptake and device temperature. And lastly, the possible problems associated with a multi-layered device using the Ciba-Geigy Probimide 412 needs to be investigated. Since no chemical reaction is taking place during the cure for this preimidized product, subsequent coatings could partially dissolve the bottom layers at the layer interface.

3.4. Low Temperature Measurements

Purpose:

The purpose of this task is to investigate low temperature mechanical properties of polymer interlevel dielectric films. Interlevel dielectrics able to withstand low temperatures and continual temperature cycling without cracking may be valuable in subambient applications and HTSC devices.

Ciba-Geigy Probimide series pre-imidized polymers may be a particularly useful as an interlevel dielectric for low temperature applications. Since the material is pre-imidized prior to spin-coating, a lower level of stress may be achieved over some of the thermal imidized polyimides. In addition, the Probimide Series can be processed at relatively low temperatures (i.e. $< 250^{\circ}\text{C}$). This is beneficial, since many of the materials used in HTSCs are damaged at high temperatures.

This study will focus on the effect of variations in processing conditions on residual stress in thin films. In addition, techniques

will be developed to measure the modulus and coefficient of thermal expansion of the polymer at subambient temperatures.

Approach:

The stress measurements were performed on a Flexus (F2320) which uses the wafer curvature to infer the residual stress in the wafer. These stress measurements were carried out over a range of temperatures. The thickness of the polymer films were measured using a Metricon prism coupler.

Micromachined structures (i.e. cantilever beams, load-deflection structure and vibrating strings) are currently being adapted to be used in a liquid nitrogen Dewar for in-situ measurement of the modulus and coefficient of thermal expansion under subambient conditions.

Results:

Ciba-Geigy polyimide Probimide 293 (preimidized) was cured at different temperatures to study the effects of temperature on the residual stress in the polymer. The films were prepared by first spinning an adhesion promoter at 2000 rpm for 60 seconds followed by spinning on the polymer at 5000 rpm for 30 seconds. Next the wafers were placed in a convection oven and soft baked at 120°C for 15 min. The hard baking (curing) and stress measurements were obtained simultaneously on the Flexus. For a curing cycle, the wafer is taken from 24°C to the desired final cure temperature, held at that temperature for 5 hours, and brought back down to 24°C. The effects of temperature cycling on the stress were also studied by reheating the wafer several times (3) up to the final cure temperature and bringing back down to room temperature. Figure 3.18 is for a final cure temperature of 250°C. After the initial cure, there is a noticeable relaxation in the stress. However, there is no significant change in the stress for the temperature cycling that follows. Since the Probimide 200 series are preimidized, there are no reactions (cross linking) occurring, and the purpose of the hard bake is to drive the solvent off which explains the relaxation in the stress for the initial cure, and its absence in the temperature cycling. This trend is seen in all the wafers processed regardless of the final curing temperature (see figures 3.19 and 3.20). For the wafer cured at 250°C, the stress was 31.5 MPa at 44°C and 3.3 MPa at 250°C. For the wafer cured at 120°C, the stress was 29.2

Figure 3.18 Curing and Temperature Cycling for PB293/250.

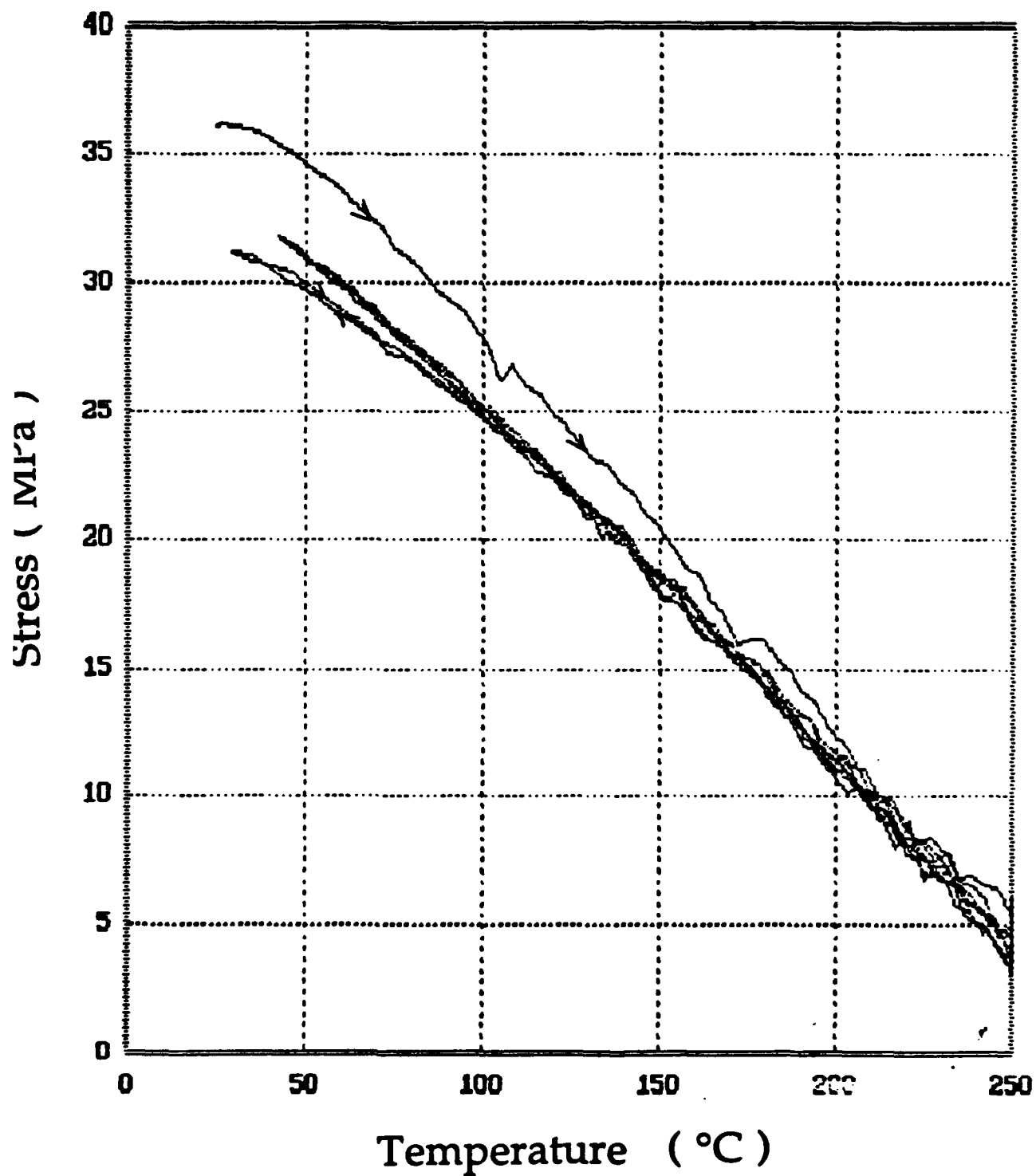


Figure 3.19 Curing and temperature cycling for PB293/120.

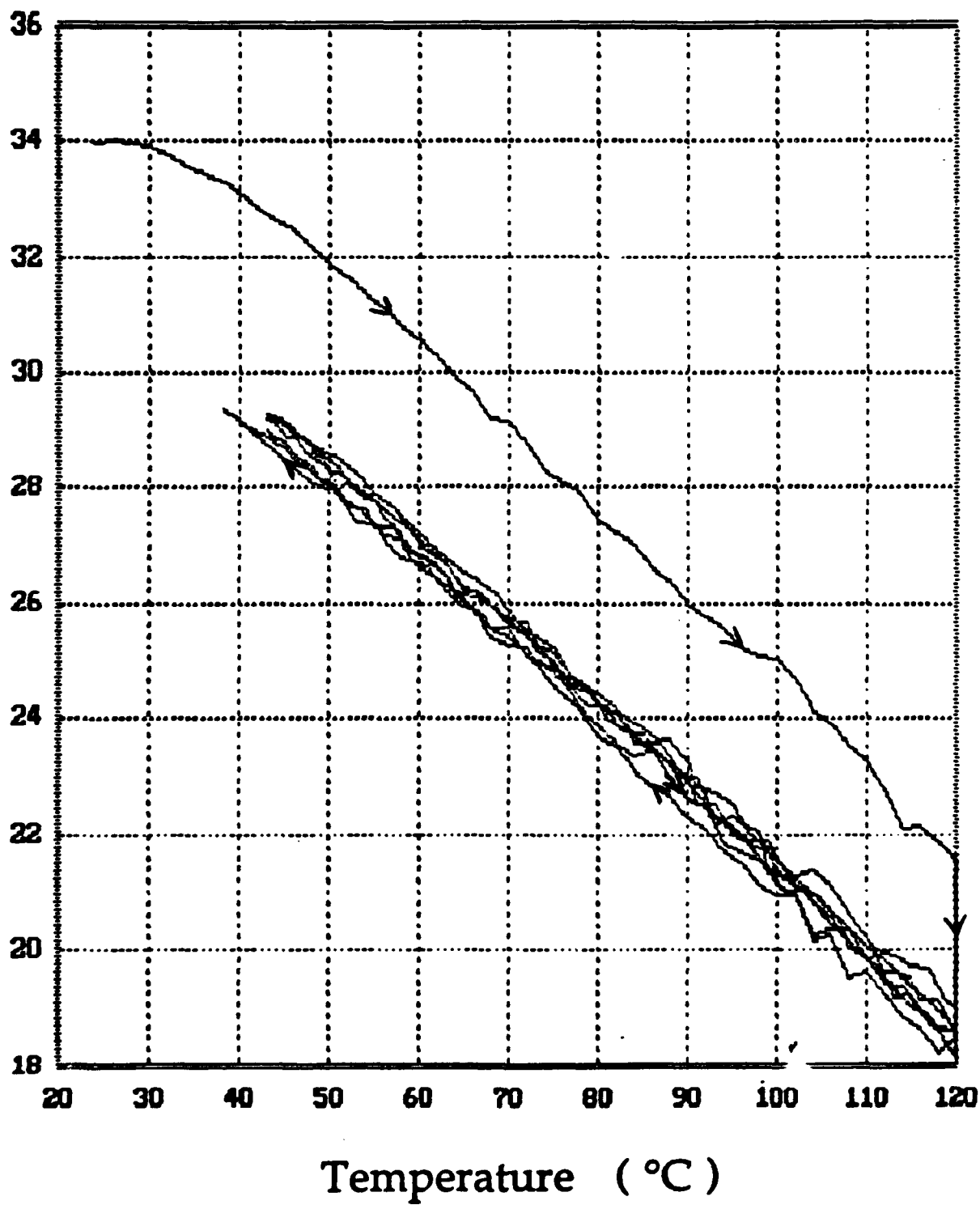
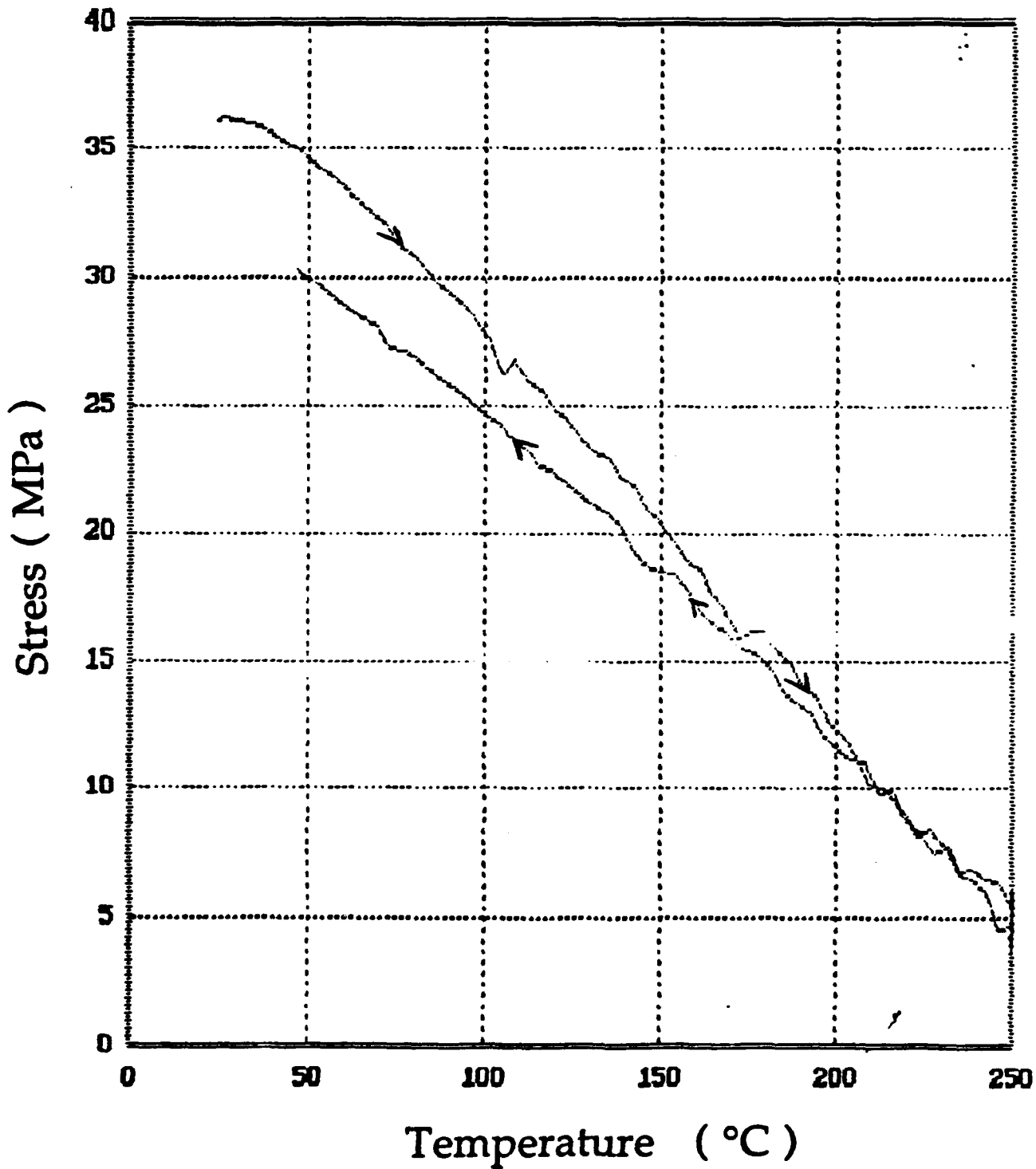


Figure 3.20 Curing Cycle for PB293/200.



MPa at 43°C and 18.4 MPa at 120°C. The thickness of the films were measured using a Metricon prism coupler. There was a 3%-4% change in the thickness after the hard bake.

Liquid nitrogen was used to lower the temperature of the wafers to -180°C, where stress measurements were also obtained and the wafer was left to warm back up to 24°C. In general, the stress was observed to increase as the temperature decreased. However, it was noted that there was a sharp decrease in the stress around 0°C (see figure 3.21). It is believed that this drop could be due to the moisture freezing in the sample. The next experiment was carried out by taking the same wafer up to 120 °C, held there for 1 hour in order to drive off all the moisture that could be present in the polymer film, and then brought down to low temperatures. However, it can be seen in figure 3.22 that the decrease in stress is still present, leading to the conclusion that there is still some water present. This hypothesis will be tested by repeating the experiment and taking the wafer to an even higher temperature and holding it there for a longer period of time. Results for the current studies are summarized in Table 3.11.

3.5 Moisture Measurements

Problem:

Moisture in polyimide films used in microelectronics is detrimental to the functionality and reliability of these films as inter-level dielectric. Moisture absorption increases the dielectric constant of the polyimide and thus reduces the insulating characteristic of the polymer; in addition, moisture migration to polymer metal interfaces may result in metal corrosion and loss of adhesion.

Approach:

To study the moisture absorption properties of spin-coated polyimide films, gravimetric measurements will be used to measure the weight change of a film sample in a controlled humidity environment. For a typical 6.44 mm polyimide film exposed to a step change in relative humidity (RH) from 19% to 50%, a weight change of 160 mg has been reported.^(3,8) In order to detect the small weight changes of the thin films upon exposure to a high

Table 3.11 Data for Probimides.

Wafer ID	Note	Final Cure Temperature (°C)	Measuring Temperature (°C)	Stress (MPa)
PB293/120	Before cure	120	24	34.0
	After cure	120	38	29.4
			120	19.0
	1st temp cycle	120	43	29.3
			120	18.6
	2nd temp cycle	120	43	29.2
			120	18.4
	3rd temp cycle	120	43	29.0
			120	18.4
PB293/250	Before cure	250	24	36.1
	After cure	250	35	31.2
			250	4.5
	1st temp cycle	250	43	31.8
			250	3.3
	2nd temp cycle	250	42	31.9
			250	3.3
	3rd temp cycle	250	44	31.5
			250	3.3
	Liquid N ₂	250	-180	50.1

Figure 3.21 Low Temperature PB293/253 without initial heating.

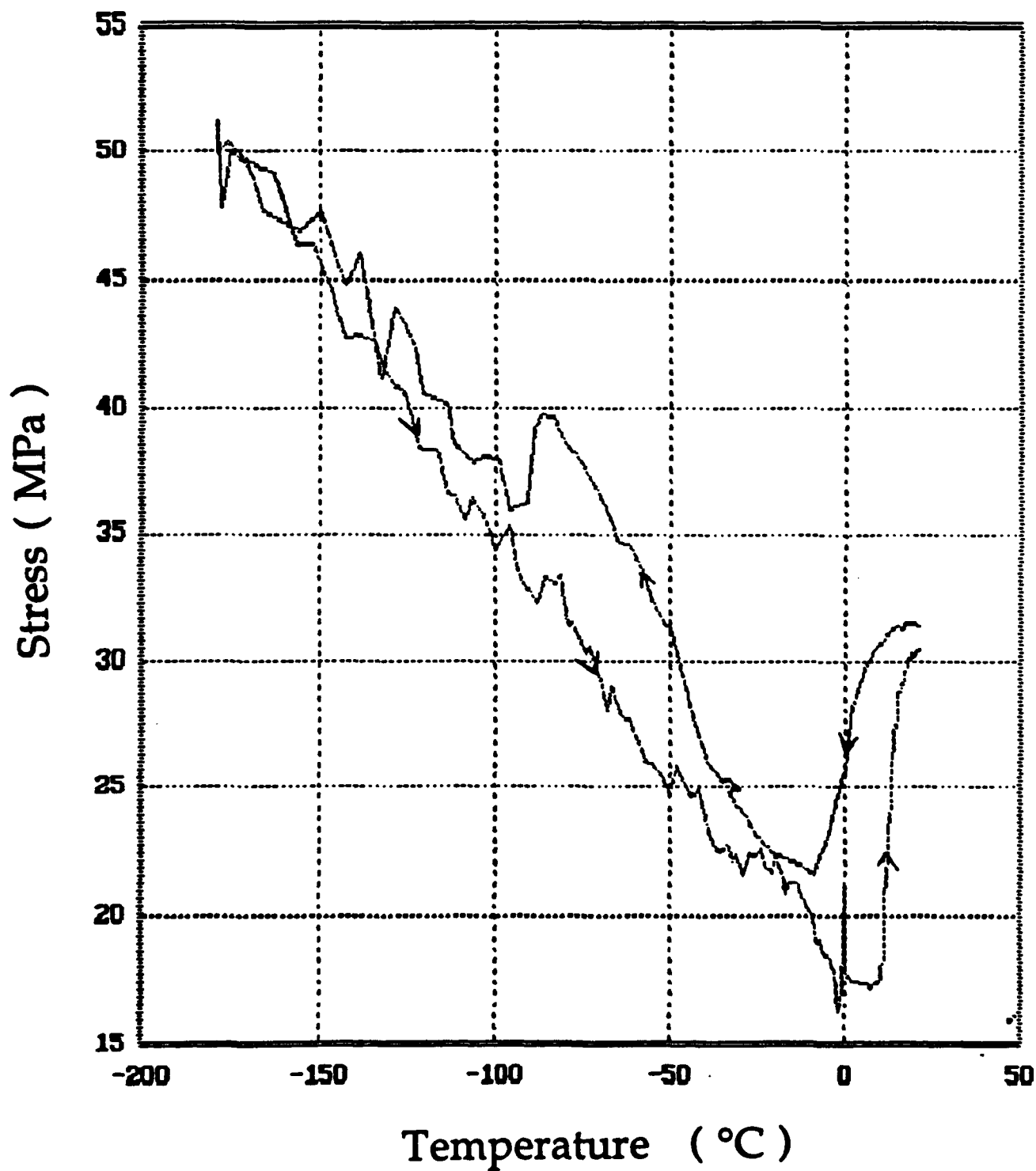
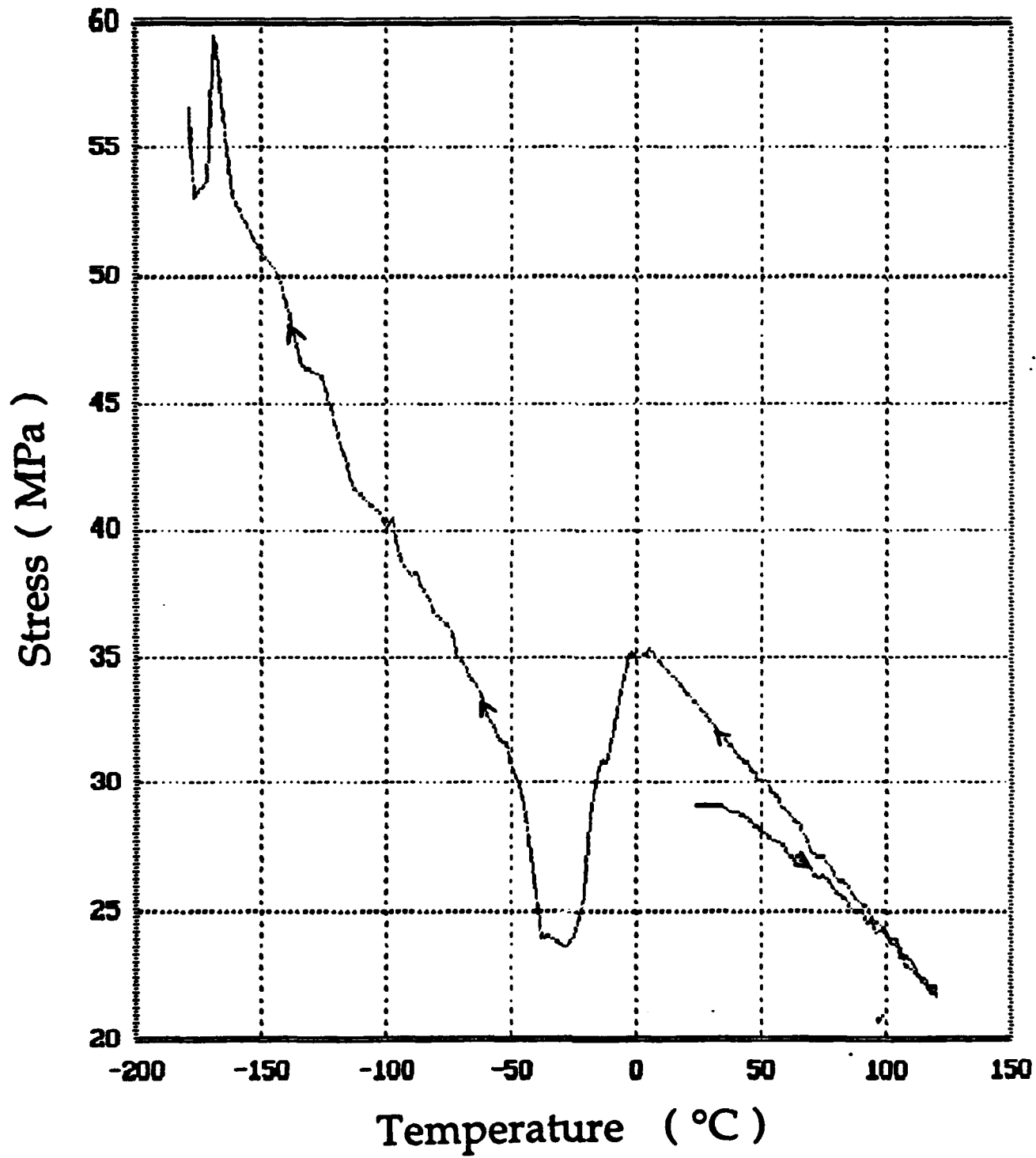


Figure 3.22 Low Temperature PB293/250 with initial heating.



humidity environment, a micro-balance of the highest sensitivity and a well-controlled humidity chamber are needed. The balance will be mounted above the humidity chamber so that the sample being weighed would be suspended inside the humidity chamber. The sample will be allowed to equilibrate at 20% RH, then the sample will be subject to a step change in humidity as the chamber humidity is increased to 80%.

The appropriate equipments for the above mentioned experiment have been identified and are currently on order. The major instrumentations include a Cahn Digital Recording Balance and a Blue M Programmable Temperature and Humidity Chamber. The Cahn Recording Balance has a 1 mg sensitivity which gives precise changes in the weight of the sample. In addition, the Cahn balance gives continuous measurement at 1 second intervals. The continuous recording feature of the micro-balance enables the determination of not only the steady-state moisture uptake, but also the transient moisture absorption process. The Blue M Programmable Temperature and Humidity Chamber can be operated between 20 to 90% RH at 25°C with humidity control accuracy of at least $\pm 3\%$. A schematic of the experimental set-up is shown in Figure 3.22.

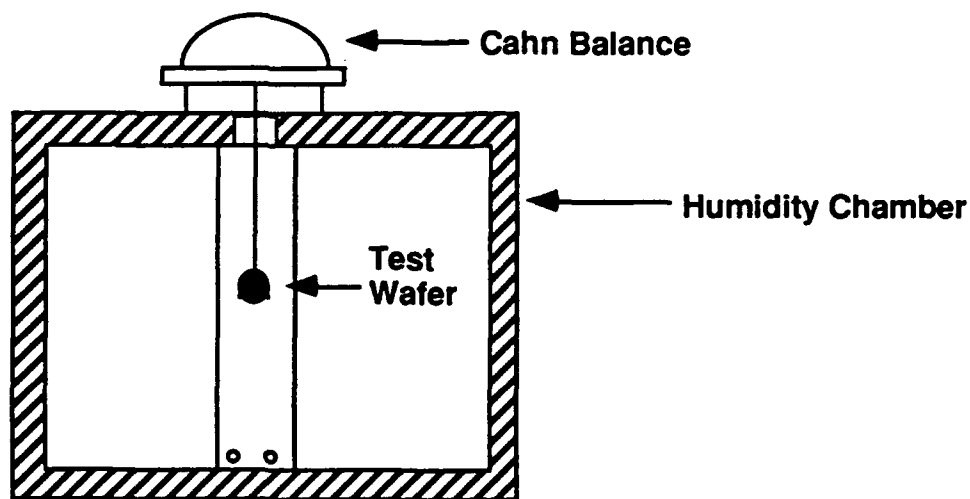


Figure 3.22: Experimental set-up for measuring moisture up-take of thin polyimide film on a substrate.

4. Inorganic Insulators

4.1. Silicon Dioxide

Purpose:

Silicon dioxide has been successfully used as an insulator in MCMs mainly because of the high degree of refinement for deposition equipment developed for the microelectronics industry. Two approaches to depositing thin oxide films (plasma-enhanced chemical vapor deposition, PECVD) and spin-on-glass processing (SOG) will be investigated here for application to GHz MCMs. The SOG work is particularly important and novel because PECVD is a non-planarizing material which requires additional process steps to achieve planarization. planarization is required after about 2 layers of PECVD SiO_2 because photolithography cannot deal with the topography changes. The development of a planarizing SOG would reduce cost and processing time. This work is with the knowledge and collaboration of n-Chip.

Approach:

Most experiments were set up as reduced factorial design experiments. In plasma-enhanced chemical vapor deposition, an alternating electric current is used to fragment the reactant gases, nitrous oxide, silane, and nitrogen, forming reactive ions and free radicals. When these ions encounter the plasma sheath, they are accelerated toward the electrode with high kinetic energy. The ions combine in the plasma and at the electrode surface producing SiO_2 . The ions also bombard the electrode and the substrate, located on the electrode. The important parameters governing the deposition are substrate temperature, pressure, radio frequency (rf), power (which dictates the amount of current passed through the gases), and reactant gas partial pressure. The substrate temperature controls the ability of reactants to dissociate and the by-products to leave the substrate surface and escape incorporation into the growing film. Hence, the temperature has the largest effect on film composition. Most notably, the substrate temperature determines the concentration of silanol (Si-OH) bonds in the film. Because of the conductive nature of the hydroxyl ($-\text{OH}$) group, higher silanol concentrations create a higher dielectric constant (i.e. a poorer insulator). The reactant gas partial pressures have a smaller effect

on the film composition and, hence, the dielectric constant. The pressure and rf power control the energy and the amount of ion bombardment. High pressure produces more collisions in the plasma and lowers the energy of the bombarding ions. High rf power induces large electric current and large amount of ion bombardment. The amount and energy of ion bombardment controls the thin film density and the film stress. Large levels of energetic ion bombardment promote low film stress and high film density. However, a denser film has a higher dielectric constant because it contains a smaller amount of air. The parameters and effects are summarized in Figure 4.1. These parameters must be manipulated to produce a low dielectric constant silicon dioxide film with the corresponding properties necessary for success as an interlevel dielectric.

Spun on glasses are another form of thin oxide films. SOG processing is nearly identical to the polymer film processing that is being explored by other members of our research group. A polysiloxane, polysilicate, or polysilsequioxane is dissolved in a solvent and spun on the substrate. The film is then cured to remove the solvent and induce formation of a polysiloxane, polysilicate, or polysilsequioxane glass. The greatest asset of spun on glasses is their ability to planarize. This facilitates the formation of the next metal layer and its connection to the previous metal layer. Hence, SOGs could be used after a series of layers to planarize the top surface and would allow the MCM to consist of more levels. However, current SOG technology will not allow production of films of sufficient thickness. The stresses formed in the cooling of SOGs after curing are high enough so that thick films crack and are of little value. These limitations must be overcome in order to incorporate SOGs as a planarizing interlevel dielectric.

Hence, the electrical and mechanical properties of the deposited oxide films must be optimized. The methods that are being employed in the characterization of the oxide films are:

- I. A parallel plate capacitor consisting of two metal layers surrounding an oxide layer is used to determine the low frequency dielectric constant and breakdown voltage/current of the insulator. The dielectric constant is found by relation of the capacitance to the geometrical features of the capacitor. The breakdown voltage and current are found by

applying a voltage across the capacitor and measuring the current through it until the dielectric breaks down and the current increases rapidly with increases in voltage.

II. A Flexus model F2320 measures the radius of curvature of the substrate which is used to calculate the residual stress and coefficient of thermal expansion of the film.

III. A Metricon model 2010 prism coupler measures the thickness and index of refraction of the films.

IV. A Perkin - Elmer Fourier Transform Infrared Spectrometer provides the IR absorption spectrum of the silicon dioxide film. The relative sizes of the spectrum peaks reflect the concentration of the film.

V. Etch rates of the silicon dioxide film in hydrofluoric acid solutions describe the relative density of the films.

VI. Controlled environment experiments utilizing the parallel plate capacitors are performed to determine the effects of humidity on the electrical properties of the films.

VII. The degree of planarization quantifies how flat a particular film is when deposited over steps or plateaus in the underlying region. Scanning Electron Microscopy (SEM) creates pictures of substrate cross-sections which show the degree of planarization.

Results:

Thus far, four different experiments are underway. The first experiment, a partial factorial experiment consisting of nine different lots investigated the effects of deposition parameters on the films produced by plasma-enhanced chemical vapor deposition. The variables examined were substrate temperature, total pressure, partial pressure of nitrogen feed, and rf power. The actual parameter settings are shown in Table 4.1. Each lot consisted of four samples. Two wafers of microstrip test patterns were fabricated for high frequency dielectric evaluation. On another wafer, twenty-eight separate parallel-plate capacitors of five different sizes were constructed. The fourth sample consists of a dielectric film placed directly on a silicon wafer for evaluation of

Table 4.1-PECVD Oxide Deposition Parameters-Preliminary Investigation

Lot	N2/sccm	Pres./Torr	Rf power/W	
18	144	0.5	150	
19	0	0.5	20	
20	0	1.8	150	
21	0	1.1	80	
22	144	1.8	80	
23	467	1.1	150	
24	144	1.1	20	
25	467	0.5	80	
26	467	1.8	20	
Note: Nitrous oxide feed rate was 900 sccm.				
Silane feed rate was 400 sccm.				
This rate refers to 2% silane in nitrogen.				
The nitrogen feed described above refers to additional nitrogen.				

film thickness, deposition rate, residual stress, thermal expansion coefficient, refractive index, and film composition. The second experiment investigated the effect of substrate temperature on film properties while at low total pressure and high rf power (the conditions for accelerated, energetic ion bombardment). The exact parameters used in these lots are shown in Table 4.2. This pattern facilitates expedient evaluation of the electrical properties (although it contains less parallel plate capacitors), along with the etch rate and residual stress. Also, the film composition is determined by using FTIR spectroscopy. The third experiment, a larger reduced factorial experiment consisting of more in-depth investigation of the effects of PECVD parameters on film properties is just underway. The parameters for these experiment are shown in Table 4.3. The fourth experiment, also in the production stages is a preliminary experiment evaluating the properties of (SOG), a research and development product, XM2-25, developed by Allied Signal, Inc. The device in this experiment is identical to that used in the second experiment which allows expedient evaluation of the dielectric constant, breakdown voltage, film stress, composition, etch rate, and degree of planarization. Further investigation will include extension of the reduced factorial design of the third experiment to lower substrate temperatures (below 200°C), more in-depth evaluation of the spun-on-glass, and utilization of hollow submicron sized silicon dioxide spheres along with the spun-on-glass to create a less dense, lower dielectric constant insulator.

The fabrication of the two microstrips for the first experiment was successfully completed and the high frequency measurements are being conducted by Kirk Larsen.

Dielectric constants have been determined from the different parallel plate capacitors of the six different lots. These data are shown in Tables 4.4-4.9. A plot of the average dielectric constant versus temperature is shown in Figure 4.1. The refractive index and thickness data is incorporated into the deposition rate data. The FTIR spectrum has been obtained for four of the six lots. These are presented in Figures 4.2-4.5.

In each of these lots, the rf power is high and the total pressure is low. Thus, ion current and ion energy are maximized. The FTIR spectra show peaks at approximately 1080, 815, and 460 cm^{-1} characteristic of silicon dioxide. The spectra of lower

Figure 4.1-Substrate Temperature vs. Dielectric Constant

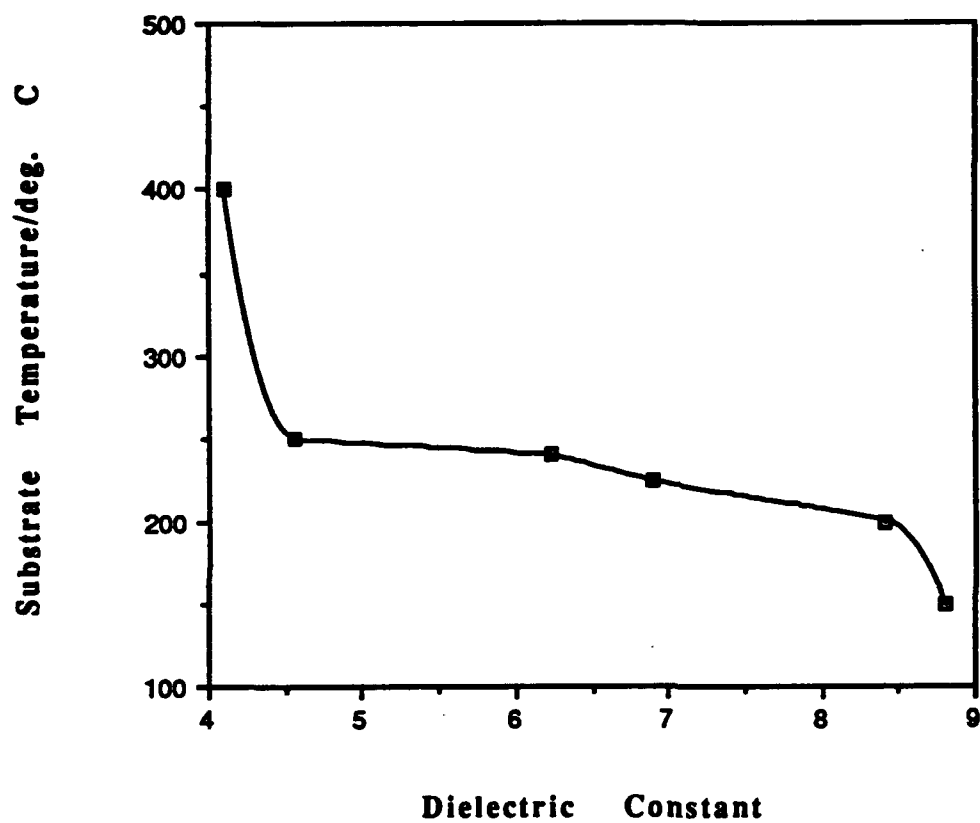


Table 4.2-PECVD Oxide Deposition Parameters-Temperature Variation

Lot	SiH₄/sccm	N₂O/sccm	Pres./Torr	Rf power/W	Temp./deg. C
TS150	400	900	0.5	150	150
TS200	400	900	0.25	190	200
TS225	400	900	0.25	175	225
TS240	400	900	0.25	175	240
TS250	400	900	0.5	150	250
TS400	200	250	0.5	150	400
Note: SiH₄ feed contains 2% silane in nitrogen.					
No additional nitrogen was fed.					
The flow rates were lowered at 400 deg. C to					
prevent premature cooling of the substrate					
by the feed gases.					

Table 4.3-PECVD Oxide Deposition Parameters-Characterization Experiment

Lot	SiH4/sccm	N2O/sccm	Pres./Torr	Rf power/W	Temp./deg. C
OX1	200	400	0.25	20	400
OX2	400	400	1.8	20	400
OX3	400	400	0.25	150	400
OX4	300	650	1.03	85	300
OX5	300	650	1.03	85	300
OX6	400	900	0.25	150	200
OX7	200	400	1.8	150	400
OX8	200	400	1.8	20	200
OX9	400	900	1.8	20	200
OX10	300	650	1.03	85	300
OX11	400	900	1.8	150	400
OX12	400	400	1.8	150	200
OX13	200	900	0.25	20	200
OX14	200	900	0.25	150	400
OX15	200	900	1.8	20	400
OX16	400	900	0.25	20	400
OX17	200	400	0.25	150	200
OX18	400	400	0.25	20	200
OX19	200	900	1.8	150	200
Note: SiH4 feed contains 2% silane in nitrogen					
No additional nitrogen was fed.					

Table 4.4-Dielectric Constant Data-Substrate Temperature=150°C

	Area/ cm^2	Capacit./nF	Thick./micr.	Dielectric Constant	
Quadrant I					
capacitor 1	0.031	0.0479	5.26		9.18
4	0.11	0.1652	5.26		8.93
5	0.6	0.7635	5.26		7.56
Quadrant II					
capacitor 1	0.031	0.0475	5.27		9.12
2	0.06	0.0866	5.27		8.60
3	0.11	0.1676	5.27		9.07
4	0.11	0.167	5.27		9.04
5	0.6	0.8043	5.27		7.98
6	0.6	0.8209	5.27		8.15
7	1.07	1.4085	5.27		7.84
Quadrant III					
capacitor 1	0.031	0.0482	5.29		9.29
2	0.06	0.092	5.29		9.17
Quadrant IV					
capacitor 1	0.031	0.0514	5.3		9.93
capacitor 2	0.06	0.0943	5.3		9.41
			Average Dielectric Constant		8.81

Table 4.5-Dielectric Constant Data-Substrate Temperature=200°C

	Area/ cm^2	Capacit./nF	Thick./micr.	Dielectric Constant	
Quadrant I					
capacitor 2	0.06	0.1011	4.37		8.32
3	0.11	0.1753	4.37		7.87
4	0.11	0.179	4.37		8.04
5	0.6	0.8784	4.37		7.23
6	0.6	0.8968	4.37		7.38
Quadrant II					
capacitor 1	0.031	0.053	4.41		8.52
2	0.06	0.0965	4.41		8.01
3	0.11	0.1727	4.41		7.82
4	0.11	0.1754	4.41		7.95
5	0.6	0.8847	4.41		7.35
7	1.07	1.6151	4.41		7.52
Quadrant III					
capacitor 1	0.031	0.0544	4.45		8.82
6	0.6	1.6434	4.45		13.77
Quadrant IV					
capacitor 1	0.031	0.054	4.66		9.17
			Average Dielectric Constant		8.41

Table 4.6-Dielectric Constant Data-Substrate Temperature=225°C

	Area/ cm^2	Capacit./nF	Thick./micr.	Dielectric Constant	
Quadrant I					
capacitor 1	0.0298	0.0643	3.21		7.83
2	0.06	0.1321	3.21		7.99
3	0.1116	0.2148	3.21		6.98
4	0.1045	0.2015	3.21		6.99
5	0.5897	1.0016	3.21		6.16
6	0.5769	0.9968	3.21		6.27
7	1.0635	1.9138	3.21		6.53
Quadrant II					
capacitor 1	0.0318	0.0757	3.21		8.63
2	0.0588	0.1205	3.21		7.43
3	0.1091	0.2047	3.21		6.81
4	0.1095	0.2157	3.21		7.15
5	0.5799	0.9119	3.21		5.70
6	0.6027	0.9783	3.21		5.89
7	1.0613	1.7678	3.21		6.04
		Average Dielectric Constant			6.89

Table 4.7-Dielectric Constant Data-Substrate Temperature=240°C

	Area/ cm^2	Capacit./nF	Thick./micr.	Dielectric Constant	
Quadrant I					
capacitor 1	0.03	0.0549	3.36		6.95
2	0.0601	0.1046	3.36		6.61
3	0.1123	0.1871	3.36		6.33
4	0.1073	0.1824	3.36		6.45
5	0.6035	0.9635	3.36		6.06
6	0.5868	0.9604	3.36		6.21
7	1.0788	1.7391	3.36		6.12
Quadrant II					
capacitor 1	0.0323	0.0553	3.33		6.44
2	0.0603	0.1042	3.33		6.50
3	0.1113	0.1795	3.33		6.07
4	0.1109	0.1807	3.33		6.13
5	0.5839	0.8683	3.33		5.60
6	0.5905	0.8935	3.33		5.69
7	1.0678	1.718	3.33		6.05
		Average Dielectric Constant			6.23

Table 4.8-Dielectric Constant Data-Substrate Temperature=250°C

	Area/ cm^2	Capacit./nF	Thick./micr.	Dielectric Constant	
Quadrant I					
capacitor 1	0.0298	0.0227	5.37		4.62
2	0.0601	0.0435	5.42		4.43
3	0.1137	0.0783	5.45		4.24
4	0.1163	0.0817	5.43		4.31
5	0.5245	0.4192	5.59		5.05
6	0.5699	0.4091	5.6		4.54
Quadrant II					
capacitor 1	0.0308	0.023	5.35		4.51
2	0.0571	0.042	5.39		4.48
3	0.1169	0.0834	5.42		4.37
4	0.1115	0.0841	5.32		4.53
6	0.6065	0.4394	5.41		4.43
7	1.0873	0.7873	5.46		4.47
Quadrant III					
capacitor 1	0.0289	0.0235	5.32		4.89
2	0.0599	0.0465	5.29		4.64
Quadrant IV					
capacitor 1	0.0295	0.0241	5.36		4.95
2	0.0612	0.0456	5.34		4.50
3	0.1083	0.0818	5.38		4.59
4	0.114	0.0834	5.38		4.45
5	0.5852	0.4214	5.47		4.45
		Average Dielectric Constant			4.55

Table 4.9-Dielectric Constant Data-Substrate Temperature=400°C

	Area/ cm^2	Capacit./nF	Thick./micr.	Dielectric Constant	
Quadrant I					
capacitor 1	0.0326	0.0403	2.92		4.08
2	0.0607	0.0767	2.91		4.16
3	0.1142	0.1389	2.9		3.99
4	0.1138	0.1422	2.9		4.09
5	0.5974	0.7389	2.89		4.04
6	0.5983	0.7444	2.9		4.08
7	1.0912	1.3774	2.9		4.14
Quadrant II					
capacitor 1	0.03	0.0387	2.92		4.26
2	0.0623	0.0749	2.9		3.94
3	0.1079	0.1356	2.9		4.12
4	0.1101	0.1373	2.91		4.10
5	0.6043	0.7443	2.92		4.06
6	0.5943	0.7375	2.9		4.07
7	1.0906	1.3661	2.92		4.13
Quadrant III					
capacitor 1	0.0292	0.0392	2.92		4.43
2	0.0581	0.0712	2.91		4.03
Quadrant IV					
capacitor 1	0.0308	0.0389	2.92		4.17
4	0.1107	0.1355	2.9		4.01
5	0.6036	0.7571	2.9		4.11
		Average Dielectric Constant			4.10

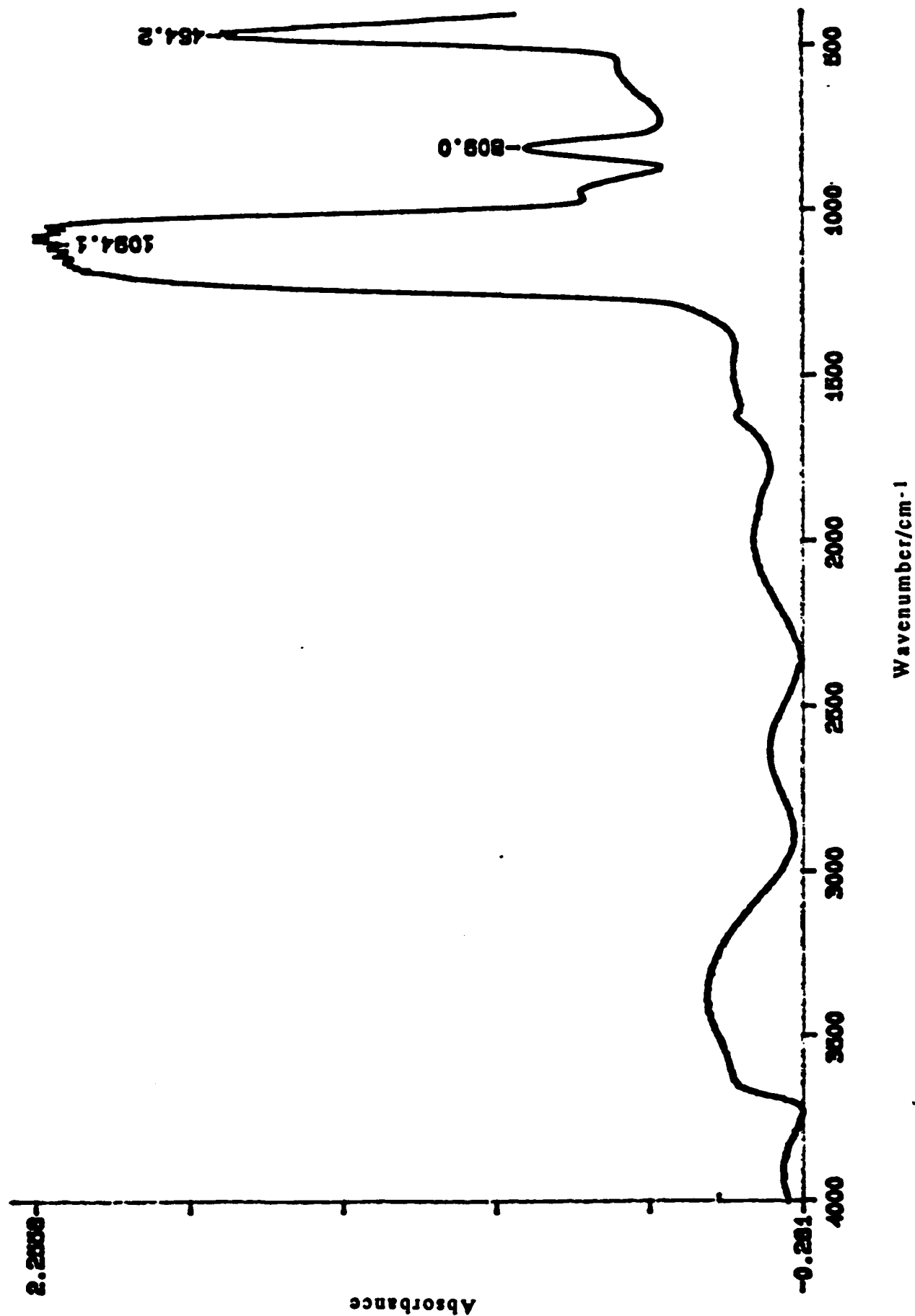


Figure 4.2-FTIR Absorbance Spectrum-Substrate Temperature=150°C

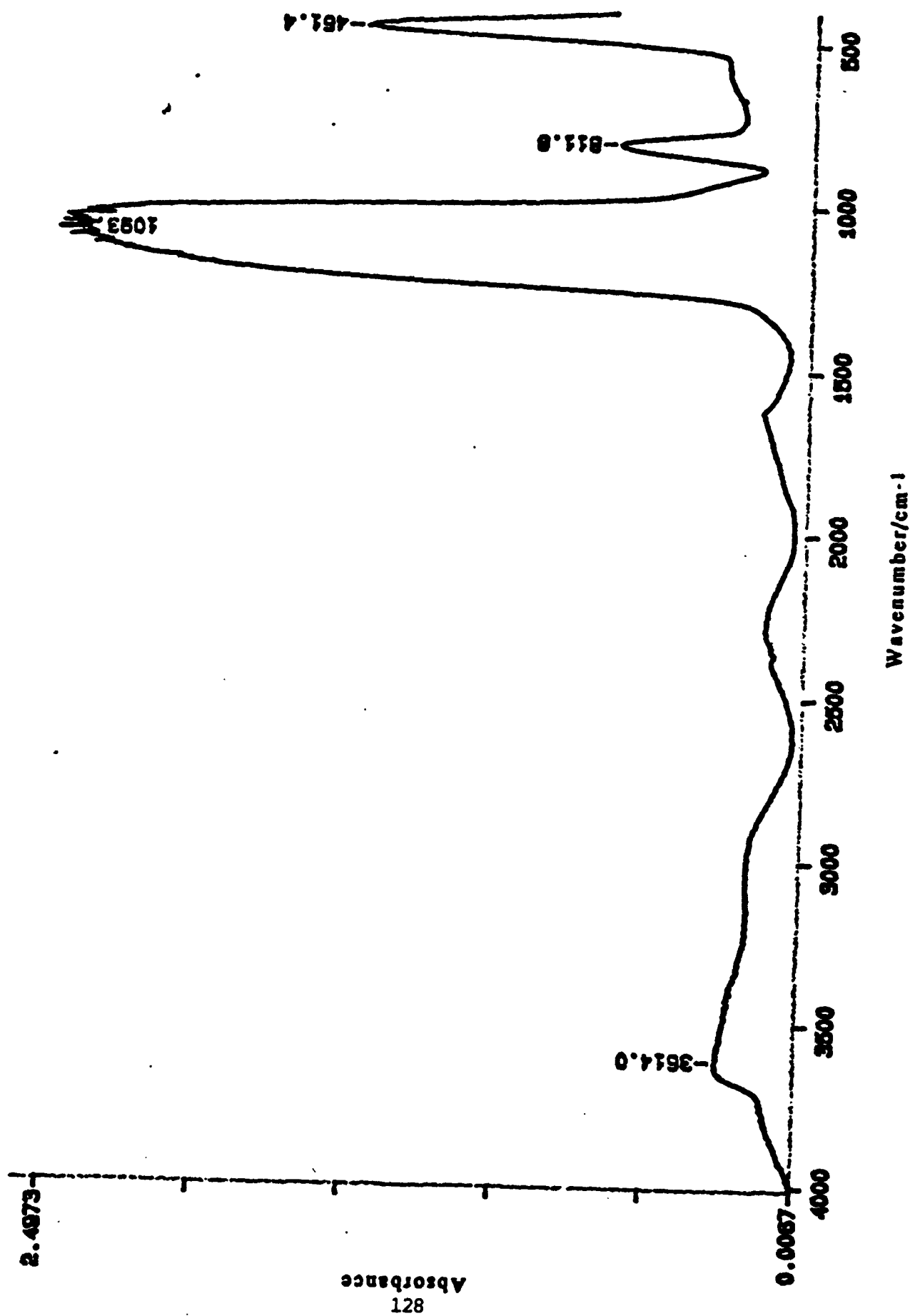


Figure 4.3-FTIR Absorbance Spectrum-Substrate Temperature=200°C

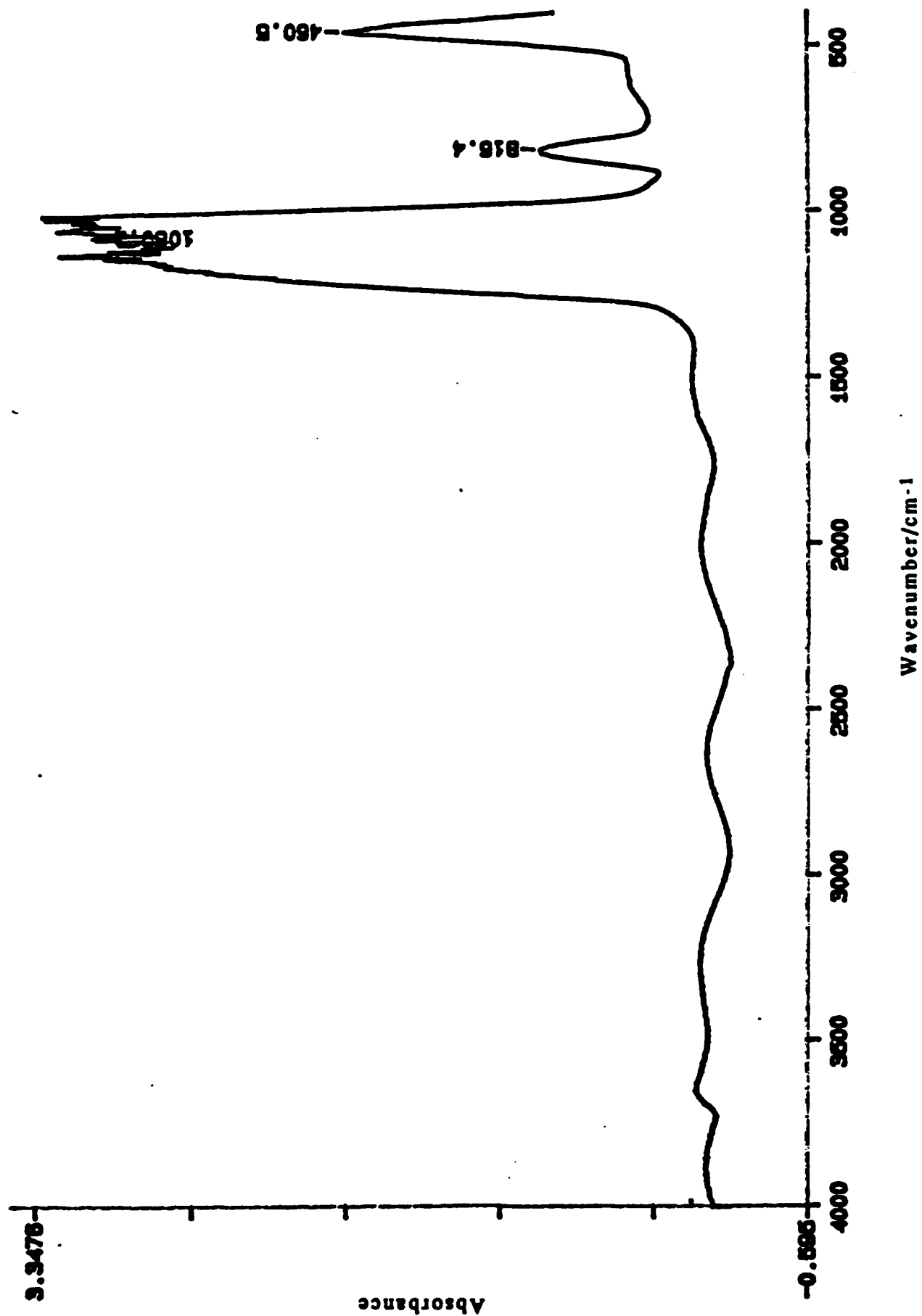


Figure 4.4-FTIR Absorbance Spectrum-Substrate Temperature=250°C

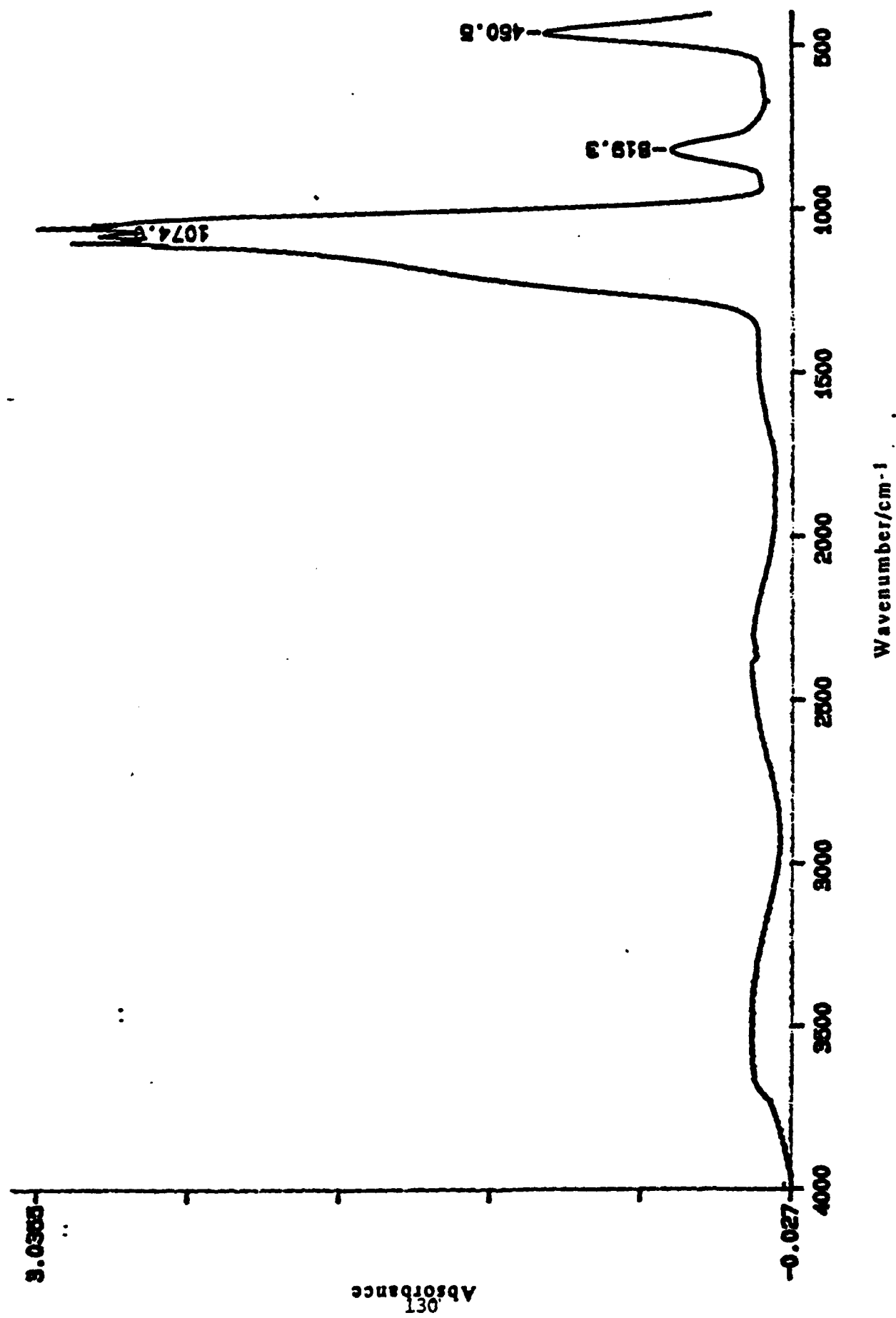


Figure 4.5-FTIR Absorbance Spectrum-Substrate Temperature=400°C

temperature oxides exhibit wide absorbance bands at approximately 3000-3500 cm^{-1} . These absorptions are O-H stretching modes resulting from silanol bonds in the film. The spectrum of the temperature oxide also exhibits an absorption peak at approximately 900 cm^{-1} due to Si-H.

Conclusions:

At low substrate temperatures with high ion bombardment, relatively high concentrations of silanol are incorporated into the film. This result is consistent with the dielectric constant data which shows high dielectric constants for the low substrate temperature films with a high silanol concentration. In order to deposit an oxide film with a truly low dielectric constant, either the reactant gas concentration must be altered or the ion current and energy lowered to produce a low density layer. This increase in pressure and/or decrease in rf power will cause a decrease in film density and dielectric constant.

4.2 Porous Silica

Purpose:

Porous silica is a silicon dioxide matrix with a high degree of porosity (e.g. 80-90%). As such, it has a low dielectric constant (as low as 1.6) and low cost because it is based on a sol-gel process. Porous silica has fair thermal conductivity, about the same as polyimide and 10% of that of SiO_2 .

The purpose of this study is to investigate its use as an interlayer dielectric in packaging applications.

Approach:

Some early work by Yarbrough et al. demonstrated the feasibility of using sol-gel silica as insulating layers in high speed, high performance substrates.^(4.1) The lowest dielectric constant they achieved was 2.50. More recent work by Gerhardt et al. has shown that bulk porous silica can be prepared with dielectric constants as low as 1.6 at 1 MHz.^(4.2,4.3)

Using colloidal sols as starting materials is a relatively simple and inexpensive synthetic route for making porous gels. In this

study the porous silica was prepared using a colloidal process originally developed by Shoup and Wein.^(4.4,4.5) Processing and microstructure of these gels in the bulk form ranging from 15-100% theoretical density have been extensively studied by the present investigator.^(4.6-4.10) However, processing of thin films by this method is a novel concept which needs to be developed for use in IC packaging.

Results:

The proposed procedure for making porous silica thin films in this pilot study is spin coating of colloidal sol-gel solutions. For the sake of simplicity, thin films were prepared by dipping a glass slide in the precursor sol solution. Various sol compositions were prepared and tested. The selected sol used in most of the experiments contains 20% colloidal silica, and 80% potassium silicate. After depositing the sol on a clean glass slide, a waiting period of several hours was necessary to insure gel formation. The formed gel was then taken through several leaching steps to remove undesirable ions that could change the dielectric constant.

The viscosity of the sol increased with time elapsed as demonstrated by placing five drops of sol on a slide and allowing it to gel. Unleached (as gelled) film thicknesses were measured with a micrometer. Table 4.10 shows the results obtained with two different compositions (10:90 and 20:80) for which room temperature and relative humidity were not monitored (hence difference in thicknesses). Each value listed is the average of three different readings. An increase in gel thickness is observed as a function of time representing that the sol viscosity gets higher as it ages.

To determine a workable sol rheology for film formation, glass slides were dipped into sols with increasing viscosity as a function of time and dried at different angles. Thicknesses were measured and the film quality with regard to even coverage was examined in all cases. Table 4.11 shows an increase of film thickness with sol age as was shown in Table 4.10. In addition, it can be concluded from visual observation of the films and sol workability that the best films were obtained when the sol age was 30-45 min. and drying angle was 45 degrees.

Table 4.10 Increase of viscosity demonstrated by increased
unleached film thickness as a function of time.
Thick Film m Commercially Cleaned Slides.

Time <u>Min:</u>	Film thickness, 10:90 sol <u>10^{-6} m</u>	Film thickness, 20:80 sol <u>10^{-6} m</u>
0	130	-
15	130	130
30	190	150
45	240	105
60	340	145
75	715	200
90	1340	-
105	-	235
120	-	305

Table 4.11 Thickness of unleached silica gel deposited on commercially cleaned glass slides at various gelation time and gelling angle.

Time min	0° Gelling Angle Film thickness, 10^{-6}		45° Gelling Angle Film thickness, 10^{-6}		90° Gelling Angle Film thickness, 10^{-6}	
	10:90 sol	20:80 sol	10:90 sol	20:80 sol	10:90 sol	20:80 sol
.	11	17.5	-	10	22.5	11.6
5	21	16.0	23	14	33.0	14.0
10	18	17.0	24	6	25.0	10.0
15	12	20.0	18	9	19.0	12.5
20	21	22.5	31	15	24.0	18.8
25	15	25.0	30	14	50.0	15.0
30	23	15.0	13.5	22.5	99.0	12.5
35	-	33.0	-	25.0	-	21.0
40	-	-	-	31.6	-	34.5

Table 4.12 shows the film thicknesses of various 20:80 leached gels formed from sols of different age (viscosity). The samples were allowed to gel at room temperature at a 45 degree angle. The glass slides used in this experiment and all others thereafter were acid cleaned, which improved the uniformity and adherence of the films. The leaching was done by soaking the samples for eight hours in NH_4NO_3 , three hours in HNO_3 , and one hour in water prior to a drying step of 20 hrs at 60°C . Comparing these results with those of the unleached 20:80 samples (Table 4.11), it seems that half the film thickness was lost during leaching.

Table 4.13 summarizes a number of experiments which were done to evaluate the effects of various processing variables on the integrity of the resultant thin films. Gelation time, temperature and atmosphere were monitored. We also varied the consolidation step and added several rinsing steps prior to leaching. 8-A and 8-B, both demonstrated a gradual increase in cracking from top to the bottom of the slide. The consolidated sample 8-B, also showed scattered number of "nuclei". Consolidation in the bulk results in shrinkage and exudation of liquids which may contain some ions. What is observed as nuclei, may indeed be ions brought up to the surface, or some form of chemical reaction. Comparison of 8-B and 8-C, showed that rinsing washed off salts that normally cause dendritic deposits on the slides. The consolidation step seemed to promote this effect (8D&C). Gelation under water was unsuccessful. Either water interferes with gel formation, or the film simply peels off (8-E1&2). The rinsing effect was also clearly observed in experiments 9-A1&2, 9-C1&2, 10-C1&2. The A series showed good coverage, and fewer cracks than the C's. The 9A&10A samples were not leached. The steam gelled/condensed samples were generally spotted, uneven, and blotchy. An improvement was observed when the slides were allowed to gel at 45 angle (10-B,D,E,F), compared to 0 (horizontal) (9-B,D,E,F). The texture of the steam-gelled films (9F and 10F) looked different as compared to the air gelled samples, and appeared to be crack free in some areas. These samples were steam leached rather than chemically leached. The steamed gelled samples (9-D,E and 10-D,E) which were chemically leached generally did not show any salt deposits, however they showed many of dark spots or "nuclei". Some appearing to be at different depths than the film itself. Air gelling in combination with steam leaching (9G2) seemed to be a better combination than steam gelling and steam leaching (9F,10F). The initial experiments for finding the ideal leaching method indicated

Table 4.12

Thickness of silica gel after leaching as a function of time.
The glass slides were acid cleaned.

Time
Min

20:80 Leached film thickness dried at 45°
 10^{-6}m

0	6.0
20	5.5
40	-
60	6.5
80	9.0
100	8.5

Table 4.13- Effects of various variables in thin film processing of low density silica gel using the 20:80 sol composition.

Expt. no	8-A	8-B	8-C	8-D	8-E ₁	8-E ₂
Process variable						
Room Temp. °F	-	-	-	-	-	-
Room humidity o/o	-	-	-	-	-	-
Rate of the sol/min	30	30	30	30	30	30
No/duration of dip	2x10sec	2x10sec	2x10sec	2x10sec	2x10sec	2x10sec
Gel time in air/hr	20	20	20	20	3.5	3.5
Gel time in water/hr	0	0	0	0	16.5	16.5
Gel time in steam/hr	0	0	0	0	0	0
Time of 1st/last rinse/hr	20	20	-	0	0	0
Rinse duration #times/min	1/30	1/30	-	1/30	1/30	1/30
Rinse interval (hr)	-	-	-	-	-	-
Consolidation/min	0	60	60	0	60	0
Consolidation temp. °C	-	80	80	-	80	-
Leach NH ₄ NO ₃ min/°C	360/RT80	360/RT80	360/RT80	360/RT80	360/RT80	360/RT80
Leach HNO ₃ min/°C	90/RT80	90/RT80	90/RT80	90/RT80	90/RT80	90/RT80
Leach water min/°C	60/RT	60/RT	60/RT	60/RT	60/RT	60/RT
Leach steam/min.	0	0	0	0	0	0
Methanol min/°C	30/RT	30/RT	30/RT	30/RT	30/RT	30/RT
Drying time/hr.	18	18	18	18	18	18
Drying temp °C	60	60	60	60	60	60

COMMENTS:

Table 4.13 Effects of various variables in thin film processing of low density silica gel using the 20:80 sol composition.

Expt. no	9-A ₁	9-A ₂	9-B	9-C ₁	9-C ₂	9-D ₁
Process variable						
Room Temp. °F	73.5	73.5	73.5	73.5	73.5	73.5
Room humidity o/o	47	47	47	47	47	47
Age of the sol/min	45	45	45	45	45	45
So/duration of dip	2x10sec	2x10sec	2x10sec	2x10sec	2x10sec	2x10sec
Gel time in air/hr	20	20	0	20	20	0
Gel time in water/hr	0	0	0	0	0	0
Gel time in steam/hr	0	0	20	0	0	20
Time of 1st/last rinse/hr	NR	20	NO	NO	20	NO
Rinse duration #times/min	0	1/10	0	0	1/10	0
Rinse interval (hr)	-	-	-	-	-	-
Consolidation/min	NO	NO	NO	60	60	NO
Consolidation temp. °C	-	-	-	80	80	-
Leach NH ₄ NO ₃ min/°C	NO	NO	NO	240/RT80	240/RT80	240/RT80
Leach HNO ₃ min/°C	NO	NO	NO	60/RT80	60/RT80	60/RT80
Leach water min/°C	NO	NO	NO	30/RT	30/RT	30/RT
Leach steam/min.	NO	NO	NO	NO	NO	NO
Methanal min/°C	NO	NO	NO	15/RT	15/RT	15/RT
Drying time/hr.	18	18	18	18	18	18
Drying temp °C	60	60	60	60	60	60

COMMENTS:

Table 4.13- Effects of various variables in thin film processing of low density silica gel using the 20:80 sol composition.

Expt. no	9-D ₂	9-E ₁	9-E ₂	9-F	9-G ₁	9-G ₂
Process variable						
Room Temp. °F	73.5	73.5	73.5	73.5	73.5	73.5
Room humidity o/o	47	47	47	47	47	47
Age of the sol/min	45	45	45	45	45	45
Dip/duration of dip	2x10sec	2x10sec	2x10sec	2x10sec	2x10sec	2x10sec
Gel time in air/hr	0	0	0	0	20	20
Gel time in water/hr	0	0	0	0	0	0
Gel time in steam/hr	20	20	20	20	0	0
Time of 1st/last rinse/hr	20	NO	20	NO	NO	20
Rinse duration #times/min	1/10	0	1/10	0	0	1/10
Rinse interval (hr)	-	-	-	-	-	-
Consolidation/min	NO	NO	NO	NO	60	60
Consolidation temp. °C	-	-	-	-	80	80
Leach NH ₄ NO ₃ min/°C	240/RT80	240/80	240/80	NO	NO	NO
Leach HNO ₃ min/°C	60/RT80	60/80	60/80	NO	NO	NO
Leach water min/°C	30/RT	30/RT	30/RT	NO	NO	NO
Leach steam/min.	NO	NO	NO	345	345	345
Ethanol min/°C	15/RT	15/RT	15/RT	15/RT	15/RT	15/RT
Drying time/hr.	18	18	18	18	18	18
Drying temp °C	60	60	60	60	60	60

COMMENTS:

Table 4.13- Effects of various variables in thin film processing of low density silica gel using the 20:80 sol composition.

Expt. no	9-H ₁	9-H ₂	9-I ₁	9-I ₂	9-J ₁	9-J ₂
Process variable						
Room Temp. °F	73.5	73.5	73.5	73.5	73.5	73.5
Room humidity o/o	47	47	47	47	47	47
Age of the sol/min	45	45	45	45	45	45
No/duration of dip	2x10sec	2x10sec	2x10sec	2x10sec	2x10sec	2x10sec
Gel time in air/hr	20	20	20	20	20	20
Gel time in water/hr	0	0	0	0	0	0
Gel time in steam/hr	0	0	0	0	0	0
Time of 1st/last rinse/hr	NO	20	NO	20	NO	20
Rinse duration #times/min	0	1/10	0	1/10	0	1/10
Rinse interval (hr)	-	-	-	-	-	-
Consolidation/min	60	60	60	60	60	60
Consolidation temp. °C	80	80	80	80	80	80
Leach NH ₄ NO ₃ min/°C	NO	NO	60/RT80	60/RT80	120/RT80	120/RT80
Leach HNO ₃ min/°C	60/RT80	60/RT80	60/RT80	60/RT80	60/RT80	60/RT80
Leach water min/°C	30/RT	30/RT	30/RT	30/RT	30/RT	30/RT
Leach steam/min.	NO	NO	NO	NO	NO	NO
Methanal min/°C	15/RT	15/RT	15/RT	15/RT	15/RT	15/RT
Drying time/hr.	18	18	18	18	18	18
Drying temp °C	60	60	60	60	60	60

COMMENTS:

table 4.13- Effects of various variables in thin film processing of low density silica gel using the 20:80 sol composition.

kpt. no	9-K ₁	9-K ₂	10-A ₁	10-A ₂	10-B	10-C ₁
process variable						
Room Temp. °F	73.5	73.5	73.6	73.6	73.6	73.6
Room humidity o/o	47	47	57	57	57	57
Rate of the sol/min	45	45	50	50	50	50
Time/duration of dip	2x10sec	2x10sec	2x10sec	2x10sec	2x10sec	2x10sec
Soak time in air/hr	20	20	20	20	0	20
Soak time in water/hr	0	0	0	0	0	0
Soak time in steam/hr	0	0	0	0	20	0
Time of 1st/last rinse/hr	NO	20	NO	20	20	NO
Rinse duration #times/min	0	1/10	0	1/10	1/10	0
Rinse interval (hr)	-	-	-	-	-	-
Consolidation/min	60	60	NO	NO	NO	60
Consolidation temp. °C	80	80	-	-	-	80
Soak NH ₄ NO ₃ min/°C	180/RT80	180/RT80	NO	NO	NO	180/80
Soak HNO ₃ min/°C	60/RT80	60/RT80	NO	NO	NO	60/80
Soak water min/°C	30/RT	30/RT	NO	NO	NO	30/80
Soak steam/min.	NO	NO	NO	NO	NO	NO
Soak ethanal min/°C	15/RT	15/RT	NO	NO	NO	15/80
Drying time/hr.	18	18	18	18	18	15/80
Drying temp °C	60	60	24	24	24	24

COMMENTS:

able4.13- Effects of various variables in thin film processing of low density silica gel using the 20:80 sol composition.

kpt. no	10-C ₂	10-D ₁	10-D ₂	10-E ₁	10-E ₂	10-F
rocess variable						
oom Temp. °F	73.6	73.6	73.6	73.6	73.6	73.6
oom humidity o/o	57	57	57	57	57	57
ge of the sol/min	50	50	50	50	50	50
o/duration of dip	2x10sec	2x10sec	2x10sec	2x10sec	2x10sec	2x10sec
el time in air/hr	20	0	0	0	0	0
el time in water/hr	0	0	0	0	0	0
el time in sleam/hr	0	20	20	20	20	20
ime of 1st/last rinse/hr 20		NO	20	NO	20	NO
inse duration #times/min 1/10		0	1/10	0	1/10	0
inse interval (hr)	-	-	-	-	-	-
onsolidation/min	60	60	60	60	60	60
onsolidation temp. °C	80	80	80	80	80	80
each NH ₄ NO ₃ min/°C	180/80	180/RT80	180/RT80	180/80	180/80	NO
each HNO ₃ min/°C	60/80	60/RT80	60/RT80	60/80	60/80	NO
each water min/°C	30/80	30/RT80	30/RT80	30/80	30/80	NO
each steam/min.	NO	NO	NO	NO	NO	120
ethanal min/°C	15/80	15/RT80	15/RT80	15/80	15/80	15/80
rying time/hr.	15/80	15/80	15/80	15/80	15/80	18
rying temp °C	24	24	24	24	24	24

OMMENTS:

Table 4.13 Effects of various variables in thin film processing of low density silica gel using the 20:80 sol composition.

Expt. no	10-G ₁	10-G ₂	10-H ₁	10-H ₂	10-I ₁	10-I ₂
Process variable						
Room Temp. °F	73.6	73.6	73.6	73.6	73.6	73.6
Room humidity o/o	57	57	57	57	57	57
Rate of the sol/min	50	50	50	50	50	50
Depth/duration of dip	2x10sec	2x10sec	2x10sec	2x10sec	2x10sec	2x10sec
Drying time in air/hr	20	20	20	20	20	20
Drying time in water/hr	0	0	0	0	0	0
Drying time in steam/hr	0	0	0	0	0	0
Time of 1st/last rinse/hr	NO	20	NO	20	NO	20
Rinse duration #times/min	0	1/10	0	1/10	0	1/10
Rinse interval (hr)	-	-	-	-	-	-
Consolidation/min	60	60	60	60	60	60
Consolidation temp. °C	80	80	80	80	80	80
Soak NH ₄ NO ₃ min/°C	NO	NO	NO	NO	30/80	30/80
Soak HNO ₃ min/°C	NO	NO	60/80	60/80	60/80	60/80
Soak water min/°C	NO	NO	30/80	30/80	30/80	30/80
Soak steam/min.	120	120	0	0	0	0
Soak ethanol min/°C	15/80	15/80	15/80	15/80	15/80	15/80
Drying time/hr.	18	18	18	18	18	18
Drying temp °C	24	24	24	24	24	24

REMARKS:

le4.13 Effects of various variables in thin film processing of low density silica gel using the 20:80 sol composition.

t. no	10-J ₁	10-J ₂	10-K ₁	10-K ₂	11-A ₁	11-A ₂
cess variable						
m Temp. °F	73.6	73.6	73.6	73.6	79.5	79.5
m humidity o/o	57	57	57	57	57	57
of the sol/min	50	50	50	50	45	45
duration of dip	2x10sec	2x10sec	2x10sec	2x10sec	2x10sec	2x10sec
time in air/hr	20	20	20	20	20	20
time in water/hr	0	0	0	0	0	0
time in sleam/hr	0	0	0	0	0	0
ie of 1st/last rinse/hr NO		20	NO	20	2½/20	2½/20
se duration #times/min 0		1/10	0	1/10	5/1+1/15	5/2+1/15
se interval (hr)	-	-	-	-	1	1-
solidation/min	60	60	60	60	60	60
solidation temp. °C	80	80	80	80	80	80
ach NH ₄ NO ₃ min/°C	60/80	60/80	120/80	120/80	120/80	120/80
ach HNO ₃ min/°C	60/80	60/80	0	0	30/80	30/80
ach water min/°C	30/80	30/80	30/80	30/80	30/80	30/80
ach steam/min.	0	0	0	0	0	0
chanal min/°C	15/80	15/80	15/80	15/80	15/80	15/80
ping time/hr.	18	18	18	18	20	20
ping temp °C	24	24	24	24	26.5	26.5

MENTS:

ble 4.12 Effects of various variables in thin film processing of low density silica gel using the 20:80 sol composition.

pt. no	11-B ₁	11-B ₂	11-C ₁	11-C ₂	11-D ₁	11-D ₂
process variable						
com Temp. °F	79.5	79.5	79.5	79.5	79.5	79.5
com humidity o/o	57	57	57	57	57	57
rate of the sol/min	45	45	45	45	45	45
duration of dip	2x10sec	2x10sec	2x10sec	2x10sec	2x10sec	2x10sec
1 time in air/hr	20	20	20	20	20	20
1 time in water/hr	0	0	0	0	0	0
1 time in steam/hr	0	0	0	0	0	0
time of 1st/last rinse/hr	2½/20	2½/20	20	20	2½/20	2½/20
rinse duration #times/min	3/1+1/15	3/2+1/15	1/15	1/15	2/2+1/15	2/2+1/15
rinse interval (hr)	2	2	-	-	3	3
consolidation/min	60	60	60	60	60	60
consolidation temp. °C	80	80	80	80	80	80
each NH ₄ NO ₃ min/°C	120/80	120/80	120/80	120/80	120/80	120/80
each HNO ₃ min/°C	30/80	30/80	30/80	30/80	30/80	30/80
each water min/°C	30/80	30/80	30/80	30/80	30/80	30/80
each steam/min.	0	0	0	0	0	0
ethanol min/°C	15/80	15/80	15/80	15/80	15/80	15/80
aging time/hr.	20	20	20	20	20	20
aging temp °C	26.5	26.5	26.5	26.5	26.5	26.5

REMARKS:

that ammonium nitrate is damaging to the film integrity. Leaching in NH_4NO_3 and HNO_3 was also investigated. As the leaching time in NH_4NO_3 increases, so does the number of cracks and tears in the film, 9-H,I,J,K and 10-H,I,J,K.

The 11 series experiments were designed to see the effects of multiple rinsing versus single rinsing prior to consolidation. Rinsing in this case (11A,B and D) was started at 2 1/2 hrs after dipping, in contrast to the usual rinsing after 20 hrs (11C and all others). The effects of rinsing duration on the quality of the film were also tested. The longer the exposure to water, the more film that was lost. Samples in 11A, showed the most film loss as compared to 11-B,&D. 11-A2 was thinner than 11-A1, since its rinsing duration was twice as long. The control samples, 11-C, had good coverage and the usual amount of cracking for chemically leached samples. The frequently-rinsed samples showed various degrees of film fragmentation and distortion directly proportional to the frequency and duration of rinsing.

Conclusions:

1. The viscosity of the 20:80 sol composition increases with time.
2. A good working rheology of this sol is reached at about 45 minutes after the sol is prepared, at 70-73 F and 47-57% humidity.
3. Drying/gelation angle influences the quality of film. 45 degrees seems to work well for sol dipped glass slides.
4. Leaching causes thinning of the film(up to nearly 50%) and cracking. Chemical leaching agents used were ammonium nitrate, nitric acid, and water. Steam leaching of air-gelled samples appeared to give some of the best films.
5. Exuded salts from the gel which form a dendritic pattern on the film can be removed by rinsing the film with deionized water prior to consolidation.
6. Consolidation seems to promote dendrite effect.
7. Gelation under water is detrimental to the film integrity.

8. Gelation in 100% humidity has been unsuccessful so far, but because small uncracked patches were observed in steam gelled/steam leached samples further experiments are warranted.
9. Increasing exposure to NH_4NO_3 , results in an increased amount of damage to the film.
10. Frequent rinsing, longer rinsing time, and shorter number of gelation hours before rinsing, all promote film distortion.

5. High Frequency Electrical Characterization

Problem:

To measure the high frequency behavior of transmission lines using low dielectric constant insulators. These measurements not only verify the low dielectric constants of the materials but also serve to verify that transmission lines using these materials will function properly in multichip modules. The data from these measurements is therefore useful to both the materials personnel fabricating the dielectric materials and to electrical designers of the multichip modules.

Approach:

Both high frequency and low frequency are being made. At low frequencies, capacitor test structures are measured with an impedance analyzer. From these measurements, the dielectric constant and loss can be determined by using a lumped element model consisting of a capacitor in parallel with a conductance.

$$Y = G + j\omega C \quad (5.1)$$

$$Y = j\omega C [\epsilon' - j\epsilon''] \quad (5.2)$$

$$C_0 = \frac{\epsilon_0 A}{h} \quad (5.3)$$

where A is the area of the capacitor plate and h is the dielectric thickness. Corrections are made for fringing fields. From the above expressions, the real and imaginary part of the dielectric constant of the material can be determined.

The high frequency measurements are made by "on wafer" probing of microstrip transmission line test structures. Capacitor test structures are also measured at high frequencies to obtain the complex dielectric constant. The transmission line test structures consist of several configurations of microstrip transmission lines. These include open circuited and short circuited transmission lines

of different lengths, transmission lines with vias, and pairs of transmission lines which are coupled.

The test structures are probed using a Design Techniques microwave probing station which is connected to an HP-8510 network analyzer. Using this experimental setup, the driving point impedance of both short circuited and open circuited transmission lines are measured. Since the open and short circuited lines are next to each other on the wafer they are considered to be identical except for the open or shorted termination. The characteristic impedance of the lines can be found using the following expression.

$$Z_o = \sqrt{Z_{sc} Z_{oc}} \quad (5.4)$$

The measured values are compared to calculated values for Z_o using commercial software packages. With a combination of computer calculations and measurements, the line parameters R , L , G , and C per unit length are obtained. Once these line parameters are known, the complex propagation constant can be calculated as follows.

$$\gamma = \sqrt{(R + j\omega L)(G + j\omega C)} \quad (5.5)$$

$$\gamma = \alpha + j\beta \quad (5.6)$$

Where alpha and beta are the loss per unit length and the phase shift per unit length, respectively.

$$\alpha + j\beta = j\omega\sqrt{\mu\epsilon} \quad (5.7)$$

$$\epsilon = \epsilon' + j\epsilon'' \quad (5.8)$$

Since there is a dielectric layer covering the top metal layer, the field is essentially contained in a homogeneous dielectric and a TEM mode is assumed to propagate on the microstrip line.

To speed up the measurement process, the data collection from the network analyzer will be computer controlled. Probing the wafers, however, will continue to be a manual operation.

Results:

The above measurements and simulations have thus far been made on wafers using a SiO₂ dielectric. Once the simulations and measurements are verified for SiO₂, measurements and simulations for various dielectric materials will be made to quantify their properties and compare their relative performance.

Tables 5.1 - 5.3 give the real and imaginary parts, R_o and X_o , of the complex Z_o as a function of frequency for a measured wafers with a SiO₂ dielectric. As can be seen from the data, the transmission line does have loss. Most of this loss is conductor loss since the metal layer is very thin. Below approximately 1.2 GHz, the metal thickness is less than the skin depth.

Accomplishments/Conclusions:

The high frequency measurement system has been assembled and preliminary measurements on microstrip transmission lines and capacitor test structures have been made. Computer simulations have been made to simulate the transmission lines and to analyze the experimental data. Work is currently underway to verify the measurements and to automate the data collection. During the next reporting period, measurements will be made on various dielectric materials to quantify and compare their performance.

6.0 Graduate Students and Tasks

Anne Sullivan

Advising Began: Winter 1990
Comprehensive Examination Passed: Summer 1991
Graduation Date: Spring 1995
Thesis Title: The Auto-catalytic Deposition of Gold

Thomas Hodge

Advising Began: Winter 1990
Comprehensive Examination Passed: Summer 1991
Graduation Date: Spring 1995
Thesis Title: Microstructures for Measuring
Mechanical and Thermal Properties of Thin Polymer
Structures.

Martin Ceiler

Advising Began: Fall 1991
Comprehensive Examination Passed:
Graduation Date: Spring 1996
Thesis Title: Inorganic Dielectrics for GHz Multi-
Chip Modules

Bilal Sinno

Advising Began: Fall 1991
Comprehensive Examination Passed:
Graduation Date: Spring 1996
Thesis Title: Properties of Polyquinoline Interlevel
Dielectrics

Kirk Laursen

Advising Began: Fall 1991
Comprehensive Examination Passed:
Graduation Date: Spring 1996
Thesis Title: High Frequency Properties of Low
Dielectric Constant Insulators

Undergraduate Students

J. Edwards, Winter 1991 to Winter 1992, "DC Magnetron Sputtering"

M. Houston, Winter 1991 to Winter 1992, "Photolithography and electron microscopy"

M. Thadhani, Winter 1991 to Winter 1992, "Electrodeposition of Gold"

G. Sampson, Winter 1991 to Winter 1992, "Reactive Ion Etching"

T. Cloud, Spring 1991 to Winter 1992, "Photosensitive Polyimides"

Ralph Redd, Fall 1991 to Winter 1992, "Semiconductor Metallization"

Cosandra Farmer, Summer 1992, "Wafer Coating Using MTI Flexifab"

Barry Coe, Summer 1992, "Electroplating of Gold"

Guerry Taylor, Summer 1992, "Reactive Ion Etching"

References

- 2.1. D.M. Mattox, *Thin Solid Films*, 18, 173 (1973).
- 2.2. J.M. Poate, P.A. Turner, W.J. DeBonte and J. Yahalom, *J. Appl. Phys.*, 46, 4275 (1975).
- 2.3. M.P. Seah and D. Briggs, "A Perspective on the Analysis of Surfaces and Interfaces", in Practical Surface Analysis by Auger and X-ray Photoelectron Spectroscopy, editors D. Briggs and M.P. Seah, Wiley, New York, 1983, p. 1.
- 2.4. C.D. Wagner, W.M. Riggs, L.E. Davis, J.F. Moulder, and G.E. Muilenberg, Handbook of X-ray Photoelectron Spectroscopy, Perkin-Elmer Corporation, Physical Electronics Division, Eden Prairie, MN, 1979.
- 2.5. W.E. Slinkard and P.B. Degroot, *J. Catal.*, 68, 1981, p.423.
- 2.6. M. Murata, W. Wakino, and S. Ikeda, *J. Electron Spectrosc. Relat. Phenom.*, 6, 1975, p. 459.
- 2.7. M.P. Seah, "Quantification of AES and XPS", in Practical Surface Analysis by Auger and X-ray Photoelectron Spectroscopy, editors D. Briggs and M.P. Seah, Wiley, New York, 1983, p. 197.
- 2.8. *Ibid.*, p. 211.
- 2.9. *Ibid.*, p. 211.
- 2.10. D.R. Penn, *Journal of Electron Spectrosc. and Related Phenomena*, 9, 1976, p. 29-40.
- 2.11. M.P. Seah, "Quantification of AES and XPS", in Practical Surface Analysis by Auger and X-ray Photoelectron Spectroscopy, editors D. Briggs and M.P. Seah, Wiley, New York, 1983, p. 213.
- 2.12. Y. Okinaka, *Journal of Electrochemical Society*, 120, 739 (1973).

2.13. G. Ramachandra Rao and L. Meites, Journal of Physical Chemistry, 70, 3620 (1966).

3.1. L. Lin and S.A. Bidstrup, Proc. ACS Division of Polymeric Materials: Science and Engineering, 66, 265 (1992).

3.2. D.Y. Yoon, D. Boese, S. Herminghaus, J.D. Swalen, and J.F. Rabolt, Mat. Res. Soc., Symp. Proc. Vol. 227, 1991.

3.3. R.W. Hoffman, in Physics of Nonmetallic Thin Films, ed. C.H.S. Dupey and A. Cachard, NATO Advanced Study Institutes, B-14, Plenum, New York, 273 (1976).

3.4. M.G. Allen, M. Mehregany, R.T. Howe and S.D. Senturia, Applied Physics Letter, 51, 241 (1987).

3.5. K.E. Peterson and C.R. Guarnieri, J. Appl. Phys., 50, 6761 (1979).

3.6. C.H. Ahn and M.G. Allen, Proceedings of the ACS Polym. Mats: Sci. and Eng., 64, 395 (1991).

3.7. H.L. Lee, S.M. Thesis, Massachusetts Institute of Technology, (1982).

3.8. D.D. Denton, "Moisture Transport in Polyimide Films in Integrated Circuits", Ph.D. Thesis, Massachusetts Institute of Technology, (1987).

4.1. W.A. Yarbrough, T.R. Gururaja, and L.E. Cross, "Materials for IC Packaging with Very Low Permittivity via Colloidal Sol-Gel Processing", Am.Ceram.Soc. Bull., 66[4] 692-98 (1987).

4.2. R. Anderson, R. Gerhardt, J.B. Wachtman, Jr., S. Becher and D.G. Onn, "Thermal, Mechanical and Dielectric Properties of Mullite-Cordierite Composites," Advances in Ceramics, Vol. 26: CERAMIC SUBSTRATES AND PACKAGING FOR ELECTRONIC APPLICATIONS, ed. M. Yan, K. Niwa, H. O'Bryan and W.S. Young, pp. 265-278, 1989.

4.3. W. Cao, R. Gerhardt and J.B. Wachtman, Jr., "Low Permittivity Porous Silica by a Colloidal Processing Method,"

Advances in Ceramics, Vol. 26 CERAMIC SUBSTRATES AND PACKAGING FOR ELECTRONIC APPLICATIONS, ed. M. Yan, Niwa, H. O'Bryan, Jr. and W.S. Young, pp. 409-418, 1989.

4.4. R.D. Shoup and W.J. Wein, "Low Temperature Production of High Purity Fused Silica," U.S. Pat. No. 4 059 65 8, Nov. 22, 1977.

4.5. R.D. Shoup, "Controlled Pore Silica Bodies Gelled from Silica Sol-Alkali Silicate Mixtures," J. Colloid Interface Sci. 3, 63-69 (1976).

4.6. W. Cao, R. Gerhardt and J.B. Wachtman, Jr., "Preparation and Sintering of Colloidal Silica: Alkali Silicate Gels," J.Amer.Ceram.Soc. 71[12] 1108-1113 (1988).

4.7. G.G. Long, S.T. Krueger and R.A. Gerhardt, "Small Angle Neutron Scattering Study of Microporous Silica", in Ceram. Trans. Vol. 5: ADVANCED CHARACTERIZATION TECHNIQUES FOR CERAMICS, ed. G. McVay and W.S. Young, pp. 171-180, 1989.

4.8. H. Kerch, R. Gerhardt and J. Grazul, "Quantitative Electron Microscopic Investigation of the Pore Structure in 10:90 Colloidal Silica-Potassium Silicate Sol-Gels", J.Am.Ceram.Soc. 73, [8] 2228-2237 (1990).

4.9. G.G. Long, S. Krueger, P.R. Jemain, D.R. Black, H.a. Burdette, J.P. Cline and R.A. Gerhardt, "Small Angle Scattering Determination of the Microstructure and Morphology of Porous Silica Precursors," J.Appl.Cryst.23, 535-544(1990).

4.10. H.M. Kerch, F. Consandey and R. Gerhardt, "Imaging of Fine Porosity in Silica Gels by a Defocus Contrast Technique," submitted to J.Non-Cryst. Solids.

APPENDIX 1

SiO₂ MICROSTRIP STEP OPERATION TASK

LOT # _____

Metal 1 Sputtering

- | | | |
|-----|-------------------|--------------------|
| 1.1 | remove thin oxide | HF soak, 2 min |
| 1.2 | sputter 75A Ti | |
| 1.3 | sputter 1000A Au | Program : Ti.Au.Ti |
| 1.4 | sputter 10A Ti | |

Metal 1 Photolithography

- | | | |
|-----|----------------------|------------------|
| 2.1 | coat 3µm positive PR | see instructions |
| 2.2 | softbake | 30 min, 90 °C |
| 2.3 | expose M1 | OAI, 15 sec |
| 2.4 | develop | 354, 25 sec |
| 2.5 | inspect | |
| 2.6 | hardbake | 30 min, 120 °C |

Metal 1 Plating

- | | | |
|-----|---------------------------|------------------------------|
| 3.1 | etch Ti | .2M EDTA, 4 min |
| 3.2 | plate M1 | 45 °C, 14 min, 100 mA, 3.0 V |
| 3.3 | remove photoresist | acetone |
| 3.4 | measure thickness, record | |

Metal 1 Etching

- | | | |
|-----|---------|-----------------|
| 4.1 | etch Ti | .2M EDTA, 4 min |
| 4.2 | etch Au | KI, 65-70 sec |
| 4.3 | etch Ti | .2M EDTA, 8 min |

Metal 1 Overcoat

- | | | |
|-----|----------------|-------------------|
| 5.1 | Sputter 10A Ti | Program : Ti(10A) |
| 5.2 | Inspect | |

Dielectric 1 Deposition

- | | | | | |
|-----|-----------------------|-------|-------------|-------|
| 6.1 | SiH ₄ flow | _____ | temperature | _____ |
| | N ₂ O flow | _____ | power | _____ |
| | N ₂ flow | _____ | dep time | _____ |
| | pressure | _____ | thickness | _____ |

6.2 deposit insulator on blank wafer

COMMENTS:

Dielectric 1 Photolithography

7.1	coat 3µm positive PR w/HMDS	see instructions
7.2	softbake	30 min, 90 °C
7.3	expose V1	OAI, 15 sec
7.4	develop	354, 25 sec
7.5	inspect	
7.6	hardbake	30 min, 120 °C

Dielectric 1 Etching

8.1	CHF ₃ flow	_____	temperature	_____
	O ₂ flow	_____	power	_____
	pressure	_____	etch time	_____

8.2 O₂ plasma for photoresist

Metal 2 Sputtering

9.1	sputter 75A Ti	
9.2	sputter 1000A Au	Program : Ti.Au.Ti
9.3	sputter 10A Ti	

Metal 2 Photolithography

10.1	coat 3µm positive PR	see instructions
10.2	softbake	30 min, 90 °C
10.3	expose M2	OAI, 23 sec
10.4	develop	354, 25 sec
10.5	inspect	
10.6	hardbake	30 min, 120 °C

Metal 2 Plating

11.1	etch Ti	.2M EDTA, 4 min
11.2	plate M2	45 °C, 25 min, 6 mA, 2.5 V
11.3	remove photoresist	acetone
11.4	measure thickness, record	

Metal 2 Etching

12.1	etch Ti	.2M EDTA, 4 min
12.2	etch Au	KI, 65-70 sec
12.3	etch Ti	.2M EDTA, 8 min
12.4	probe for contact	

Metal 2 Overcoat

13.1	sputter 10A Ti	Program : Ti(10A)
------	----------------	-------------------

13.2 inspect

Dielectric 2 Deposition

14.1	SiH ₄ flow	_____	temperature	_____
	N ₂ O flow	_____	power	_____
	N ₂ flow	_____	dep time	_____
	pressure	_____	thickness	_____

COMMENTS:

Dielectric 2 Photolithography

15.1	coat 3μm positive PR w/HMDS	see instructions
15.2	softbake	30 min, 90 °C
15.3	expose V2	OAI, 23 sec
15.4	develop	354, 25 sec
15.5	inspect	
15.6	hardbake	30 min, 120 °C

Dielectric 2 Etching

16.1	CHF ₃ flow	_____	temperature	_____
	O ₂ flow	_____	power	_____
	pressure	_____	etch time	_____

16.2 O₂ plasma for photoresist

Probe Pad/Metal Three Sputtering

17.1	sputter 75A Ti	
17.2	sputter 1000A Au	Program : Ti.Au.Ti
17.3	sputter 10A Ti	

Probe Pad/Metal Three Photolithography

18.1	coat 3μm positive PR	see instructions
18.2	softbake	30 min, 90 °C
18.3	expose GOLD	OAI, 15 sec
18.4	expose M3	OAI, 15 sec
18.5	develop	354, 25 sec
18.6	inspect	
18.7	hardbake	30 min, 120 °C

Probe Pad/Metal Three Plating

19.1	etch Ti	.2M EDTA, 4 min
19.2	plate Probe Pad/Metal Three	45 °C, ___ min, ___mA, ___V

- 19.3 remove photoresist
- 19.4 measure thickness

acetone

Probe Pad/Metal Three Etching

- 20.1 etch Ti .2M EDTA, 4 min
- 20.2 etch Au KI, 65-70 sec
- 20.3 etch Ti .2M EDTA, 8 min
- 20.4 probe for contact

CAPACITORS STEP OPERATION TASK

- 1. sputter Ti, Au, Ti
- 2. deposit insulator as above
- 3. sputter Ti, Au, Ti
- 4. coat 1 μ m photoresist
- 5. pattern top plate
- 6. etch Ti, Au, Ti
- 7. measure capacitance

MEASUREMENTS

QUAD I

- 1. pF
- 2. pF
- 3. pF
- 4. pF
- 5. pF
- 6. pF
- 7. pF

QUAD II

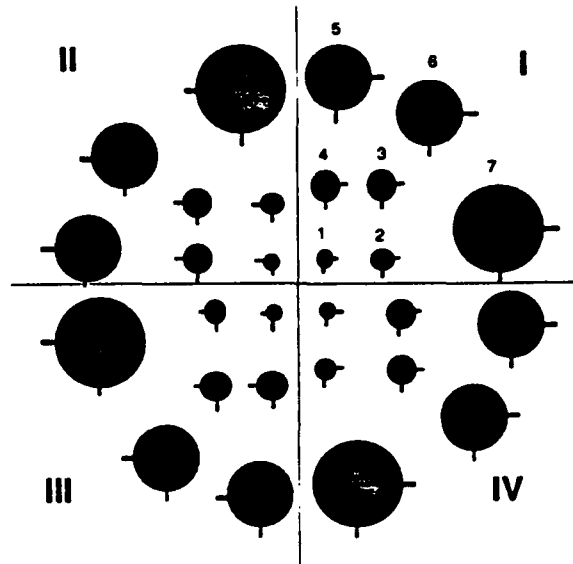
- 1. pF
- 2. pF
- 3. pF
- 4. pF
- 5. pF
- 6. pF
- 7. pF

QUAD III

- 1. pF
- 2. pF
- 3. pF
- 4. pF
- 5. pF
- 6. pF
- 7. pF

QUAD IV

- 1. pF
- 2. pF
- 3. pF
- 4. pF
- 5. pF
- 6. pF
- 7. pF



DATE LOT STARTED :
DATE LOT FINISHED :

APPENDIX 2 **POLYIMIDE** **MICROSTRIP** **STEP OPERATION TASK**

LOT # _____

Metal 1 Sputtering

- | | | |
|-----|-------------------|--------------------|
| 1.1 | remove thin oxide | HF soak, 2 min |
| 1.2 | sputter 75A Ti | |
| 1.3 | sputter 1000A Au | Program : Ti.Au.Ti |
| 1.4 | sputter 10A Ti | |

Metal 1 Photolithography

- | | | |
|-----|----------------------|------------------|
| 2.1 | coat 3µm positive PR | see instructions |
| 2.2 | softbake | 30 min, 90 °C |
| 2.3 | expose M1 | OAI, 15 sec |
| 2.4 | develop | 354, 25 sec |
| 2.5 | inspect | |
| 2.6 | hardbake | 30 min, 120 °C |

Metal 1 Plating (remember blank wafer)

- | | | |
|-----|---------------------------|------------------------------|
| 3.1 | etch Ti | .2M EDTA, 4 min |
| 3.2 | plate M1 | 45 °C, 17 min, 100 mA, 3.0 V |
| 3.3 | remove photoresist | acetone |
| 3.4 | measure thickness, record | |

Metal 1 Etching

- | | | |
|-----|---------|-----------------|
| 4.1 | etch Ti | .2M EDTA, 4 min |
| 4.2 | etch Au | KI, 65-70 sec |
| 4.3 | etch Ti | .2M EDTA, 8 min |

Metal 1 Overcoat (remember blank wafer)

- | | | |
|-----|----------------|-------------------|
| 5.1 | Sputter 10A Ti | Program : Ti(10A) |
| 5.2 | Inspect | |

Dielectric 1 Deposition (remember blank wafer)

- | | | | | |
|-----|----------------|-------|----------------|-------|
| 6.1 | polyimide type | _____ | acceleration | _____ |
| | spin speed | _____ | deceleration | _____ |
| | spin time | _____ | soft bake temp | _____ |
| | thickness | _____ | soft bake time | _____ |

6.2 deposit 1000A SiO₂

CURING CONDITIONS / COMMENTS

Dielectric 1 Photolithography

7.1	coat 3μm positive PR w/HMDS	see instructions
7.2	softbake	30 min, 90 °C
7.3	expose V1	OAI, 15 sec
7.4	develop	354, 25 sec
7.5	inspect	:
7.6	hardbake	30 min, 120 °C

Dielectric 1 Etching

8.1	CHF ₃ flow /time	_____	pressure	_____
	O ₂ flow /time	_____	temperature	_____
	CHF ₃ flow /time	_____	power	_____

Metal 2 Sputtering

9.1	sputter 75A Ti	
9.2	sputter 1000A Au	Program : Ti.Au.Ti
9.3	sputter 10A Ti	

Metal 2 Photolithography

10.1	coat 3μm positive PR	see instructions
10.2	softbake	30 min, 90 °C
10.3	expose M2	OAI, 23 sec
10.4	develop	354, 25 sec
10.5	inspect	
10.6	hardbake	30 min, 120 °C

Metal 2 Plating

11.1	etch Ti	.2M EDTA, 4 min
11.2	plate M2	45 °C, 25 min, 6mA, 2.5 V
11.3	remove photoresist	acetone
11.4	measure thickness, record	

Metal 2 Etching

12.1	etch Ti	.2M EDTA, 4 min
12.2	etch Au	KI, 65-70 sec
12.3	etch Ti	.2M EDTA, 8 min
12.4	probe for contact	

Metal 2 Overcoat

13.1 sputter 10A Ti
13.2 inspect
Dielectric 2 Deposition

Program : Ti(10A)

14.1 polyimide type _____
spin speed _____
spin time _____
thickness _____

acceleration _____
deceleration _____
soft bake temp _____
soft bake time _____

14.2 deposit 1000A SiO₂

CURING CONDITIONS / COMMENTS

Dielectric 2 Photolithography

15.1 coat 3μm positive PR w/HMDS
15.2 softbake
15.3 expose V2
15.4 develop
15.5 inspect
15.6 hardbake

see instructions
30 min, 90 °C
OAI, 23 sec
354, 25 sec

30 min, 120 °C

Dielectric 2 Etching

16.1 CHF₃ flow /time _____
O₂ flow /time _____
CHF₃ flow /time _____

pressure _____
temperature _____
power _____

Probe Pad Sputtering

17.1 sputter 75A Ti
17.2 sputter 1000A Au
17.3 sputter 10A Ti

Program : Ti.Au.Ti

Probe Pad/Metal Three Photolithography

18.1 coat 3μm positive PR
18.2 softbake
18.3 expose GOLD
18.4 expose M3
18.5 develop
18.6 inspect
18.7 hardbake

see instructions
30 min, 90 °C
OAI, 15 sec
OAI, 15 sec
354, 25 sec

30 min, 120 °C

Probe Pad/Metal Three Plating

19.1 etch Ti

.2M EDTA, 4 min

- 19.2 plate Probe Pad
- 19.3 remove photoresist
- 19.4 measure thickness

45 °C, ___min, ___mA, ___V
acetone

Probe Pad/Metal Three Etching

- 20.1 etch Ti
- 20.2 etch Au
- 20.3 etch Ti
- 20.4 probe for contact

.2M EDTA, 4 min
KI, 65-70 sec
.2M EDTA, 8 min

CAPACITORS STEP OPERATION TASK

- 1. sputter Ti, Au, Ti
- 2. deposit insulator
- 3. sputter Ti, Au, Ti
- 4. coat 1µm photoresist
- 5. pattern top plate
- 6. etch Ti, Au, Ti
- 7. measure capacitance

as above

MEASUREMENTS

QUAD I

- 1. pF
- 2. pF
- 3. pF
- 4. pF
- 5. pF
- 6. pF
- 7. pF

QUAD II

- 1. pF
- 2. pF
- 3. pF
- 4. pF
- 5. pF
- 6. pF
- 7. pF

QUAD III

- 1. pF
- 2. pF
- 3. pF
- 4. pF
- 5. pF
- 6. pF
- 7. pF

QUAD IV

- 1. pF
- 2. pF
- 3. pF
- 4. pF
- 5. pF
- 6. pF
- 7. pF

APPENDIX 3

WAFER HANDLING GUIDELINES

In order to keep defects and confusion to a minimum, here are a few tips on how to handle and process the wafers. Please read and follow them at all times.

1. The wafers are to be stored in clearly labeled boxes either in the photolithography bay, the sputtering bay, or in the RIE/PECVD bay. The wafers are also to be numbered in their boxes, starting from the back proceeding forward. Normal lots will consist of under six wafers so keep plenty of space between the individual wafers, both in the boxes and in the quartz boats.
2. Keep track of where your tweezers are! Tweezers are a very hot item in the cleanroom and disappear frequently. We have two types of tweezers: one type for getting the wafers in and out of the RIE/PECVD, and the other type for everything else. Our tweezers are marked with a white piece of tape for easy identification.
3. Throughout the process, the wafers are to be kept in order. As you remove the wafers from their boxes or the quartz boats, do so starting from the back and proceed forward. This will help keep the wafers in order and will minimize scratches, since the only thing that can be scratched is the back of the next wafer. During the SiO_2 and sputtering processes, pay particular attention to the manner in which the wafers are placed in the chambers. A clockwise ordering should be employed to ensure this order is maintained.
4. At all times, and particularly during the photolithography processes, handle the wafers by picking them up on the flat part of the wafer. Always place the wafers in the boxes and boats so you can easily grab the wafers in this manner. This will keep Au

plating and SiO_2 etching in unwanted places to a minimum when the wafer holder scratches through the photoresist.

5. Never take soft-baked photoresist out of the photolithography bay. Use the microscope in this protected bay for examining the wafers, and be sure the orange filter is activated. Also, turn off the hood lamp when developing the wafers. The filters for the lights under the hood are old and the light will expose your photoresist.

6. Clean the masks very carefully before each lot is to be patterned. A gentle swabbing with Microclean should be sufficient. Check the mask after every exposure to make sure no photoresist has stuck to the mask, and make frequent use of the nitrogen gun before and after exposures.

7. Run the cleaning program in the PECVD and RIE after every twelve wafers or so. Both machines will ruin a batch of wafers if not properly cleaned.

8. Avoid use of any solvents of any kind on a wafer before sputtering or depositing SiO_2 . The solvents will leave a residue that can only be seen after the Au or SiO_2 is put down. If for some reason this can't be avoided, put the wafer in the barrel etcher for 60 seconds at 50 watts to remove all traces of the solvent residue.

9. As of now we are plating outside of the cleanroom. Extreme care must be taken to expose the wafers as little as possible to this environment. When small particles contaminate the wafer, the Au will plate over the particle and when etched, a black blotch appears. Do not carry the wafers around in the lab or inspect under a microscope. Go from the box to the bath and straight back to the box.

10. Always put the binder containing all the process sheets, process instructions, etc. in the photolithography bay on top of the nitrogen cabinet at the end of the day. This way anyone who needs to see it knows exactly where it is. Dr. Kohl has an exact and up to

date copy in his office if you need to discuss something with him or with the rest of the group.

11. **Never, ever do a process without the process sheet!** Always fill the process sheets out completely and accurately, adding any comments that you think may be even remotely important. It is important that years from now we have an exact record of what was done to which wafers.

PHOTOLITHOGRAPHY

Preparing the Wafers

For new lots, the wafers that we will be using will be brand new so a quick blow off with the nitrogen gun is all that will be necessary. Proper handling of the wafers during subsequent processing will preclude the need for any solvent cleanings. It is often important to maintain the order in which the wafers were originally placed, so be aware of this when placing the wafers in the quartz boat.

Preparing the Mask

Always handle the masks with the greatest of care, for they are invaluable to this project. The masks should be cleaned before every use. A gentle and careful swabbing with Microclean should be sufficient. If during the patterning the mask becomes dirty, run this cleaning process again. If a mask appears to be uncleanable with Microclean, Dr. Kohl will have some alternative suggestions.

Applying the Photoresist

Place the wafer on the chuck and apply the vacuum. Test spin the wafer to make sure it will spin uniformly. Center the wafer on the chuck and repeat this process until the wafer spins with very little wobble. The only cycles that should be activated are the coat, spread and spin cycles, and make sure the automatic resist

dispenser is off. Set the coat cycle to 500 rpm for 10 seconds, the spread cycle to 500 rpm for 2 seconds, and set the spin cycle to 3250 rpm for 25 seconds. These speeds need to be tested before coating an actual wafer; a dummy wafer may be used for this purpose. If you are applying a via pattern, first coat the surface of the wafer with HMDS and spin until dry. Take the thick resist (PR 1400-37) out of the refrigerator and pour approximately 50mL into the small beaker labeled for this use. Clean the beaker with acetone only and blow dry when you are finished; no other solvents should ever touch this beaker. Start the coat cycle and place your finger on the coat button as you slowly pour the resist onto the center of the spinning wafer. When you are satisfied the wafer is covered sufficiently, close the cover on the coater, and click the coat cycle off, bringing in the spread and spin cycles. The 10 second coat time is meant to give you plenty of time to pour before the next cycle starts; you should not use all ten seconds. When the spin cycle has stopped, disengage the vacuum, click the coat cycle back on, and remove the wafer. Only pick up the wafer with the tweezers on the flat part of the wafer; we want to keep resist defects, no matter where they are on the wafer, to an absolute minimum. At this point the wafers will be noticeably tacky so handle with caution, and check to make sure that none of the photoresist sticks to your tweezers. Soft bake the wafers in the quartz boat for 30 minutes at 90 °C. Always check the temperature of the oven before inserting the wafers because the ovens are often changed to different temperatures for other uses.

Exposing the Pattern

Turn on the OAI mask aligner, turn on the microscope, and start the lamp, allowing about 5 minutes for the lamp to warm up. Make sure the adapters currently on the aligner are for 4 inch wafers and 5 inch masks. Using extreme care, place the cleaned mask on the OAI mask aligner, place the maskclamp on top, and apply the maskclamp vacuum. Take a clean practice wafer and level the wafer chuck by placing the wafer on the chuck, closing the maskframe, and releasing the chuck release *slowly* until it contacts with the mask. Then apply the contact vacuum. Take the contact vacuum off, disengage the chuck release, and remove the wafer. Check the mask for any particles that will ruin the exposure. Place a coated wafer on the chuck with the flat side squared against the

two pins at the bottom of the chuck. Apply the substrate vacuum, and lower the maskframe. Set the correct exposure length and pay particular attention to the decimal point. Bring the chuck up fairly close to the mask, apply the contact vacuum, and expose. When the exposure is completed, take the contact vacuum off, remove the lamp, raise the maskframe, disengage the substrate vacuum, and remove the wafer. Remove the vacuum contact first or the jerking motion of the lamp will ruin the wafer.

Aligning the Mask

If you are exposing a pattern other than Metal One, you will need to align the top pattern to the pattern below it. This will not be difficult at all if a few simple rules are followed. First, always put the mask in the same way every time; you should be able to read the writing on the mask. Second, always put the wafer on the wafer chuck as described in the preceding section. If these two procedures are consistently followed, it should take you no more than thirty seconds to align a pattern. Place the wafer on the chuck, close the maskframe, and bring over the microscope. Adjust the microscope lenses so the alignment patterns on the extreme right and left are visible. Bring the chuck up until both the mask and the wafer below are fairly in focus. Always use the stars and crosses for alignment; they have proven to be the easiest and most effective to use. The crosses will be on the wafer and the stars will be on the mask. Line up the crosses under the stars by first using the theta rotation manipulator, and then use the up/down and left/right manipulators.

If you need to, decrease the magnification to see how unique features of the entire pattern are lining up. Make sure the wafer is very close to the mask before applying contact since the wafer has a tendency to jump off of alignment if the contact has too far to go. Apply the contact, check the alignment one last time, and expose. The next wafers will go even quicker than the first, since the mask isn't going to move and you will place the next wafer in the exact same place on the chuck.

Developing the Pattern

Pour 1000mL of 354 into a beaker under the hood. *Make sure the hood lamp is turned off!* The filters for the lights under the hood are old and the light will expose your photoresist. Place the wafer in a plastic holder and immerse in the developer for 25 seconds. During this developing time be sure to agitate the wafer thoroughly by moving and rotating it. Immediately withdraw the wafer and rinse off well with a gentle stream of DI. Blow off with the nitrogen gun. Hard bake the photoresist for 30 minutes at 120 °C.

Au PLATING

Current process

Preparing the Solution

Initial preparation: To 5 liters of DI add 103.5 mL of 14.5 M H_3PO_4 . To this add 140.28 grams of KOH. Shake well to ensure all the KOH is dissolved. Finally, add 100 grams of $\text{KAu}(\text{CN})_2$. Dr. Kohl has the gold in his office and the solution will be replenished as necessary.

Preparing the Apparatus

Uncover the plating bath, turn on the hood, turn on the variac and set the dial to 55% power. Check the water level to see that it comes up to the correct height; if not, add water until it reaches the mark. With this variac setting and water level, the water should not be spilling over the top - all the water will circulate through the small holes drilled through the divider. It is very important that the apparatus be operating in this fashion before any wafers are plated since the uniformity of the plating depends on it. Place the thermocouple in the drainage compartment, turn the thermocouple on, and plug in the second heater. It is important that the pump be turned on first to keep the heaters sufficiently submerged. The thermocouple should be set to 46 °C. The bath will take about 20 minutes to heat up, and once it has, unplug the second heater. The first heater will be sufficient to maintain the correct temperature.

Plating

As of now, we are plating outside of the cleanroom in lab 150 so great care must be taken to keep the exposure of the wafers to this environment to a minimum. Handle the wafers as little as possible; do not inspect under a microscope or carry around the lab. They should go straight from the box to the bath and back to the box. We are currently using only the left plating station. Close the circuit by clipping the alligator clips together and set the current and voltage using the multimeter for accuracy. Check the task sheet for the proper voltage, current, and time. Set the voltage at 5.0 V for both Metal One and Metal Two and then set the current; the voltage will adjust itself. Turn the power off, unclip the leads, and place a wafer carefully into the bath. Clip the negative lead to the wafer, the positive lead to the cathode, and turn on the power. A timer is present for exact results. At low current settings, the current tends to rise as you plate so pay attention. When the time is up, turn off the power, unclip the negative lead, and *carefully* remove the wafer. Wash the gold solution off the front and back of the wafer with the DI bottle into the waste jug. Wait until you get back into the cleanroom before fully rinsing and drying. Do not blow off with the air valve under the hood. After every wafer check the water level once again, since a small amount will evaporate.

Measurements

Every time you plate, choose a sampling of your lot and take 8 height measurements as shown below. It is important to have identical points of measurement for all of the wafers all of the time. Record your data clearly and precisely, for later the information will be evaluated on Cricket Graph in terms of range and standard deviation.

SPUTTERING

Current process

1. Turn on power to all systems on the main unit
 - a. Ion gauge toggle switch
 - b. Work heater breaker switch
 - c. MDX-1.5K power button
 - d. Rotostrate toggle switch

- e. DC Temp Interlock control power button
- f. MDX-10K Magnetron Drive key to lock position
- 2. Turn on water interlock toggle switch on process chamber
- 3. Turn up screen brightness
- 4. Load the wafers
 - a. Enter password to get to initial menu screen
 - b. Type 'O' to get to operate subroutine
 - c. If not on the LOGO screen type 'S' and then highlight LOGO and press return
 - d. Next, type 'D' for Direct Control and the block *RUN* will be highlighted
 - e. Press return when *RUN* is highlighted and a list of programs will appear at the top of the screen
 - f. Use the cursor keys to go through the list of programs and highlight the program *VENT* and press return
 - g. When the message 'CHAMBER VENTED HOIST ENABLED' appears at the bottom of the screen, press the hoist up button until lid is high enough to load the wafers
 - h. Load the wafers into the appropriate trays. If the right trays are not in the machine they should be in the glass cabinet and can easily be swapped into the machine
 - i. Set rotostrate speed. Flip the toggle switch to the run position and slowly turn dial to appropriate speed. For all sputtering the dial should be set at 10. These speed requirements dictate that only six wafers may be loaded when sputtering
 - j. Once the wafers are loaded, press the hoist down button until the lid is securely closed

5. Sputter

- a. If not in operate subroutine Type 'O'
- b. If not on the logo screen type 'S' and then highlight LOGO and press return
- c. Next, type 'D' for Direct Control and the block *RUN* will be highlighted below
- d. Press return when *RUN* is highlighted and a list of programs will appear at the top of the screen
- e. Use the cursor keys to go through the list of programs and

highlight the program you want and press return. The programs are as follows:

Metal One/Two/Three : **Ti.Au.Ti(M23)**
Overcoat : **Ti(50A)**

Make absolutely certain you choose the correct program ! The program will then run and vent when finished

6. Unload wafers

- a. Make sure screen says 'CHAMBER VENTED HOIST ENABLED'
- b. Press hoist up button until lid is raised
- c. Stop the rotostrate by first turning the dial to zero and then flipping the toggle switch to INDEX. Do not flip the switch while the rotostrate is still moving.
- d. Unload the wafers
- e. Press hoist down button until lid is securely closed

7. Power down

- a. If not in operate subroutine , then Type 'O'
- b. If not on the logo screen type 'S' and then highlight *LOGO* and press return
- c. Next, type 'D' for Direct Control and the block *RUN* will be highlighted
- d. Press return when *RUN* is highlighted and a list of programs will appear at the top of the screen
- e. Use the cursor keys to go through the list of programs and highlight the program *PUMPDOWN* and press return
- f. Turn the ion gauge off while program is running. This cuts down on program running time
- g. Turn off all power on the main unit that was turned on when starting up
- h. When program is finished (the screen will no longer say- 'Press any key for manual page selection') press escape to get to initial menu screen. Then, press escape again and you will see a message that says 'Exit from PAL automation system'. Type 'N' to say no and the password screen will come up. IF YOU

**ACCIDENTALLY SAY YES, IMMEDIATELY
NOTIFY SOMEONE FROM THE CLEANROOM
STAFF THE CRYO PUMP HAS JUST BEEN
TURNED OFF**

- i. Turn down screen brightness and turn off water interlock switch

**PECVD/SiO₂
DEPOSITION**
Current process

System Startup

1. If the mechanical pump is not on (check the console for this message), open up the cabinet doors and push the clearly labeled start button for the mechanical pump
2. Check the back of the machine cabinet to see if the turbo pump is on. If not, do the following:
 - a. press the ON button
 - b. press the MENU button use the cursor keys to highlight 'power hi-vacuum pump' and press ENTER
 - c. highlight 'power up turbo' and press ENTER
 - d. when the task is complete, press the STANDBY button
3. Check the temperatures of the heat exchanger and the substrate on the console. The heat exchanger should read 70 °C and the substrate should read 240 °C. If they do not, press STANDBY until they do
4. Check to see that chamber 2 is active. If not, do the following:
 - a. press the ON button to close the gate valves
 - b. press the MENU button, highlight 'select active chamber', and press ENTER
 - c. highlight 'chamber 2 and press ENTER
 - d. press the STANDBY button

Etching

1. Get the 'DEPOSITION' disk from the nitrogen cabinet and place the disk into the floppy drive on the PECVD machine with the label facing left
2. Press the STANDBY button. The monitor will give the message 'applying standby parameters'
3. Press the ON-LINE button to load the program. When the program is loaded the message 'Program D204-C777 loaded' will appear
4. To load the wafers, press the VENT button to vent the chamber
5. When the message 'Vent completed' appears the chamber lid on the right chamber can be raised and the wafers loaded (4 four-inch wafers per run). CAUTION : the substrate is intensely hot and will melt your gloves to your hands if you touch it
6. Lower the lid to close the chamber
7. Press the READY button. Then press the RUN button to begin the process
8. When the process has finished, press the VENT button, wait for the 'Vent completed' message, and unload the wafers
9. If another run is to be done, go back to step #5

Cleaning

1. The PECVD should be cleaned after every twelve wafers or at the end of the day
2. Press the STANDBY button, insert the 'Cleaning program Chamber 2' disk into the disk drive (label facing left) and press the ON-LINE button
3. Once the program is loaded, press the READY button and then the RUN button
5. This process will take about 1 hour and 15 minutes, and the machine can then be left in this status

RIE/SiO₂
ETCHING
Current process

System Startup

1. If the mechanical pump is not on (check the console for this message), open up the cabinet doors and push the clearly labeled start button for the mechanical pump
2. Check the back of the machine cabinet to see if the turbo pump is on. If not, do the following:
 - a. press the ON button
 - b. press the MENU button use the cursor keys to highlight 'power hi-vacuum pump' and press ENTER
 - c. highlight 'power up turbo' and press ENTER
 - d. when the task is complete, press the STANDBY button
3. Check the temperatures of the chambers on the console. The temperatures must read 25 °C. If they do not, press STANDBY until they do
4. Check to see that chamber 2 is active. If not, do the following:
 - a. press the ON button to close the gate valves
 - b. press the MENU button, highlight 'select active chamber', and press ENTER
 - c. highlight 'chamber 2 and press ENTER
 - d. press the STANDBY button

Etching

1. Get the 'RIE - SiO₂' disk from the nitrogen cabinet and place the disk into the floppy drive on the RIE machine with the label facing left
2. Press the STANDBY button. The monitor will give the message 'applying standby parameters'
3. Press the ON-LINE button to load the program. When the program is loaded the message 'Program D204-C100 loaded' will appear
4. To load the wafers, press the VENT button to vent the

- chamber
5. When the message 'Vent completed' appears the chamber lid on the right chamber can be raised and the wafers loaded (4 four-inch wafers per run)
 6. Lower the lid to close the chamber
 7. Press the READY button. Then press the RUN button to begin the process
 8. When the process has finished, press the VENT button, wait for the 'Vent completed' message, and unload the wafers
 9. If another run is to be done, go back to step #5

Cleaning

1. The RIE should be cleaned after every twelve wafers or at the end of the day
2. Press the STANDBY button, insert the 'Cleaning program Chamber 2' disk into the disk drive (label facing left) and press the ON-LINE button
3. Once the program is loaded, press the READY button and then the RUN button
5. This process will take about 1 hour and 15 minutes, and the machine can then be left in this status

KI Au ETCH

Current process

Preparing the Solution

Measure out 100 grams of KI and add this to 1 liter of DI. To this, add 25 grams of I₂ and stir until all the I₂ is dissolved. Place in the bottles clearly marked for this purpose; they should be kept in the RIE/PECVD bay under the hood.

Using the Solution

Place 1000mL of the KI into a Nalgene beaker and place the beaker into a sonic bath machine. Fill the sonic bath with as much water as it will hold. Place the wafer in a plastic holder, turn the power on, and immerse the wafer in the beaker. Rotate the wafer

holder once every 15 seconds or so. The wafer should be etched for a total of 55-60 seconds. When you are done, carefully pour the solution back into its storage container and put the sonic bath back into the cabinet. It is important to save this solution because the gold can be recovered from it at a later date.

EDTA Ti ETCH

Current process

Preparing the Solution

Measure 323.4 grams of EDTA and dissolve in 9.8 liters of DI. There is a 10 liter container clearly marked in the chemical cart in the metallization bay for this purpose. To this add approximately 50mL of ammonium hydroxide 5-10 ml at a time until the pH reads between 9.4 and 9.6. It is very important that the pH be within these parameters; the pH meter and buffer solution are kept in the photolithography bay. Do not allow the pH to go above 9.6 by adding too much ammonium hydroxide.

Using the Solution

Before every use, vigorously shake the container to ensure a homogeneous solution. Mix the EDTA with hydrogen peroxide in a 2:1 ratio; adding 333 ml of hydrogen peroxide to 667 ml of EDTA in a 1000mL Nalgene beaker works very well for four inch wafers. Use a 250mL/500mL combination for three inch wafers. Etch at room temperature, placing the wafer in a plastic holder and immersing upside down in the solution. For a thickness of 200A, we are currently etching for 6 minutes. Wash the wafer off with a gentle stream of DI and dry with the nitrogen gun. When you are done, pour the solution down the drain with plenty of water. Do not put the solution back into the EDTA jug.